# INTEGRAL EQUATIONS IN COMPUTATIONAL ELECTROMAGNETICS AND THEIR IMPLEMENTATIONS

By

Luke Baumann

#### A DISSERTATION

Submitted to Michigan State University in partial fulfillment of the requirements for the degree of

Electrical and Computer Engineering—Doctor of Philosophy Computational Mathematics, Science, and Engineering—Dual Major

#### ABSTRACT

Integral equations in Computational Electromagnetics (CEM) are one branch of a diverse field. There are many methods to solve for electromagnetic scattering and transmission, with boundary integral equations being one of the most efficient. This is due to only needing to discretize the object's surface, leading to smaller, dense systems as opposed to the larger, sparse systems encountered with Finite Element Method (FEM). Combining the boundary integral method with FEM leads to the creatively named Finite Element Boundary Integral (FEBI) method. It can use the more appropriate method as needed for a given region of space. We turn our focus to boundary integral methods and their implementations.

The subfield of boundary integral equations comprises many subparts, including formulations, representations, testing, singularity treatment, acceleration techniques, solvers, preconditioning, and others. In this thesis, I will present several new and existing formulations using the same formulation framework, demonstrate how to perform the integrals for analytic and piecewise basis and testing functions, modify acceleration techniques for various integral equations, and present supporting results.

The new formulations are well-conditioned, free from traditional breakdowns, and comparable to state-of-the-art formulations. Most of the implementation of all the formulations presented is shared to limit unintended comparisons.

Copyright by LUKE BAUMANN 2023 To my loving wife and kids, Ocean and Bode, you are everything

#### ACKNOWLEDGEMENTS

I want to acknowledge my advisor first and foremost for his continued support through the years. He is incredibly passionate about excellence and has shaped how I approach life, work, and research. It has been my joy and great privilege to study under him.

A special thanks to my committee members, Drs. Aktulga, Qian, Rothwell, Van, and Zayernouri. I made it a point to attend official and unofficial office hours as much as possible for each of them and have a broader and deeper understanding because of it.

I owe so much thanks to my fellow group members, both past and present. I have many memories of that first semester in the group with Drs. Li, Hughey, O'Connor, Crawford, Alsnayyan, Glisson. I want to thank the current members of the group, Jacob Hawkins, Chad Moorman, Omkar Ramachandranharishankar, and Elliot Lu, for making this experience more fulfilling and collaborative.

The Electromagnetics Research Group at Michigan State University is incredible. The faculty have been extremely accessible for advice and eager to help. The students are brilliant and motivated.

Most of all, I would like to thank my family. My wife, for all of her sacrifices, encouragement, and love. I would not have finished this journey without her. My wonderful kids Ocean and Bode who are probably halfway to a degree from all of the online classes and meetings they have been present for. My parents and brother who have always supported and loved me.

## TABLE OF CONTENTS

CHAPTER	1 INTRODUCTION
1.1	What is a Formulation?
1.2	Organization
CHAPTER	2 FORMULATIONS
2.1	Introduction
2.2	Common Formulation Framework
2.3	Operators
2.4	DFIE
2.5	DPIE
2.6	LC-CFIE
2.7	Conclusion
CHAPTER	3 DISCRETIZATION
3.1	Introduction
3.2	Analytic Analysis
3.3	Piecewise Analysis
3.4	Conclusion
CHAPTER	4 ACCELERATION
4.1	Introduction
4.2	Multilevel Fast Multipole Algorithm (MLFMA) Background 64
4.3	Implementation Details
4.4	Results
4.5	Conclusion
4.0	Conclusion
CHAPTER	5 CONCLUSION
5.1	Future Work
BIBLIOGR	APHY 74

#### CHAPTER 1

#### INTRODUCTION

This thesis builds on decades of research in the field of CEM, a vast and varied field that spans physics, mathematics, engineering, and computer science. This conflux of disciplines makes for a fertile research environment where there is rarely a lack of topics to expand upon. This thesis is razor-focused and aimed at developing new surface integral equation formulations capable of solving problems over a broad band of frequencies. Background on surface equivalence theorem, surface integral equations, direct methods, and current formulations is necessary to fully appreciate this body of work. As an introduction, a brief overview of the key concepts will be covered.

#### 1.1 What is a Formulation?

In our context, a formulation is a boundary value problem that can be used to model electromagnetic physics. A formulation can be separated into two parts: the differential equation that governs the behavior of fields interior to a region and boundary conditions relating fields between touching regions.

#### 1.1.1 Differential Equations

Maxwell's equations are the cornerstone of all electromagnetic formulations because they are the differential equations that govern all electromagnetic phenomena. For the scenarios that we are interested in, we can specialize Maxwell's equations for homogeneous, source-free regions with linear materials

$$\nabla \times \mathbf{E} = -j\kappa \eta \mathbf{H} \tag{1.1}$$

$$\nabla \times \mathbf{H} = \frac{j\kappa}{\eta} \mathbf{E} \tag{1.2}$$

$$\nabla \cdot \mathbf{E} = 0 \tag{1.3}$$

$$\nabla \cdot \mathbf{H} = 0 \tag{1.4}$$

with electric field **E**, magnetic field **H**, imaginary unit  $j = \sqrt{-1}$ , wavenumber  $\kappa = \omega \sqrt{\mu \epsilon}$ , wave impedance  $\eta = \sqrt{\frac{\mu}{\epsilon}}$ , permittivity  $\epsilon$ , permeability  $\mu$ . Other material constants used throughout include relative permittivity  $\epsilon_r$  and permeability  $\mu_r$  defined with respect to the permittivity and permeability of free space  $\epsilon = \epsilon_r \epsilon_0$ ,  $\mu = \mu_r \mu_0$  and the refractive index  $n = \sqrt{\mu_r \epsilon_r}$ . These equations describe how the fields interact with each other and can be combined to see that each field satisfies the vector Helmholtz differential equation

$$\nabla \times \mathbf{E} = -j\kappa \eta \mathbf{H} \tag{1.5}$$

$$\nabla \times \nabla \times \mathbf{E} = -j\kappa \eta \nabla \times \mathbf{H} \tag{1.6}$$

$$\nabla \times \nabla \times \mathbf{E} = -j\kappa \eta \frac{j\kappa}{\eta} \mathbf{E}$$
 (1.7)

$$\nabla \left(\nabla \cdot \mathbf{E}\right) - \nabla^2 \mathbf{E} = \kappa^2 \mathbf{E} \tag{1.8}$$

$$\nabla^2 \mathbf{E} + \kappa^2 \mathbf{E} = 0 \tag{1.9}$$

$$\nabla \times \mathbf{H} = \frac{j\kappa}{\eta} \mathbf{E} \tag{1.10}$$

$$\nabla \times \nabla \times \mathbf{H} = \frac{j\kappa}{\eta} \nabla \times \mathbf{E} \tag{1.11}$$

$$\nabla \times \nabla \times \mathbf{H} = \frac{j\kappa}{\eta} \left( -j\kappa \eta \mathbf{H} \right) \tag{1.12}$$

$$\nabla \left(\nabla \cdot \mathbf{H}\right) - \nabla^2 \mathbf{H} = \kappa^2 \mathbf{H} \tag{1.13}$$

$$\nabla^2 \mathbf{H} + \kappa^2 \mathbf{H} = 0 \tag{1.14}$$

#### 1.1.2 Boundary Conditions

The boundary conditions can be formed by examining a pill-box and Stokesian loop across an interface separating two regions of different materials as is typically done [Balanis, 2012]. Boundary conditions for more complex junctions are easily developed as in [Ylä-Oijala et al., 2005]. Still, for simplicity, we restrict ourselves to a single object, dividing space into two regions with a single interface. Once we denote values associated with each region with the proper subscript p and equip the interface with two normal vectors that point into their

respective regions, we can write the boundary conditions as

$$\mathbf{E}_1 \times \hat{\mathbf{n}}_1 + \mathbf{E}_2 \times \hat{\mathbf{n}}_2 = \mathbf{M}_s \tag{1.15}$$

$$\hat{\mathbf{n}}_1 \times \mathbf{H}_1 + \hat{\mathbf{n}}_2 \times \mathbf{H}_2 = \mathbf{J}_s \tag{1.16}$$

$$\epsilon_{r1}\hat{\mathbf{n}}_1 \cdot \mathbf{E}_1 + \epsilon_{r2}\hat{\mathbf{n}}_2 \cdot \mathbf{E}_2 = \frac{\rho_s}{\epsilon_0}$$
(1.17)

$$\mu_{r1}\hat{\mathbf{n}}_1 \cdot \mathbf{H}_1 + \mu_{r2}\hat{\mathbf{n}}_2 \cdot \mathbf{H}_2 = \frac{\rho_{ms}}{\mu_0}$$

$$\tag{1.18}$$

with electric surface current and charge densities  $\mathbf{J}_s$  and  $\rho_s$  along with fictitious magnetic surface current and charge densities  $\mathbf{M}_s$  and  $\rho_{ms}$  as is typically done.

#### 1.1.3 Surface Integral Formulations

Surface integral formulations reformulate Maxwell's equations into an integrodifferential equation, discretize the boundary, and introduce unknown surface sources responsible for the scattered fields within each region. There are two classes of surface integral equations: direct and indirect methods. For direct methods, the sources are directly related to physical quantities. This means the boundary conditions can be imposed on the surface sources. For indirect methods, the sources have no direct physical meaning but can still represent the scattered field within each region. Because there is no physical meaning to the sources, the boundary conditions are imposed on the measurement of the field or charge on the boundary. This thesis will exclusively utilize the direct method, but equivalent indirect method corollaries exist.

For all of the formulations, we decompose the fields into the incident and scattered parts  $\mathbf{x}_p^t = \mathbf{x}_p^i + \mathbf{x}_p^s$  with  $\mathbf{x}$  being any vector that satisfies the vector Helmholtz equation  $\nabla^2 \mathbf{x} + \kappa^2 \mathbf{x} = 0$  and superscripts t, i, and s denoting the total, incident, and scattered part. The incident field is given due to a primary source. This incident field induces a reactionary scattered field such that the boundary conditions on the total fields are satisfied at the interface. In addition, the scattered field must also satisfy a radiating condition to generate a practical and unique solution. The scattered field is written such that it is due to unknown sources on the surface of the boundary. The integral equation used to represent the scattered

field on the surface is derived from Green's vector identity and the vector Helmholtz equation. We let  $\mathbf{x}_p^s$  be the scattered field, and  $G_p$  be the Green's function for the inhomogeneous Helmholtz equation

$$G_p(\mathbf{r}, \mathbf{r}') = \frac{\exp(-j\kappa_p R)}{4\pi R}$$
(1.19a)

$$\nabla^{2} G_{p}(\mathbf{r}, \mathbf{r}') + \kappa_{p}^{2} G_{p}(\mathbf{r}, \mathbf{r}') = -\delta(R)$$
(1.19b)

with  $\mathbf{r}$  as the observation point,  $\mathbf{r}'$  as the source point,  $\mathbf{R} = \mathbf{r} - \mathbf{r}'$ , and  $R = ||\mathbf{R}||_2$ . After much manipulation, we can arrive at what is known as Green's representation theorem

$$\mathbf{x}_{p}^{s} = \mathcal{S}_{p} \circ \left(\hat{\mathbf{n}}_{p} \times \nabla \times \mathbf{x}_{p}^{t}\right) + \nabla \times \mathcal{S}_{p} \circ \left(\hat{\mathbf{n}}_{p} \times \mathbf{x}_{p}^{t}\right) - \nabla \mathcal{S}_{p} \circ \left(\hat{\mathbf{n}}_{p} \cdot \mathbf{x}_{p}^{t}\right) - \mathcal{S}_{p} \circ \left(\hat{\mathbf{n}}_{p} \nabla \cdot \mathbf{x}_{p}^{t}\right)$$
(1.20)

where

$$S_p \circ f_p = \int G_p(\mathbf{r}, \mathbf{r}') f_p(\mathbf{r}') dS'$$
(1.21a)

$$S_{p} \circ \mathbf{f}_{p} = \int G_{p}(\mathbf{r}, \mathbf{r}') \, \mathbf{f}_{p}(\mathbf{r}') \, dS'. \tag{1.21b}$$

is the Single-Layer potential for vectors and scalars. We identify four surface sources per region  $\hat{\mathbf{n}}_p \times \nabla \times \mathbf{x}_p^t$ ,  $\hat{\mathbf{n}}_p \times \mathbf{x}_p^t$ ,  $\hat{\mathbf{n}}_p \times \mathbf{x}_p^t$ , and  $\nabla \cdot \mathbf{x}_p^t$ . The complete steps from Green's identity to (1.20) can be found in [Wilcox, 1956].

We can immediately substitute  ${\bf E}$  and  ${\bf H}$  in for  ${\bf x}$  because they satisfy the vector Helmholtz equation and arrive at

$$\mathbf{E}_{p}^{s} = \mathcal{S}_{p} \circ \left(\hat{\mathbf{n}}_{p} \times \nabla \times \mathbf{E}_{p}^{t}\right) + \nabla \times \mathcal{S}_{p} \circ \left(\hat{\mathbf{n}}_{p} \times \mathbf{E}_{p}^{t}\right) - \nabla \mathcal{S}_{p} \circ \left(\hat{\mathbf{n}}_{p} \cdot \mathbf{E}_{p}^{t}\right) - \mathcal{S}_{p} \circ \left(\hat{\mathbf{n}}_{p} \nabla \cdot \mathbf{E}_{p}^{t}\right)$$

$$(1.22a)$$

$$\mathbf{H}_{p}^{s} = \mathcal{S}_{p} \circ \left(\hat{\mathbf{n}}_{p} \times \nabla \times \mathbf{H}_{p}^{t}\right) + \nabla \times \mathcal{S}_{p} \circ \left(\hat{\mathbf{n}}_{p} \times \mathbf{H}_{p}^{t}\right) - \nabla \mathcal{S}_{p} \circ \left(\hat{\mathbf{n}}_{p} \cdot \mathbf{H}_{p}^{t}\right) - \mathcal{S}_{p} \circ \left(\hat{\mathbf{n}}_{p} \nabla \cdot \mathbf{H}^{t}\right).$$

$$(1.22b)$$

Because we are using electromagnetic fields and have Maxwell's equations, we can simplify by using Gauss' Laws

$$\mathbf{E}_{p}^{s} = \mathcal{S}_{p} \circ \left(\hat{\mathbf{n}}_{p} \times \nabla \times \mathbf{E}_{p}^{t}\right) + \nabla \times \mathcal{S}_{p} \circ \left(\hat{\mathbf{n}}_{p} \times \mathbf{E}^{t}\right) - \nabla \mathcal{S}_{p} \circ \left(\hat{\mathbf{n}}_{p} \cdot \mathbf{E}^{t}\right)$$
(1.23a)

$$\mathbf{H}_{p}^{s} = \mathcal{S}_{p} \circ \left(\hat{\mathbf{n}}_{p} \times \nabla \times \mathbf{H}_{p}^{t}\right) + \nabla \times \mathcal{S}_{p} \circ \left(\hat{\mathbf{n}}_{p} \times \mathbf{H}_{p}^{t}\right) - \nabla \mathcal{S}_{p} \circ \left(\hat{\mathbf{n}}_{p} \cdot \mathbf{H}_{p}^{t}\right). \tag{1.23b}$$

It is also possible to use Faraday's and Ampere's Laws to create two additional representations by taking the curl of both sides and substituting for  $\nabla \times \mathbf{E}$  and  $\nabla \times \mathbf{H}$ 

$$\mathbf{E}_{p}^{s} = \nabla \times \mathcal{S}_{p} \circ \left(\hat{\mathbf{n}}_{p} \times \mathbf{E}_{p}^{t}\right) + \frac{\eta_{p}}{j\kappa_{p}} \nabla \times \nabla \times \mathcal{S}_{p} \circ \left(\hat{\mathbf{n}}_{p} \times \mathbf{H}_{p}^{t}\right)$$
(1.24a)

$$\mathbf{H}_{p}^{s} = \nabla \times \mathcal{S}_{p} \circ \left(\hat{\mathbf{n}}_{p} \times \mathbf{H}_{p}^{t}\right) - \frac{1}{j\kappa_{p}\eta_{p}} \nabla \times \nabla \times \mathcal{S}_{p} \circ \left(\hat{\mathbf{n}}_{p} \times \mathbf{E}_{p}^{t}\right). \tag{1.24b}$$

We have three representation integrals for each field and will use them to develop several formulations with different properties.

To introduce the formulation process, we will step through it for the Electric Field Integral Equation (EFIE), Magnetic Field Integral Equation (MFIE), Combined Field Integral Equation (CFIE), Poggio-Miller-Chang-Harrington-Wu-Tsai (PMCHWT), and Müller formulations. The process for all direct method formulations is similar: use the surface equivalence principle to break the problem into a homogeneous problem for each region, represent the field in each region with an integral equation, enforce boundary conditions on the surface, and solve for the unknowns.

#### 1.1.4 EFIE

We focus on a single Perfect Electrical Conductor (PEC) object immersed in free space with a plane wave incident upon it. For the incident electric and magnetic field plane wave, we will utilize

$$\mathbf{E}_{1}^{i}\left(\mathbf{r}\right) = \mathbf{E}_{0} \exp\left(-j\boldsymbol{\kappa}_{1} \cdot \mathbf{r}\right) \tag{1.25a}$$

$$\mathbf{H}_{1}^{i}\left(\mathbf{r}\right) = \mathbf{H}_{0} \exp\left(-j\boldsymbol{\kappa}_{1} \cdot \mathbf{r}\right) \tag{1.25b}$$

where  $\mathbf{E}_0$  and  $\mathbf{H}_0 = \frac{1}{\eta_1} \hat{\boldsymbol{\kappa}} \times \mathbf{E}_0$  are polarization vectors that are perpendicular to the propagation direction  $\hat{\boldsymbol{\kappa}}$  and each other. There is no incident field produced within the interior of the object  $\mathbf{E}_2^i = \mathbf{H}_2^i = \mathbf{0}$ .

We use the surface equivalence principle to break our problem into two problems. For the first problem, we replace the PEC object with free space, prescribe a null field interior to the object boundary, and place equivalent currents  $J_1$  and  $M_1$  on its surface. For the second

problem, we replace free space with PEC (such that everything is PEC), the field exterior to the object boundary is the null field, and  $\mathbf{J}_2$  and  $\mathbf{M}_2$  are placed on its surface. This second problem is already solved because no field is supported inside a PEC, so the interior fields are also the null field, and consequently  $\mathbf{J}_2 = \mathbf{M}_2 = \mathbf{0}$ . We use the scattered field representation integral (1.24a), add the incident field, and take  $-\hat{\mathbf{n}}_p \times \hat{\mathbf{n}}_p \times$  on both sides

$$-\hat{\mathbf{n}}_{p} \times \hat{\mathbf{n}}_{p} \times \mathbf{E}_{p}^{t} = -\hat{\mathbf{n}}_{p} \times \hat{\mathbf{n}}_{p} \times \left(\mathbf{E}_{p}^{i} + \nabla \times \mathcal{S}_{p} \circ \left(\hat{\mathbf{n}}_{p} \times \mathbf{E}_{p}^{t}\right) + \frac{\eta_{p}}{j\kappa_{p}} \nabla \times \nabla \times \mathcal{S}_{p} \circ \left(\hat{\mathbf{n}}_{p} \times \mathbf{H}_{p}^{t}\right)\right). \tag{1.26}$$

At this point, we can apply the boundary conditions (1.15) and (1.16), recall that  $\mathbf{E}_2^t = \mathbf{H}_2^t = \mathbf{M}_s = \mathbf{0}$  because the PEC supports no fields interior to it and no magnetic currents on the surface, and substitute

$$\mathbf{E}_1^t \times \hat{\mathbf{n}}_1 = 0 \tag{1.27a}$$

$$\hat{\mathbf{n}}_1 \times \mathbf{H}_1^t = \mathbf{J}_s \tag{1.27b}$$

$$-\hat{\mathbf{n}}_1 \times \hat{\mathbf{n}}_1 \times \mathbf{E}_1^i = \frac{\eta_1}{j\kappa_1} \hat{\mathbf{n}}_1 \times \hat{\mathbf{n}}_1 \times \nabla \times \nabla \times \mathcal{S}_1 \circ \hat{\mathbf{n}}_1 \times \mathbf{H}_1^t$$
 (1.27c)

$$\mathcal{L}_p \circ \mathbf{x} = \frac{1}{\kappa_p^2} \nabla \times \nabla \times \mathcal{S}_p \circ \mathbf{x}$$
 (1.27d)

$$-\hat{\mathbf{n}}_1 \times \hat{\mathbf{n}}_1 \times \mathbf{E}_1^i = -j\kappa_1 \eta_1 \hat{\mathbf{n}}_1 \times \hat{\mathbf{n}}_1 \times \mathcal{L}_1 \circ \mathbf{J}_s. \tag{1.27e}$$

#### 1.1.5 MFIE

We reuse some of the work done for the EFIE to formulate the MFIE. This time we use (1.24b) to represent the scattered field. Following a similar procedure, we add the incident field and take  $\hat{\mathbf{n}}_p \times$  on either side

$$\hat{\mathbf{n}}_p \times \mathbf{H}_p^t = \hat{\mathbf{n}}_p \times \left( \mathbf{H}_p^i + \nabla \times \mathcal{S}_p \circ \left( \hat{\mathbf{n}}_p \times \mathbf{H}_p^t \right) - \frac{1}{j\kappa_p\eta_p} \nabla \times \nabla \times \mathcal{S}_p \circ \left( \hat{\mathbf{n}}_p \times \mathbf{E}_p^t \right) \right). \tag{1.28}$$

We apply the boundary conditions (1.15) and (1.16), recall that  $\mathbf{E}_2^t = \mathbf{H}_2^t = \mathbf{M}_s = \mathbf{0}$ , and substitute

$$\mathbf{E}_1^t \times \hat{\mathbf{n}}_1 = \mathbf{0} \tag{1.29a}$$

$$\hat{\mathbf{n}}_1 \times \mathbf{H}_1^t = \mathbf{J}_s \tag{1.29b}$$

$$\mathbf{J}_{s} = \hat{\mathbf{n}}_{1} \times \mathbf{H}_{1}^{i} + \hat{\mathbf{n}}_{p} \times \nabla \times \mathcal{S}_{1} \circ \hat{\mathbf{n}}_{1} \times \mathbf{H}_{1}^{t}$$

$$(1.29c)$$

$$\mathcal{K}_p \circ \mathbf{x} = \hat{\mathbf{n}}_p \times \nabla \times \mathcal{S}_p \circ \mathbf{x} \tag{1.29d}$$

$$\hat{\mathbf{n}}_1 \times \mathbf{H}_1^i = \mathbf{J}_s - \mathcal{K}_1 \circ \mathbf{J}_s. \tag{1.29e}$$

#### 1.1.6 CFIE

The EFIE and MFIE operators each have a null space, meaning there exist corresponding sources  $\mathbf{J}_s$  that produce no scattered field that can be added to any solution. To eliminate the null space, we add the two formulations together with a scaling factor for each equation

$$\begin{pmatrix} \frac{\alpha}{\eta_0} & 1 \end{pmatrix} \begin{pmatrix} -\hat{\mathbf{n}}_1 \times \hat{\mathbf{n}}_1 \times \mathbf{E}_1^i \\ \hat{\mathbf{n}}_1 \times \mathbf{H}_1^i \end{pmatrix} = \begin{pmatrix} \frac{\alpha}{\eta_0} & 1 \end{pmatrix} \begin{pmatrix} -j\kappa_1\eta_1\hat{\mathbf{n}}_1 \times \hat{\mathbf{n}}_1 \times \mathcal{L}_1 \\ \mathcal{I} - \mathcal{K}_1 \end{pmatrix} \circ \mathbf{J}_s. \tag{1.30}$$

The purpose of dividing the EFIE formulation by  $\eta_0$  is so that both integral equations and incident fields are of the same scale, which leads to a better-conditioned system. The purpose of  $\alpha$  is to give the ability to tune the formulation with different relative weights for each formulation as desired.

#### 1.1.7 PMCHWT

We enter the world of dielectrics with the PMCHWT formulation [Poggio and Miller, 1973]. We will make use of two representation integrals (1.24b) and (1.24a), add the incident

fields, and take  $\hat{\mathbf{n}}_p \times \hat{\mathbf{n}}_p \times$  on (1.24b) and  $-\hat{\mathbf{n}}_p \times \hat{\mathbf{n}}_p \times$  on (1.24a) to either side

$$-\hat{\mathbf{n}}_{p} \times \hat{\mathbf{n}}_{p} \times \mathbf{E}_{p}^{t} = -\hat{\mathbf{n}}_{p} \times \hat{\mathbf{n}}_{p} \times \left(\mathbf{E}_{p}^{i} + \nabla \times \mathcal{S}_{p} \circ \left(\hat{\mathbf{n}}_{p} \times \mathbf{E}_{p}^{t}\right) + \frac{\eta_{p}}{j\kappa_{p}} \nabla \times \nabla \times \mathcal{S}_{p} \circ \left(\hat{\mathbf{n}}_{p} \times \mathbf{H}_{p}^{t}\right)\right)$$

$$(1.31a)$$

$$\hat{\mathbf{n}}_{p} \times \hat{\mathbf{n}}_{p} \times \mathbf{H}_{p}^{t} = \hat{\mathbf{n}}_{p} \times \hat{\mathbf{n}}_{p} \times \left(\mathbf{H}_{p}^{i} + \nabla \times \mathcal{S}_{p} \circ \left(\hat{\mathbf{n}}_{p} \times \mathbf{H}_{p}^{t}\right) - \frac{1}{j\kappa_{p}\eta_{p}}\nabla \times \nabla \times \mathcal{S}_{p} \circ \left(\hat{\mathbf{n}}_{p} \times \mathbf{E}_{p}^{t}\right)\right).$$

$$(1.31b)$$

We apply the boundary conditions (1.15) and (1.16), but this time, neither electric nor magnetic currents are supported on the boundary  $\mathbf{J}_s = \mathbf{M}_s = \mathbf{0}$ . However, we can relate the two traces that satisfy the boundary conditions to each other by creating two common "source-like" functions  $\bar{\mathbf{J}}$  and  $\bar{\mathbf{M}}$ 

$$\hat{\mathbf{n}}_1 \times \mathbf{H}_1^t = -\hat{\mathbf{n}}_2 \times \mathbf{H}_2^t \tag{1.32a}$$

$$\mathbf{E}_1^t \times \hat{\mathbf{n}}_1 = -\mathbf{E}_2^t \times \hat{\mathbf{n}}_2 \tag{1.32b}$$

$$\underline{\mathcal{P}}_{1} \begin{pmatrix} \hat{\mathbf{n}}_{1} \times \mathbf{H}_{1}^{t} \\ \mathbf{E}_{1}^{t} \times \hat{\mathbf{n}}_{1} \end{pmatrix} = \underline{\mathcal{P}}_{2} \begin{pmatrix} \hat{\mathbf{n}}_{2} \times \mathbf{H}_{2}^{t} \\ \mathbf{E}_{2}^{t} \times \hat{\mathbf{n}}_{2} \end{pmatrix} = \begin{pmatrix} \bar{\mathbf{J}} \\ \bar{\mathbf{M}} \end{pmatrix}$$
(1.32c)

$$\underline{\mathcal{P}}_{p} = \operatorname{diag}\left(\varepsilon_{p}, \frac{\varepsilon_{p}}{\eta_{0}}\right) \tag{1.32d}$$

where  $\varepsilon_p$  is + for one region and - for the other (e.g.,  $\varepsilon_p = 3 - 2p$  for the two region case and  $p \in \{1, 2\}$ ) and  $\underline{\mathcal{P}}_p$  contains the boundary condition relationship between the traces of the fields on either side of the interface and a scaling parameter such that  $\bar{\mathbf{J}}$  and  $\bar{\mathbf{M}}$  are of the same scale. We can use a scaling matrix,  $\underline{\mathcal{W}}_p$  (along with  $\underline{\mathcal{P}}_p$ ), to combine the equations

from each region

$$\mathcal{Z}_{p} = \begin{pmatrix} -j\kappa_{p}\eta_{p}\hat{\mathbf{n}}_{p} \times \hat{\mathbf{n}}_{p} \times \mathcal{L}_{p} & \hat{\mathbf{n}}_{p} \times (\mathcal{I} - \mathcal{K}_{p}) \\ \hat{\mathbf{n}}_{p} \times (\mathcal{I} - \mathcal{K}_{p}) & \frac{j\kappa_{p}}{\eta_{p}}\hat{\mathbf{n}}_{p} \times \hat{\mathbf{n}}_{p} \times \mathcal{L}_{p} \end{pmatrix}$$
(1.33a)

$$\begin{pmatrix}
\hat{\mathbf{n}}_p \times \mathbf{E}_p^i \times \hat{\mathbf{n}}_p \\
\hat{\mathbf{n}}_p \times \hat{\mathbf{n}}_p \times \mathbf{H}_p^i
\end{pmatrix} = \mathcal{Z}_p \begin{pmatrix}
\hat{\mathbf{n}}_p \times \mathbf{H}_p^t \\
\mathbf{E}_p^t \times \hat{\mathbf{n}}_p
\end{pmatrix}$$
(1.33b)

$$\sum_{p=1}^{2} \underline{\mathcal{P}}_{p} \underline{\mathcal{W}}_{p} \begin{pmatrix} \hat{\mathbf{n}}_{p} \times \mathbf{E}_{p}^{i} \times \hat{\mathbf{n}}_{p} \\ \hat{\mathbf{n}}_{p} \times \hat{\mathbf{n}}_{p} \times \mathbf{H}_{p}^{i} \end{pmatrix} = \left( \sum_{p=1}^{2} \underline{\mathcal{P}}_{p} \underline{\mathcal{W}}_{p} \mathcal{Z}_{p} \left( \underline{\mathcal{P}}_{p} \right)^{-1} \right) \begin{pmatrix} \bar{\mathbf{J}} \\ \bar{\mathbf{M}} \end{pmatrix}. \tag{1.33c}$$

The  $\hat{\mathbf{n}}_p \times \mathcal{I}$  operator can result in degenerate matrices if not correctly discretized. With the right choice of  $\underline{\mathcal{W}}_p$ , we can eliminate it, analytically, canceling out the operator, and preconditioning the system

$$\underline{\mathcal{W}}_p = \operatorname{diag}\left(\frac{1}{\eta_0}, \eta_0\right). \tag{1.34}$$

#### 1.1.8 Müller

The Müller formulation [Müller, 1969] is the final formulation covered in the introduction. We employ the same representation integrals (1.24b) and (1.24a), add the incident fields, but this time take  $\hat{\mathbf{n}}_p \times$  on (1.24b) and  $-\hat{\mathbf{n}}_p \times$  on (1.24a) to either side resulting in

$$\hat{\mathbf{n}}_{p} \times \mathbf{H}_{p}^{t} = \hat{\mathbf{n}}_{p} \times \left(\mathbf{H}_{p}^{i} + \nabla \times \mathcal{S}_{p} \circ \left(\hat{\mathbf{n}}_{p} \times \mathbf{H}_{p}^{t}\right) - \frac{1}{j\kappa_{p}\eta_{p}} \nabla \times \nabla \times \mathcal{S}_{p} \circ \left(\hat{\mathbf{n}}_{p} \times \mathbf{E}_{p}^{t}\right)\right)$$
(1.35a)

$$-\hat{\mathbf{n}}_{p} \times \mathbf{E}_{p}^{t} = -\hat{\mathbf{n}}_{p} \times \left(\mathbf{E}_{p}^{i} + \nabla \times \mathcal{S}_{p} \circ \left(\hat{\mathbf{n}}_{p} \times \mathbf{E}_{p}^{t}\right) + \frac{\eta_{p}}{j\kappa_{p}} \nabla \times \nabla \times \mathcal{S}_{p} \circ \left(\hat{\mathbf{n}}_{p} \times \mathbf{H}_{p}^{t}\right)\right). \quad (1.35b)$$

As before, we apply the boundary conditions (1.15) and (1.16), eliminate sources  $\mathbf{J}_s = \mathbf{M}_s = \mathbf{0}$ , and relate the two boundary condition traces by creating two common "source-like" functions

 $\bar{\mathbf{J}}$  and  $\bar{\mathbf{M}}$ 

$$\hat{\mathbf{n}}_1 \times \mathbf{H}_1^t = -\hat{\mathbf{n}}_2 \times \mathbf{H}_2^t \tag{1.36a}$$

$$\mathbf{E}_1^t \times \hat{\mathbf{n}}_1 = -\mathbf{E}_2^t \times \hat{\mathbf{n}}_2 \tag{1.36b}$$

$$\underline{\mathcal{P}}_{1} \begin{pmatrix} \hat{\mathbf{n}}_{1} \times \mathbf{H}_{1}^{t} \\ \mathbf{E}_{1}^{t} \times \hat{\mathbf{n}}_{1} \end{pmatrix} = \underline{\mathcal{P}}_{2} \begin{pmatrix} \hat{\mathbf{n}}_{2} \times \mathbf{H}_{2}^{t} \\ \mathbf{E}_{2}^{t} \times \hat{\mathbf{n}}_{2} \end{pmatrix} = \begin{pmatrix} \bar{\mathbf{J}} \\ \bar{\mathbf{M}} \end{pmatrix}$$
(1.36c)

$$\underline{\mathcal{P}}_{p} = \operatorname{diag}\left(\varepsilon_{p}, \frac{\varepsilon_{p}}{\eta_{0}}\right). \tag{1.36d}$$

We use a scaling matrix,  $\underline{\mathcal{W}}_p$  (along with  $\underline{\mathcal{P}}_p$ ), to combine the equations from each region

$$\mathcal{Z}_{p} = \begin{pmatrix} \mathcal{I} - \mathcal{K}_{p} & \frac{j\kappa_{p}}{\eta_{p}} \hat{\mathbf{n}}_{p} \times \mathcal{L}_{p} \\ -j\kappa_{p}\eta_{p} \hat{\mathbf{n}}_{p} \times \mathcal{L}_{p} & \mathcal{I} - \mathcal{K}_{p} \end{pmatrix}$$
(1.37a)

$$\begin{pmatrix}
\hat{\mathbf{n}}_p \times \mathbf{H}_p^i \\
\mathbf{E}_p^i \times \hat{\mathbf{n}}_p
\end{pmatrix} = \mathcal{Z}_p \begin{pmatrix}
\hat{\mathbf{n}}_p \times \mathbf{H}^t \\
\mathbf{E}^t \times \hat{\mathbf{n}}_p
\end{pmatrix}$$
(1.37b)

$$\sum_{p=1}^{2} \underline{\mathcal{P}}_{p} \underline{\mathcal{W}}_{p} \begin{pmatrix} \hat{\mathbf{n}}_{p} \times \mathbf{H}_{p}^{i} \\ \mathbf{E}_{p}^{i} \times \hat{\mathbf{n}}_{p} \end{pmatrix} = \left( \sum_{p=1}^{2} \underline{\mathcal{P}}_{p} \underline{\mathcal{W}}_{p} \mathcal{Z}_{p} \left( \underline{\mathcal{P}}_{p} \right)^{-1} \right) \begin{pmatrix} \bar{\mathbf{J}} \\ \bar{\mathbf{M}} \end{pmatrix}. \tag{1.37c}$$

For the Müller formulation, we can make a second-kind formulation by using the linear factors

$$\underline{\mathcal{W}}_p = \operatorname{diag}(\mu_{rp}, \epsilon_{rp}).$$
 (1.38)

#### 1.1.9 Need and Outline of this Thesis

Well-conditioned formulations free of low-frequency, dense-mesh, and topology breakdowns have recently been developed. These new well-conditioned surface integral equation formulations apply to the same problems as current formulations, can be solved with a few iterations across a broad band of frequencies, and are free from typical breakdowns. Like the ones presented above, existing formulations suffer from one breakdown or another. For that reason, I will present several new formulations and the necessary details needed to implement the operators involved in these formulations on spheres and tessellated objects. Much of what is covered will apply tried and true methods and techniques to new formulations. Here is an incomplete list of existing tools and techniques that will be enlisted to take the new formulations to market.

- 1. A surface equivalence framework to represent scattered fields with surface sources
- 2. Using a direct method formulation and enforcing boundary conditions to link surface unknowns between regions
- 3. Spherical harmonics, Rao-Wilton-Glisson (RWG), and pulse basis functions to represent unknowns and measure functions
- 4. Method of Moments to create the system of equations
- 5. Iterative solvers to find the solution for the unknown sources
- 6. Using MLFMA to accelerate the matrix-vector multiplications needed for an iterative solver.

#### 1.2 Organization

This thesis will be organized into three main sections. Chapter 2 will cover the new formulations and discretization process. Chapter 3 will cover implementing these new formulations with piecewise basis sets. Chapter 4 will cover the acceleration details needed to implement the new formulations with MLFMA. Results will be presented throughout as appropriate.

#### CHAPTER 2

#### **FORMULATIONS**

#### 2.1 Introduction

A formulation serves as the foundation for a numerical method. The discretized system of equations to be solved depends on the equations, first and foremost. Many main formulations utilized today were introduced decades ago and have been under constant development. In addition to the formulations introduced in Chapter 1, other formulations include the single integral equation [Marx, 1984, Glisson, 1984] as well as various combinations of surface equivalence theorems; see [Yla-Oijala and Taskinen, 2005], [Li et al., 2014], and references therein for some varieties. The necessity of analyzing composite objects has driven vast advances in the machinery and techniques necessary to compute scattering accurately. The primary challenges include dense mesh breakdown [Cools et al., 2009b], low-frequency breakdown [Vecchi, 1999, Qian and Chew, 2008], and topology breakdown [Cools et al., 2009a]. These breakdowns find their cause in the formulation due to either catastrophic cancellation, bad constraints, or improper scaling. When representing and measuring these integral equations on tessellated representations, they manifest as ill-conditioned and poorly convergent discrete systems. As a result, there has been a concerted effort to develop wellconditioned formulations in both the electromagnetics and applied mathematics communities for a while [Kress and Roach, 1978, Costabel and Stephan, 1988, Wilde, 1987, Costabel, 1991, Dely, 2020].

Indeed, early work recognizing these challenges and efforts toward amelioration date back four decades [Wilton and Glisson, 1981, Wu et al., 1995, Burton and Kashyap, 1995, Vecchi, 1999] with the introduction of loop-star and loop-tree decompositions. Developing preconditioners, formulations, and appropriate basis sets to work around these breakdowns numerically has been a topic of intense research over the past decade [Andriulli et al., 2008]. These methods rely on the representation integrals (1.24b) and (1.24a). More recently, research has focused on alternative formulations which use (1.22a), (1.22b), and in general

(2.17) and (1.20). The two main classes of new formulations are the Decoupled Field Integral Equation (DFIE) [Vico et al., 2018] and Decoupled Potential Integral Equation (DPIE) [Chew, 2014, Liu et al., 2015, Vico et al., 2016, Li et al., 2017]. Other formulations and techniques to overcome some of the bottlenecks of the classical integral equations have been the reliance on Debye potentials [Epstein and Greengard, 2010, Fu et al., 2017], projectors [Andriulli et al., 2008, Adrian et al., 2019], and Dirac formulations [Helsing et al., 2020].

The DPIE is a solution to the transmission problem posed in terms of potentials, whereas the DFIE utilizes fields directly. It has been shown that the DFIE and DPIE are robust to breakdowns associated with low frequency, mesh discretization, and topology Vico et al., 2018, Vico et al., 2016. The DPIE, as is usually the case, was first developed to analyze scattering from PECs [Chew, 2014, Liu et al., 2015, Vico et al., 2016]. A corrected Nyström's method implementation was presented in [Vico et al., 2015], and a time domain potential based integral equation solvers [Roth and Chew, 2018, Roth and Chew, 2020] currently exist. As an aside, it can be shown that [Liu et al., 2015], while based on potential, is akin to an Augmented Electric Field Integral Equation (A-EFIE) [Qian and Chew, 2009]. As expected, developing equations for analyzing scattering from dielectric objects is more complicated. It has its genesis in [Vico et al., 2016, Li et al., 2017, Li et al., 2019]. It is well-conditioned and not susceptible to non-uniqueness due to resonances (under assumptions on constitutive parameters [Vico et al., 2018, Helsing et al., 2020]) nor breakdown due to either low frequencies or topology. All these features were demonstrated using analytic basis sets on spheres or Nyström's method on canonical geometries. The analysis using potentials was first presented by [Vico et al., 2016], who then continued their work by developing the DFIE formulation for dielectrics using an indirect method [Vico et al., 2018]. It has been noted that the DFIE is non-unique for specific pairs of constitutive parameters when loss is present. The formulations presented here are presumed to have the same problem; only lossless materials are considered. The Dirac formulation has recently been introduced with similar properties for a broader range of constitutive properties [Helsing et al., 2020]. Since

the publication of [Vico et al., 2016, Li et al., 2019, Vico et al., 2018], there has yet to be transition to scattering analysis on tessellated geometries. The complexity of the operators is deceptively daunting. In what follows, we present details necessary to implement all of the operators used by the formulations in this chapter in Chapter 3 on spheres using spherical harmonics basis functions and on tessellated surfaces using piecewise basis functions and show that the properties demonstrated using analytic basis sets are preserved.

This chapter uses a general formulation process to describe each formulation presented concisely. Several DFIE and DPIE formulations are developed for dielectric objects, and the Local Calderón-Combined Field Integral Equation (LC-CFIE) formulation for PEC objects is presented using a Calderón identity that was encountered while developing the DFIE and DPIE.

#### 2.2 Common Formulation Framework

It is not difficult to see from looking at Chapter 1 that there is a fairly general way of writing all of these formulations

$$\mathbf{b}_{p}^{\chi} = \mathcal{Z}_{p}^{\chi} \circ \left( \left( \underline{\mathcal{P}}_{p}^{\chi} \right)^{-1} \mathbf{x}^{\chi} \right) \tag{2.1a}$$

$$\sum_{p=1}^{N_p} \underline{\mathcal{P}}_p^{\chi} \underline{\mathcal{W}}_p^{\chi} \mathbf{b}_p^{\chi} = \left( \sum_{p=1}^{N_p} \underline{\mathcal{P}}_p^{\chi} \underline{\mathcal{W}}_p^{\chi} \mathcal{Z}_p^{\chi} \left( \underline{\mathcal{P}}_p^{\chi} \right)^{-1} \right) \circ \mathbf{x}^{\chi}$$
 (2.1b)

with  $\chi$  being a placeholder for a specific formulation,  $N_p$  being the number of regions,  $\mathbf{b}_p^{\chi}$  being a collection of incident functions,  $\mathbf{x}_p^{\chi}$  being a collection of source or "source-like" unknown functions,  $\underline{\mathcal{P}}_p^{\chi}$  enforcing boundary conditions (for dielectric formulations) and scaling unknowns and measurements,  $\underline{\mathcal{W}}_p^{\chi}$  being another scaling matrix, and  $\mathcal{Z}_p^{\chi}$  being the block operator matrix. While this common formulation framework is not entirely general, it applies to all the formulations discussed in this thesis. We can further incorporate the sum over p by creating a stacked  $\underline{\mathcal{P}}^{\chi}$ ,  $(\underline{\mathcal{P}}^{\chi})^{\circ -1}^T$ , and  $\mathbf{b}^{\chi}$  and block  $\underline{\mathcal{W}}^{\chi}$  and  $\mathcal{Z}^{\chi}$ 

$$\underline{\mathcal{P}}^{\chi}\underline{\mathcal{W}}^{\chi}\mathbf{b}^{\chi} = \underline{\mathcal{P}}^{\chi}\underline{\mathcal{W}}^{\chi}\mathcal{Z}^{\chi}(\underline{\mathcal{P}}^{\chi})^{\circ -1} \circ \mathbf{x}^{\chi}$$
(2.2)

where  $\mathbf{x}^{\chi}$  is now the number of independent unknowns and  $\underline{\mathcal{A}} = \underline{\mathcal{B}}^{\circ -1}, \underline{\mathcal{A}}_{ij} = \underline{\mathcal{B}}_{ij}^{-1}$  denotes the element-wise inverse.

For the remainder of this thesis, we will concern ourselves with only the two region cases with either a PEC or dielectric closed object immersed in free space. However, it is important to note that our discussion is mainly extendable to composite and open objects.

We will recast the formulations from the introduction within this framework for completeness. For EFIE, we have

$$\underline{\mathcal{P}}_{1}^{\text{EFIE}} = 1$$
 (2.3a)

$$\underline{\mathcal{W}}_{1}^{\text{EFIE}} = \frac{1}{\eta_{0}} \tag{2.3b}$$

$$\mathcal{Z}_1^{\text{EFIE}} = -j\kappa_1 \eta_1 \hat{\mathbf{n}}_1 \times \hat{\mathbf{n}}_1 \times \mathcal{L}_1 \tag{2.3c}$$

$$\mathbf{b}_{1}^{\text{EFIE}} = -\,\hat{\mathbf{n}}_{1} \times \hat{\mathbf{n}}_{1} \times \mathbf{E}_{1}^{i} \tag{2.3d}$$

$$\mathbf{x}^{\text{EFIE}} = \mathbf{J}_s. \tag{2.3e}$$

For MFIE, we have

$$\underline{\mathcal{P}}_{1}^{\text{MFIE}} = 1 \tag{2.4a}$$

$$\underline{\mathcal{W}}_{1}^{\text{MFIE}} = 1 \tag{2.4b}$$

$$\mathcal{Z}_1^{\text{MFIE}} = \mathcal{I} - \mathcal{K}_1 \tag{2.4c}$$

$$\mathbf{b}_{1}^{\mathrm{MFIE}} = \hat{\mathbf{n}}_{1} \times \mathbf{H}_{1}^{i} \tag{2.4d}$$

$$\mathbf{x}^{\text{MFIE}} = \mathbf{J}_s. \tag{2.4e}$$

For CFIE, we scale and combined the EFIE and MFIE formulations

$$\underline{\mathcal{P}}_{1}^{\text{CFIE}} = \begin{pmatrix} \underline{\mathcal{P}}_{1}^{\text{EFIE}} \\ \underline{\mathcal{P}}_{1}^{\text{MFIE}} \end{pmatrix}^{T}$$
(2.5a)

$$\underline{\mathcal{W}}_{1}^{\text{CFIE}} = \operatorname{diag}\left(\alpha \underline{\mathcal{W}}_{1}^{\text{EFIE}}, \underline{\mathcal{W}}_{1}^{\text{MFIE}}\right) \tag{2.5b}$$

$$\mathcal{Z}_{1}^{\text{CFIE}} = \text{diag}\left(\mathcal{Z}_{1}^{\text{EFIE}}, \mathcal{Z}_{1}^{\text{MFIE}}\right)$$
 (2.5c)

$$\mathbf{b}_{1}^{\text{CFIE}} = \begin{pmatrix} \mathbf{b}_{1}^{\text{EFIE}} \\ \mathbf{b}_{1}^{\text{MFIE}} \end{pmatrix}$$
 (2.5d)

$$\mathbf{x}^{\text{CFIE}} = \mathbf{J}_s. \tag{2.5e}$$

For the PMCHWT, we have

$$\underline{\mathcal{P}_p^{\text{PMCHWT}}} = \text{diag}\left(\varepsilon_p, \frac{\varepsilon_p}{\eta_0}\right) \tag{2.6a}$$

$$\underline{\mathcal{W}}_{p}^{\text{PMCHWT}} = \text{diag}\left(\frac{1}{\eta_{0}}, \eta_{0}\right) \tag{2.6b}$$

$$\mathcal{Z}_{p}^{\text{PMCHWT}} = \begin{pmatrix} -j\kappa_{p}\eta_{p}\hat{\mathbf{n}}_{p} \times \hat{\mathbf{n}}_{p} \times \mathcal{L}_{p} & \hat{\mathbf{n}}_{p} \times (\mathcal{I} - \mathcal{K}_{p}) \\ \hat{\mathbf{n}}_{p} \times (\mathcal{I} - \mathcal{K}_{p}) & \frac{j\kappa_{p}}{\eta_{p}}\hat{\mathbf{n}}_{p} \times \hat{\mathbf{n}}_{p} \times \mathcal{L}_{p} \end{pmatrix}$$
(2.6c)

$$\mathbf{b}_{1}^{\text{PMCHWT}} = \begin{pmatrix} \hat{\mathbf{n}}_{p} \times \mathbf{E}_{p}^{i} \times \hat{\mathbf{n}}_{p} \\ \hat{\mathbf{n}}_{p} \times \hat{\mathbf{n}}_{p} \times \mathbf{H}_{p}^{i} \end{pmatrix}$$
(2.6d)

$$\mathbf{x}^{\text{PMCHWT}} = \begin{pmatrix} \bar{\mathbf{J}} \\ \bar{\mathbf{M}} \end{pmatrix}. \tag{2.6e}$$

For Müller, we have

$$\underline{\mathcal{P}}_{p}^{\text{Müller}} = \operatorname{diag}\left(\varepsilon_{p}, \frac{\varepsilon_{p}}{\eta_{0}}\right) \tag{2.7a}$$

$$\underline{\mathcal{W}}_{p}^{\text{Müller}} = \operatorname{diag}(\mu_{rp}, \epsilon_{rp})$$
(2.7b)

$$\mathcal{Z}_{p}^{\text{Müller}} = \begin{pmatrix}
\mathcal{I} - \mathcal{K}_{p} & \frac{j\kappa_{p}}{\eta_{p}} \hat{\mathbf{n}}_{p} \times \mathcal{L}_{p} \\
-j\kappa_{p}\eta_{p} \hat{\mathbf{n}}_{p} \times \mathcal{L}_{p} & \mathcal{I} - \mathcal{K}_{p}
\end{pmatrix}$$
(2.7c)

$$\mathbf{b}_{1}^{\text{Müller}} = \begin{pmatrix} \hat{\mathbf{n}}_{p} \times \mathbf{H}_{p}^{i} \\ \mathbf{E}_{p}^{i} \times \hat{\mathbf{n}}_{p} \end{pmatrix}$$
(2.7d)

$$\mathbf{x}^{\text{Müller}} = \begin{pmatrix} \bar{\mathbf{J}} \\ \bar{\mathbf{M}} \end{pmatrix}. \tag{2.7e}$$

#### 2.3 Operators

Before presenting additional formulations, all of the operators used will be defined. In total, fifteen different integral operators are defined as follows:

$$S_{p} \circ \begin{pmatrix} \mathbf{x} \\ x \end{pmatrix}^{T} = \int G_{p}(\mathbf{r}, \mathbf{r}') \begin{pmatrix} \mathbf{x}(\mathbf{r}') \\ x(\mathbf{r}') \end{pmatrix}^{T} dS'$$
(2.8a)

$$\mathcal{D}_p \circ x = -\nabla \cdot \mathcal{S}_p \circ \left(\hat{\mathbf{n}}_p x\right) \tag{2.8b}$$

$$\mathcal{N}_p \circ x = -\hat{\mathbf{n}}_p \cdot \nabla \nabla \cdot \mathcal{S}_p \circ (\hat{\mathbf{n}}_p x)$$
 (2.8c)

$$\mathcal{D}_p' \circ x = \hat{\mathbf{n}}_p \cdot \nabla \mathcal{S}_p \circ x \tag{2.8d}$$

$$\mathcal{K}'_p \circ \mathbf{x} = -\nabla \times \mathcal{S}_p \circ (\hat{\mathbf{n}}_p \times \mathbf{x})$$
 (2.8e)

$$\mathcal{J}_p^{(2)} \circ \mathbf{x} = \hat{\mathbf{n}}_p \times \mathcal{S}_p \circ (\hat{\mathbf{n}}_p \times \mathbf{x})$$
 (2.8f)

$$\mathcal{J}_p^{(3)} \circ \mathbf{x} = \hat{\mathbf{n}}_p \cdot \mathcal{S}_p \circ (\hat{\mathbf{n}}_p \times \mathbf{x})$$
 (2.8g)

$$\mathcal{J}^{(4)} \circ \mathbf{x} = \nabla \cdot \mathcal{S}_p \circ \left( \hat{\mathbf{n}}_p \times \mathbf{x} \right) \tag{2.8h}$$

$$\mathcal{L}_p \circ \mathbf{x} = \frac{1}{\kappa_p^2} \nabla \times \nabla \times \mathcal{S}_p \circ \mathbf{x}$$
 (2.8i)

$$\mathcal{K}_p \circ \mathbf{x} = \hat{\mathbf{n}}_p \times \nabla \times \mathcal{S}_p \circ \mathbf{x} \tag{2.8j}$$

$$\mathcal{M}_{p}^{(3)} \circ \mathbf{x} = \hat{\mathbf{n}}_{p} \cdot \nabla \times \mathcal{S}_{p} \circ \mathbf{x} \tag{2.8k}$$

$$\mathcal{P}_p^{(2)} \circ x = \hat{\mathbf{n}}_p \times \nabla \mathcal{S}_p \circ x \tag{2.81}$$

$$Q_p^{(1)} \circ x = \hat{\mathbf{n}}_p \times \hat{\mathbf{n}}_p \times \nabla \times \mathcal{S}_p \circ (\hat{\mathbf{n}}_p x)$$
(2.8m)

$$Q_n^{(2)} \circ x = \hat{\mathbf{n}}_n \times \mathcal{S}_p \circ (\hat{\mathbf{n}}_n x) \tag{2.8n}$$

$$Q_p^{(3)} \circ x = \hat{\mathbf{n}}_p \cdot \mathcal{S}_p \circ (\hat{\mathbf{n}}_p x). \tag{2.80}$$

We define the Single Layer Potential operator (2.8a) as accepting either a scalar or vectorvalued function, denote adjoint operators with a prime, and introduce the shorthand for operators  $\mathcal{O}_p^t = \hat{\mathbf{n}}_p \times \hat{\mathbf{n}}_p \times \mathcal{O}_p$ .

#### 2.4 **DFIE**

The DFIE formulations represent and enforce boundary conditions on fields on either side of an interface as was done for the PMCHWT and Müller formulations. There are two forms of the DFIE, one for **E** and one for **H** that are very closely related to each other.

### 2.4.1 E-Decoupled Field Integral Equation (E-DFIE)

For the E-DFIE, we employ the representation integral (1.22a), add the incident fields, and take  $\hat{\mathbf{n}}_p \times \hat{\mathbf{n}}_p \times \hat{\mathbf$ 

$$\mathbf{E}^{s} = -\mathcal{S}_{p} \circ \left(\hat{\mathbf{n}}_{p} \times \hat{\mathbf{n}}_{p} \times \hat{\mathbf{n}}_{p} \times \nabla \times \mathbf{E}_{p}^{t}\right) + \nabla \times \mathcal{S}_{p} \circ \left(\hat{\mathbf{n}}_{p} \times \mathbf{E}^{t}\right) - \nabla \mathcal{S}_{p} \circ \left(\hat{\mathbf{n}}_{n} \cdot \mathbf{E}^{t}\right) - \mathcal{S}_{p} \circ \left(\hat{\mathbf{n}}_{n} \nabla \cdot \mathbf{E}_{n}^{t}\right).$$

$$(2.9)$$

This is not strictly required but is done so that Galerkin testing with the piecewise RWG basis functions can easily be used with *both* vector unknowns being represented and measured with RWG functions as will be done in Section 3.3.

$$\hat{\mathbf{n}}_{p} \times \hat{\mathbf{n}}_{p} \times \nabla \times \mathbf{E}_{p}^{t} = \hat{\mathbf{n}}_{p} \times \hat{\mathbf{n}}_{p} \times \nabla \times \left(\mathbf{E}^{i} - \mathcal{S}_{p} \circ \left(\hat{\mathbf{n}}_{p} \times \hat{\mathbf{n}}_{p} \times \hat{\mathbf{n}}_{p} \times \nabla \times \mathbf{E}_{p}^{t}\right) + \nabla \times \mathcal{S}_{p} \circ \left(\hat{\mathbf{n}}_{p} \times \mathbf{E}^{t}\right) - \nabla \mathcal{S}_{p} \circ \left(\hat{\mathbf{n}}_{p} \cdot \mathbf{E}^{t}\right) - \mathcal{S}_{p} \circ \left(\hat{\mathbf{n}}_{p} \nabla \cdot \mathbf{E}_{p}^{t}\right) \\
\hat{\mathbf{n}}_{p} \times \mathbf{E}_{p}^{t} = \hat{\mathbf{n}}_{p} \times \left(\mathbf{E}^{i} - \mathcal{S}_{p} \circ \left(\hat{\mathbf{n}}_{p} \times \hat{\mathbf{n}}_{p} \times \hat{\mathbf{n}}_{p} \times \nabla \times \mathbf{E}_{p}^{t}\right) + \nabla \times \mathcal{S}_{p} \circ \left(\hat{\mathbf{n}}_{p} \times \mathbf{E}^{t}\right) - \nabla \mathcal{S}_{p} \circ \left(\hat{\mathbf{n}}_{p} \cdot \mathbf{E}^{t}\right) - \mathcal{S}_{p} \circ \left(\hat{\mathbf{n}}_{p} \nabla \cdot \mathbf{E}_{p}^{t}\right) \\
\hat{\mathbf{n}}_{p} \cdot \mathbf{E}_{p}^{t} = \hat{\mathbf{n}}_{p} \cdot \left(\mathbf{E}^{i} - \mathcal{S}_{p} \circ \left(\hat{\mathbf{n}}_{p} \times \hat{\mathbf{n}}_{p} \times \hat{\mathbf{n}}_{p} \times \nabla \times \mathbf{E}_{p}^{t}\right) + \nabla \times \mathcal{S}_{p} \circ \left(\hat{\mathbf{n}}_{p} \times \mathbf{E}^{t}\right) - \nabla \mathcal{S}_{p} \circ \left(\hat{\mathbf{n}}_{p} \cdot \mathbf{E}^{t}\right) - \mathcal{S}_{p} \circ \left(\hat{\mathbf{n}}_{p} \nabla \cdot \mathbf{E}_{p}^{t}\right) \\
\nabla \cdot \mathbf{E}_{p}^{t} = \nabla \cdot \left(\mathbf{E}^{i} - \mathcal{S}_{p} \circ \left(\hat{\mathbf{n}}_{p} \times \hat{\mathbf{n}}_{p} \times \hat{\mathbf{n}}_{p} \times \nabla \times \mathbf{E}_{p}^{t}\right) + \nabla \times \mathcal{S}_{p} \circ \left(\hat{\mathbf{n}}_{p} \nabla \cdot \mathbf{E}_{p}^{t}\right) \\
+ \nabla \times \mathcal{S}_{p} \circ \left(\hat{\mathbf{n}}_{p} \times \hat{\mathbf{n}}_{p} \times \hat{\mathbf{n}}_{p} \times \nabla \times \mathbf{E}_{p}^{t}\right) + \nabla \mathcal{S}_{p} \circ \left(\hat{\mathbf{n}}_{p} \nabla \cdot \mathbf{E}_{p}^{t}\right)$$
(2.10d)
$$+ \nabla \times \mathcal{S}_{p} \circ \left(\hat{\mathbf{n}}_{p} \times \mathbf{E}^{t}\right) - \nabla \mathcal{S}_{p} \circ \left(\hat{\mathbf{n}}_{p} \cdot \mathbf{E}^{t}\right) - \mathcal{S}_{p} \circ \left(\hat{\mathbf{n}}_{p} \nabla \cdot \mathbf{E}_{p}^{t}\right)$$

We apply the boundary conditions (1.15), (1.16), (1.17), and create a fourth boundary condition on  $\nabla \cdot \mathbf{E}_p^t$  (such that it is continuous across the boundary). As for PMCHWT and Müller, there are no currents or charges supported on the boundary  $\mathbf{J}_s = \mathbf{M}_s = \mathbf{0}$  and

 $\rho_s == \rho_{ms} = 0$  but we can create four "source-like" functions,  $\bar{\mathbf{a}}$ ,  $\bar{\mathbf{b}}$ ,  $\bar{\gamma}$ , and  $\bar{\sigma}$  to use

$$\frac{1}{\mu_{r1}}\hat{\mathbf{n}}_1 \times \hat{\mathbf{n}}_1 \times \nabla \times \mathbf{E}_1^t = \frac{1}{\mu_{r2}}\hat{\mathbf{n}}_2 \times \hat{\mathbf{n}}_2 \times \nabla \times \mathbf{E}_2^t$$
(2.11a)

$$\hat{\mathbf{n}}_1 \times \mathbf{E}_1^t = -\hat{\mathbf{n}}_2 \times \mathbf{E}_2^t \tag{2.11b}$$

$$\epsilon_{r1}\hat{\mathbf{n}}_1 \cdot \mathbf{E}_1^t = -\epsilon_{r2}\hat{\mathbf{n}}_2 \cdot \mathbf{E}_2^t \tag{2.11c}$$

$$\nabla \cdot \mathbf{E}_1^t = \nabla \cdot \mathbf{E}_2^t \tag{2.11d}$$

$$\underline{\mathcal{P}}_{1}^{\mathbf{EDFIE}}\begin{pmatrix} \hat{\mathbf{n}}_{1} \times \hat{\mathbf{n}}_{1} \times \nabla \times \mathbf{E}_{1}^{t} \\ \hat{\mathbf{n}}_{1} \times \mathbf{E}_{1}^{t} \\ \hat{\mathbf{n}}_{1} \cdot \mathbf{E}_{1}^{t} \\ \nabla \cdot \mathbf{E}_{1}^{t} \end{pmatrix} = \underline{\mathcal{P}}_{2}^{\mathbf{EDFIE}}\begin{pmatrix} \hat{\mathbf{n}}_{2} \times \hat{\mathbf{n}}_{2} \times \nabla \times \mathbf{E}_{2}^{t} \\ \hat{\mathbf{n}}_{2} \times \mathbf{E}_{2}^{t} \\ \hat{\mathbf{n}}_{2} \cdot \mathbf{E}_{2}^{t} \\ \nabla \cdot \mathbf{E}_{2}^{t} \end{pmatrix} = \begin{pmatrix} \bar{\mathbf{a}} \\ \bar{\mathbf{b}} \\ \bar{\gamma} \\ \bar{\sigma} \end{pmatrix} \tag{2.11e}$$

We can define the matrices, operators, and vectors for this formulation as

$$\underline{\mathcal{P}_{p}^{\mathbf{EDFIE}}} = \operatorname{diag}\left(\frac{1}{\mu_{rp}}, -j\kappa_{0}\varepsilon_{p}, -j\kappa_{0}\varepsilon_{p}\epsilon_{rp}, 1\right)$$
(2.12a)

$$\underline{\mathcal{W}}_{p}^{\text{EDFIE}} = \operatorname{diag}\left(\mu_{rp}, \epsilon_{rp}, \frac{1}{\epsilon_{rp}}, \frac{1}{\mu_{rp}}\right)$$
(2.12b)

$$\mathcal{Z}_{p}^{\mathbf{EDFIE}} = \begin{pmatrix}
\mathcal{I} - \mathcal{K}_{p}^{\prime t} & -\kappa_{p}^{2} \mathcal{L}_{p}^{t} & 0 & \mathcal{Q}_{p}^{(1)} \\
\mathcal{J}_{p}^{(2)} & \mathcal{I} - \mathcal{K}_{p} & \mathcal{P}_{p}^{(2)} & \mathcal{Q}_{p}^{(2)} \\
\mathcal{J}_{p}^{(3)} & -\mathcal{M}_{p}^{(3)} & \mathcal{I} + \mathcal{D}_{p}^{\prime} & \mathcal{Q}_{p}^{(3)} \\
\mathcal{J}_{p}^{(4)} & 0 & -\kappa^{2} \mathcal{S}_{p} & \mathcal{I} - \mathcal{D}_{p}
\end{pmatrix} \tag{2.12c}$$

$$\mathbf{b}_{p}^{\mathbf{E}\mathrm{DFIE}} = \begin{pmatrix} \hat{\mathbf{n}}_{p} \times \hat{\mathbf{n}}_{p} \times \nabla \times \mathbf{E}_{p}^{i} \\ \hat{\mathbf{n}}_{p} \times \mathbf{E}_{p}^{i} \\ \hat{\mathbf{n}}_{p} \cdot \mathbf{E}_{p}^{i} \\ \nabla \cdot \mathbf{E}_{p}^{i} \end{pmatrix}$$
(2.12d)

$$\mathbf{x}^{\mathbf{EDFIE}} = \begin{pmatrix} \bar{\mathbf{a}} & \bar{\mathbf{b}} & \bar{\gamma} & \bar{\sigma} \end{pmatrix}^{T}.$$
 (2.12e)

The linear factors of  $\underline{\mathcal{W}}_p^{\text{EDFIE}}$  are chosen such that the E-DFIE formulation results in a second-kind integral equation.

#### 2.4.2 E-Reduced Decoupled Field Integral Equation (E-RDFIE)

Rather than using (1.22a), we could explicitly enforce Gauss's law (1.3) by using (1.23a). A second-kind integral equation can be made by removing the fourth row and column of the E-DFIE.

By reusing many of the same definitions from the E-DFIE, we can jump straight to

$$\underline{\mathcal{P}_p^{\text{ERDFIE}}} = \operatorname{diag}\left(\frac{1}{\mu_{rp}}, -j\kappa_0\varepsilon_p, -j\kappa_0\varepsilon_p\varepsilon_{rp}\right)$$
(2.13a)

$$\underline{\mathcal{W}}_{p}^{\text{ERDFIE}} = \operatorname{diag}\left(\mu_{rp}, \epsilon_{rp}, \frac{1}{\epsilon_{rp}}\right)$$
(2.13b)

$$\mathcal{Z}_{p}^{\text{ERDFIE}} = \begin{pmatrix}
\mathcal{I} - \mathcal{K}_{p}^{\prime t} & -\kappa_{p}^{2} \mathcal{L}_{p}^{t} & 0 \\
\mathcal{J}_{p}^{(2)} & \mathcal{I} - \mathcal{K}_{p} & \mathcal{P}_{p}^{(2)} \\
\mathcal{J}_{p}^{(3)} & -\mathcal{M}_{p}^{(3)} & \mathcal{I} + \mathcal{D}_{p}^{\prime}
\end{pmatrix} (2.13c)$$

$$\mathbf{b}_{p}^{\mathbf{E}RDFIE} = \begin{pmatrix} \hat{\mathbf{n}}_{p} \times \hat{\mathbf{n}}_{p} \times \nabla \times \mathbf{E}_{p}^{i} \\ \hat{\mathbf{n}}_{p} \times \mathbf{E}_{p}^{i} \\ \hat{\mathbf{n}}_{p} \cdot \mathbf{E}_{p}^{i} \end{pmatrix}$$
(2.13d)

$$\mathbf{x}^{\mathbf{E}RDFIE} = \begin{pmatrix} \bar{\mathbf{a}} & \bar{\mathbf{b}} & \bar{\gamma} \end{pmatrix}^T \tag{2.13e}$$

#### 2.4.3 H-Decoupled Field Integral Equation (H-DFIE)

For the H-DFIE, we employ the same tactics as with the E-DFIE, and because of duality, we can replace  $\mathbf{E}$  with  $\mathbf{H}$ ,  $\mu$  with  $\epsilon$ , and  $\epsilon$  with  $\mu$  and arrive at the formulation. Boundary conditions are expressed as

$$\underline{\mathcal{P}}_{1}^{\mathbf{HDFIE}} \begin{pmatrix} \hat{\mathbf{n}}_{1} \times \hat{\mathbf{n}}_{1} \times \nabla \times \mathbf{H}_{1}^{t} \\ \hat{\mathbf{n}}_{1} \times \mathbf{H}_{1}^{t} \\ \hat{\mathbf{n}}_{1} \cdot \mathbf{H}_{1}^{t} \\ \nabla \cdot \mathbf{H}_{1}^{t} \end{pmatrix} = \underline{\mathcal{P}}_{2}^{\mathbf{HDFIE}} \begin{pmatrix} \hat{\mathbf{n}}_{2} \times \hat{\mathbf{n}}_{2} \times \nabla \times \mathbf{H}_{2}^{t} \\ \hat{\mathbf{n}}_{2} \times \mathbf{H}_{2}^{t} \\ \hat{\mathbf{n}}_{2} \cdot \mathbf{H}_{2}^{t} \\ \nabla \cdot \mathbf{H}_{2}^{t} \end{pmatrix} = \begin{pmatrix} \bar{\mathbf{a}} \\ \bar{\mathbf{b}} \\ \bar{\gamma} \\ \bar{\sigma} \end{pmatrix} \tag{2.14a}$$

and the remaining matrices, operators, and vectors are

$$\underline{\mathcal{P}}_{p}^{\mathbf{H}\mathrm{DFIE}} = \operatorname{diag}\left(\frac{1}{\epsilon_{rp}}, -j\kappa_{0}\varepsilon_{p}, -j\kappa_{0}\varepsilon_{p}\mu_{rp}, 1\right)$$
(2.14b)

$$\underline{\mathcal{W}}_{p}^{\mathbf{H}\mathrm{DFIE}} = \operatorname{diag}\left(\epsilon_{rp}, \mu_{rp}, \frac{1}{\mu_{rp}}, \frac{1}{\epsilon_{rp}}\right)$$
(2.14c)

$$\mathcal{Z}_{p}^{\mathbf{HDFIE}} = \begin{pmatrix}
\mathcal{I} - \mathcal{K}_{p}^{\prime t} & -\kappa_{p}^{2} \mathcal{L}_{p}^{t} & 0 & \mathcal{Q}_{p}^{(1)} \\
\mathcal{J}_{p}^{(2)} & \mathcal{I} - \mathcal{K}_{p} & \mathcal{P}_{p}^{(2)} & \mathcal{Q}_{p}^{(2)} \\
\mathcal{J}_{p}^{(3)} & -\mathcal{M}_{p}^{(3)} & \mathcal{I} + \mathcal{D}_{p}^{\prime} & \mathcal{Q}_{p}^{(3)} \\
\mathcal{J}_{p}^{(4)} & 0 & -\kappa^{2} \mathcal{S}_{p} & \mathcal{I} - \mathcal{D}_{p}
\end{pmatrix} \tag{2.14d}$$

$$\mathbf{b}_{p}^{\mathbf{HDFIE}} = \begin{pmatrix} \hat{\mathbf{n}}_{p} \times \hat{\mathbf{n}}_{p} \times \nabla \times \mathbf{H}_{p}^{i} \\ \hat{\mathbf{n}}_{p} \times \mathbf{H}_{p}^{i} \\ \hat{\mathbf{n}}_{p} \cdot \mathbf{H}_{p}^{i} \\ \nabla \cdot \mathbf{H}_{p}^{i} \end{pmatrix}$$
(2.14e)

$$\mathbf{x}^{\mathbf{HDFIE}} = \begin{pmatrix} \bar{\mathbf{a}} & \bar{\mathbf{b}} & \bar{\gamma} & \bar{\sigma} \end{pmatrix}^T \tag{2.14f}$$

#### 2.4.4 H-Reduced Decoupled Field Integral Equation (H-RDFIE)

Similarly, we could enforce Gauss's law (1.4) explicitly by using (1.23b). A second-kind integral equation can be made by removing the fourth row and column of the H-DFIE.

$$\underline{\mathcal{P}_p^{\mathbf{H}RDFIE}} = \operatorname{diag}\left(\frac{1}{\epsilon_{rp}}, -j\kappa_0 \varepsilon_p, -j\kappa_0 \varepsilon_p \mu_{rp}\right)$$
(2.15a)

$$\underline{\mathcal{W}}_{p}^{\mathbf{H}RDFIE} = \operatorname{diag}\left(\epsilon_{rp}, \mu_{rp}, \frac{1}{\mu_{rp}}\right)$$
(2.15b)

$$\mathcal{Z}_{p}^{\mathbf{H}RDFIE} = \begin{pmatrix}
\mathcal{I} - \mathcal{K}_{p}^{\prime t} & -\kappa_{p}^{2} \mathcal{L}_{p}^{t} & 0 \\
\mathcal{J}_{p}^{(2)} & \mathcal{I} - \mathcal{K}_{p} & \mathcal{P}_{p}^{(2)} \\
\mathcal{J}_{p}^{(3)} & -\mathcal{M}_{p}^{(3)} & \mathcal{I} + \mathcal{D}_{p}^{\prime}
\end{pmatrix} (2.15c)$$

$$\mathbf{b}_{p}^{\mathbf{H}RDFIE} = \begin{pmatrix} \hat{\mathbf{n}}_{p} \times \hat{\mathbf{n}}_{p} \times \nabla \times \mathbf{H}_{p}^{i} \\ \hat{\mathbf{n}}_{p} \times \mathbf{H}_{p}^{i} \\ \hat{\mathbf{n}}_{p} \cdot \mathbf{H}_{p}^{i} \end{pmatrix}$$
(2.15d)

$$\mathbf{x}^{\mathbf{H}RDFIE} = \begin{pmatrix} \bar{\mathbf{a}} & \bar{\mathbf{b}} & \bar{\gamma} \end{pmatrix}^{T} \tag{2.15e}$$

#### 2.5 **DPIE**

All other formulations discussed thus far have used representations of fields, either **E** or **H**, as a starting point. The novelty of the DPIE formulation is that it uses potentials.

It is well-known that fields can be represented with potentials. For the vector magnetic and scalar electric potential  $\mathbf{A} - \phi$  decomposition and the vector electric and scalar magnetic potential  $\mathbf{F} - \psi$  decomposition, we have

$$\mathbf{E} = -j\omega\mathbf{A} - \nabla\phi \tag{2.16a}$$

$$\mathbf{H} = \frac{1}{\mu} \nabla \times \mathbf{A} \tag{2.16b}$$

$$\mathbf{H} = -j\omega\mathbf{F} - \nabla\psi \tag{2.16c}$$

$$\mathbf{E} = \frac{-1}{\epsilon} \nabla \times \mathbf{F}. \tag{2.16d}$$

Furthermore, under the Lorenz gauge,

$$\nabla \cdot \mathbf{A} = \frac{\kappa^2}{j\omega} \phi \tag{2.16e}$$

$$\nabla \cdot \mathbf{F} = \frac{\kappa^2}{i\omega} \psi \tag{2.16f}$$

these potentials satisfy the Helmholtz equation

$$\nabla^2 \mathbf{A} + \kappa^2 \mathbf{A} = 0 \tag{2.16g}$$

$$\nabla^2 \phi + \kappa^2 \phi = 0 \tag{2.16h}$$

$$\nabla^2 \mathbf{F} + \kappa^2 \mathbf{F} = 0 \tag{2.16i}$$

$$\nabla^2 \psi + \kappa^2 \psi = 0. \tag{2.16j}$$

We start diverging from the previous formulations by representing the potentials **A** and **F** rather than the fields with (1.20). The scalar counterpart to Green's Vector Representation Theorem is derived from Green's scalar identities. With x being any scalar that satisfies the scalar Helmholtz equation  $\nabla^2 x + \kappa^2 x = 0$ , we have

$$x_p^s = -\nabla \cdot \mathcal{S}_p \circ \left(\hat{\mathbf{n}}_p x_p^t\right) - \mathcal{S}_p \circ \left(\hat{\mathbf{n}}_p \cdot \nabla x_p^t\right). \tag{2.17}$$

We use Green's Scalar Representation Theorem to represent  $\phi$  and  $\psi$ .

Explicitly, we have four representation equations

$$\mathbf{A}_{p}^{s} = \mathcal{S}_{p} \circ \left(\hat{\mathbf{n}}_{p} \times \nabla \times \mathbf{A}_{p}^{t}\right) + \nabla \times \mathcal{S}_{p} \circ \left(\hat{\mathbf{n}}_{p} \times \mathbf{A}_{p}^{t}\right) - \nabla \mathcal{S}_{p} \circ \left(\hat{\mathbf{n}}_{p} \cdot \mathbf{A}_{p}^{t}\right) - \mathcal{S}_{p} \circ \left(\hat{\mathbf{n}}_{p} \nabla \cdot \mathbf{A}_{p}^{t}\right)$$

$$(2.18a)$$

$$\phi_p^s = -\nabla \cdot \mathcal{S}_p \circ (\hat{\mathbf{n}}_p \phi_p^t) - \mathcal{S}_p \circ (\hat{\mathbf{n}}_p \cdot \nabla \phi_p^t)$$
(2.18b)

$$\mathbf{F}_{p}^{s} = \mathcal{S}_{p} \circ \left(\hat{\mathbf{n}}_{p} \times \nabla \times \mathbf{F}_{p}^{t}\right) + \nabla \times \mathcal{S}_{p} \circ \left(\hat{\mathbf{n}}_{p} \times \mathbf{F}_{p}^{t}\right) - \nabla \mathcal{S}_{p} \circ \left(\hat{\mathbf{n}}_{p} \cdot \mathbf{F}_{p}^{t}\right) - \mathcal{S}_{p} \circ \left(\hat{\mathbf{n}}_{p} \nabla \cdot \mathbf{F}_{p}^{t}\right)$$

$$(2.18c)$$

$$\psi_p^s = -\nabla \cdot \mathcal{S}_p \circ (\hat{\mathbf{n}}_p \psi_p^t) - \mathcal{S}_p \circ (\hat{\mathbf{n}}_p \cdot \nabla \psi_p^t). \tag{2.18d}$$

At this point, we can impose boundary conditions; however, the boundary conditions we have available are on the fields, not potentials. Because there is a many-to-one relationship

from potentials to fields, many options exist for deriving potential-based boundary conditions from the field boundary conditions. One method in particular results in decoupling the vector and scalar potentials [Li et al., 2019].

As for the DFIE, there are several variants to the DPIE, and a collection of them will be covered in the following sections.

#### 2.5.1 Incident Wave

The incident waves  $\phi_1^i$  and  $\mathbf{A}_1^i$  decompose  $\mathbf{E}_1^i$  (1.25a) while  $\psi_1^i$  and  $\mathbf{F}_1^i$  decompose  $\mathbf{H}_1^i$  (1.25b) and are in the form found in [Vico et al., 2015]:

$$\phi_1^i = -\left(\mathbf{r} \cdot \mathbf{E}_0\right) \exp\left(-j\boldsymbol{\kappa}_1 \cdot \mathbf{r}\right) \tag{2.19a}$$

$$\mathbf{A}_{1}^{i} = -\frac{\boldsymbol{\kappa}_{1}}{\omega} \left( \mathbf{r} \cdot \mathbf{E}_{0} \right) \exp \left( -j \boldsymbol{\kappa}_{1} \cdot \mathbf{r} \right) \tag{2.19b}$$

$$\psi_1^i = -(\mathbf{r} \cdot \mathbf{H}_0) \exp(-j\kappa_1 \cdot \mathbf{r})$$
(2.19c)

$$\mathbf{F}_{1}^{i} = -\frac{\boldsymbol{\kappa}_{1}}{\omega} \left( \mathbf{r} \cdot \mathbf{H}_{0} \right) \exp \left( -j \boldsymbol{\kappa}_{1} \cdot \mathbf{r} \right). \tag{2.19d}$$

Alternate decompositions, such as

$$\phi_1^i = \phi_0 \exp\left(-j\boldsymbol{\kappa}_1 \cdot \mathbf{r}\right) \tag{2.20a}$$

$$\mathbf{A}_{1}^{i} = \mathbf{A}_{0} \exp\left(-j\boldsymbol{\kappa}_{1} \cdot \mathbf{r}\right) \tag{2.20b}$$

$$\mathbf{A}_0 = \frac{-1}{j\omega} \left( \mathbf{E}_0 - j \boldsymbol{\kappa}_1 \phi_0 \right) \tag{2.20c}$$

$$\psi_1^i = \psi_0 \exp\left(-j\boldsymbol{\kappa}_1 \cdot \mathbf{r}\right) \tag{2.20d}$$

$$\mathbf{F}_{1}^{i} = \mathbf{F}_{0} \exp\left(-j\boldsymbol{\kappa}_{1} \cdot \mathbf{r}\right) \tag{2.20e}$$

$$\mathbf{F}_0 = \frac{-1}{j\omega} \left( \mathbf{H}_0 - j\boldsymbol{\kappa}_1 \psi_0 \right). \tag{2.20f}$$

with  $\phi_0$  and  $\psi_0$  being arbitrary constants, have limitations at low frequencies but can be useful for analysis with spherical harmonics as done in Section 3.2.4.2.

# 2.5.2 A $-\phi$ -Decoupled Potential Integral Equation (A $-\phi$ -DPIE)

We use boundary conditions derived from the boundary conditions on fields (1.15), (1.16), (1.17), and (1.18) that decouples **A** from  $\phi$ . We create six "source-like" functions,  $\bar{\mathbf{a}}$ ,  $\bar{\mathbf{b}}$ ,  $\bar{\gamma}$ ,  $\bar{\sigma}$ ,

 $\bar{\alpha}$ , and  $\bar{\beta}$  to use

$$\frac{1}{\mu_{r1}}\hat{\mathbf{n}}_1 \times \hat{\mathbf{n}}_1 \times \nabla \times \mathbf{A}_1^t = \frac{1}{\mu_{r2}}\hat{\mathbf{n}}_2 \times \hat{\mathbf{n}}_2 \times \nabla \times \mathbf{A}_2^t$$
(2.21a)

$$\hat{\mathbf{n}}_1 \times \mathbf{A}_1^t = -\hat{\mathbf{n}}_2 \times \mathbf{A}_2^t \tag{2.21b}$$

$$\frac{1}{\epsilon_{r1}}\hat{\mathbf{n}}_1 \cdot \mathbf{A}_1^t = \frac{-1}{\epsilon_{r2}}\hat{\mathbf{n}}_2 \cdot \mathbf{A}_2^t \tag{2.21c}$$

$$\frac{1}{\mu_{r1}\epsilon_{r1}} \nabla \cdot \mathbf{A}_1^t = \frac{1}{\mu_{r2}\epsilon_{r2}} \nabla \cdot \mathbf{A}_2^t \tag{2.21d}$$

$$\phi_1 = \phi_2 \tag{2.21e}$$

$$\epsilon_{r1}\hat{\mathbf{n}}_1 \cdot \nabla \phi_1 = -\epsilon_{r2}\hat{\mathbf{n}}_2 \cdot \nabla \phi_2 \tag{2.21f}$$

$$\underline{\mathcal{P}}_{1}^{\mathbf{A}-\phi\mathrm{DPIE}}\begin{pmatrix}
\hat{\mathbf{n}}_{1} \times \hat{\mathbf{n}}_{1} \times \nabla \times \mathbf{A}_{1}^{t} \\
\hat{\mathbf{n}}_{1} \times \mathbf{A}_{1}^{t} \\
\hat{\mathbf{n}}_{1} \cdot \mathbf{A}_{1}^{t} \\
\nabla \cdot \mathbf{A}_{1}^{t} \\
\phi_{1} \\
\hat{\mathbf{n}}_{1} \cdot \nabla \phi_{1}
\end{pmatrix} = \underline{\mathcal{P}}_{2}^{\mathbf{A}-\phi\mathrm{DPIE}}\begin{pmatrix}
\hat{\mathbf{n}}_{2} \times \hat{\mathbf{n}}_{2} \times \nabla \times \mathbf{A}_{2}^{t} \\
\hat{\mathbf{n}}_{2} \times \mathbf{A}_{2}^{t} \\
\hat{\mathbf{n}}_{2} \cdot \mathbf{A}_{2}^{t} \\
\nabla \cdot \mathbf{A}_{2}^{t} \\
\phi_{2} \\
\hat{\mathbf{n}}_{2} \cdot \nabla \phi_{2}
\end{pmatrix} = \begin{pmatrix}
\bar{\mathbf{a}} \\
\bar{\mathbf{b}} \\
\bar{\mathbf{b}} \\
\bar{\mathbf{p}} \\
\bar{\sigma} \\
\bar{\sigma} \\
\bar{\beta}
\end{pmatrix} (2.21g)$$

We can define the matrices, operators, and vectors for this formulation as

$$\underline{\mathcal{P}_{p}^{\mathbf{A}-\phi\mathrm{DPIE}}} = \operatorname{diag}\left(\frac{1}{\mu_{rp}}, -j\kappa_{0}\varepsilon_{p}, -j\kappa_{0}\varepsilon_{p}\epsilon_{rp}, \frac{1}{n_{p}^{2}}, \frac{-j\kappa_{0}}{c_{0}}, \frac{\varepsilon_{p}\epsilon_{rp}}{c_{0}}\right)$$
(2.22a)

$$\underline{\mathcal{W}}_{p}^{\mathbf{A}-\phi \mathrm{DPIE}} = \mathrm{diag}\left(\mu_{rp}, \epsilon_{rp}, \frac{1}{\epsilon_{rp}}, \epsilon_{rp}, 1, \frac{1}{\epsilon_{rp}}\right)$$
(2.22b)

$$\mathcal{P}_{p}^{\mathbf{A}-\phi\mathrm{DPIE}} = \operatorname{diag}\left(\frac{1}{\mu_{rp}}, -j\kappa_{0}\varepsilon_{p}, -j\kappa_{0}\varepsilon_{p}\epsilon_{rp}, \frac{1}{n_{p}^{2}}, \frac{j\kappa_{0}}{c_{0}}, \frac{sperp}{c_{0}}\right) \tag{2.22a}$$

$$\mathcal{W}_{p}^{\mathbf{A}-\phi\mathrm{DPIE}} = \operatorname{diag}\left(\mu_{rp}, \epsilon_{rp}, \frac{1}{\epsilon_{rp}}, \epsilon_{rp}, 1, \frac{1}{\epsilon_{rp}}\right) \tag{2.22b}$$

$$\mathcal{Z}_{p}^{\mathbf{A}-\phi\mathrm{DPIE}} = \begin{pmatrix}
\mathcal{I} - \mathcal{K}_{p}^{\prime t} & -\kappa_{p}^{2}\mathcal{L}_{p}^{t} & 0 & \mathcal{Q}_{p}^{(1)} & 0 & 0 \\
\mathcal{J}_{p}^{(2)} & \mathcal{I} - \mathcal{K}_{p} & \mathcal{P}_{p}^{(2)} & \mathcal{Q}_{p}^{(2)} & 0 & 0 \\
\mathcal{J}_{p}^{(3)} & -\mathcal{M}_{p}^{(5)} & \mathcal{I} + \mathcal{D}_{p}^{\prime} & \mathcal{Q}_{p}^{(3)} & 0 & 0 \\
\mathcal{J}_{p}^{(4)} & 0 & -\kappa_{p}^{2}\mathcal{S}_{p} & \mathcal{I} - \mathcal{D}_{p} & 0 & 0 \\
0 & 0 & 0 & \mathcal{I} - \mathcal{D}_{p} & \mathcal{S}_{p} \\
0 & 0 & 0 & -\mathcal{N}_{p} & \mathcal{I} + \mathcal{D}_{p}^{\prime}
\end{pmatrix}$$

$$\mathbf{b}_{p}^{\mathbf{A}-\phi\mathrm{DPIE}} = \begin{pmatrix} \hat{\mathbf{n}}_{p} \times \hat{\mathbf{n}}_{p} \times \nabla \times \mathbf{A}_{p}^{i} \\ \hat{\mathbf{n}}_{p} \times \mathbf{A}_{p}^{i} \\ \hat{\mathbf{n}}_{p} \cdot \mathbf{A}_{p}^{i} \\ \nabla \cdot \mathbf{A}_{p}^{i} \\ \phi_{p}^{i} \\ \hat{\mathbf{n}}_{p} \cdot \nabla \phi_{p}^{i} \end{pmatrix}$$

$$(2.22d)$$

$$\mathbf{x}^{\mathbf{A}-\phi\mathrm{DPIE}} = \begin{pmatrix} \bar{\mathbf{a}} & \bar{\mathbf{b}} & \bar{\gamma} & \bar{\sigma} & \bar{\alpha} & \bar{\beta} \end{pmatrix}^{T}.$$
 (2.22e)

The linear factors of  $\underline{\mathcal{W}}_p$  are chosen such that the DPIE formulation only has one operator whose strong singularity is not canceled.

# $A - \phi$ -Reduced Decoupled Potential Integral Equation $(A - \phi$ -RDPIE)

Alternate formulations are possible due to the Lorenz gauge, which relates two unknowns to each other  $\bar{\sigma} = \bar{\alpha}$ . We can immediately create several Reduced-Decoupled Potential Integral Equation (R-DPIE) formulations with the six equations and five unknowns and show two as examples. The first is created by eliminating  $\bar{\sigma}$ 

$$\underline{\mathcal{P}_{p}^{\mathbf{A}-\phi\text{RDPIE }1}} = \operatorname{diag}\left(\frac{1}{\mu_{rp}}, -j\kappa_{0}\varepsilon_{p}, -j\kappa_{0}\varepsilon_{p}\epsilon_{rp}, \frac{-j\kappa_{0}}{c_{0}}, \frac{\varepsilon_{p}\epsilon_{rp}}{c_{0}}\right)$$
(2.23a)

$$\underline{\mathcal{W}}_{p}^{\mathbf{A}-\phi\text{RDPIE }1} = \operatorname{diag}\left(\mu_{rp}, \epsilon_{rp}, \frac{1}{\epsilon_{rp}}, 1, \frac{1}{\epsilon_{rp}}\right)$$
(2.23b)

$$\mathcal{Z}_{p}^{\mathbf{A}-\phi\text{RDPIE 1}} = \begin{pmatrix}
\mathcal{I} - \mathcal{K}_{p}^{\prime t} & -\kappa_{p}^{2} \mathcal{L}_{p}^{t} & 0 & \frac{\kappa_{p}^{2}}{j\omega} \mathcal{Q}_{p}^{(1)} & 0 \\
\mathcal{J}_{p}^{(2)} & \mathcal{I} - \mathcal{K}_{p} & \mathcal{P}_{p}^{(2)} & \frac{\kappa_{p}^{2}}{j\omega} \mathcal{Q}_{p}^{(2)} & 0 \\
\mathcal{J}_{p}^{(3)} & -\mathcal{M}_{p}^{(5)} & \mathcal{I} + \mathcal{D}_{p}^{\prime} & \frac{\kappa_{p}^{2}}{j\omega} \mathcal{Q}_{p}^{(3)} & 0 \\
0 & 0 & 0 & \mathcal{I} - \mathcal{D}_{p} & \mathcal{S}_{p} \\
0 & 0 & 0 & -\mathcal{N}_{p} & \mathcal{I} + \mathcal{D}_{p}^{\prime}
\end{pmatrix} (2.23c)$$

$$\mathbf{b}_{p}^{\mathbf{A}-\phi\text{RDPIE 1}} = \begin{pmatrix} \hat{\mathbf{n}}_{p} \times \hat{\mathbf{n}}_{p} \times \nabla \times \mathbf{A}_{p}^{i} \\ \hat{\mathbf{n}}_{p} \times \mathbf{A}_{p}^{i} \\ \hat{\mathbf{n}}_{p} \cdot \mathbf{A}_{p}^{i} \\ \phi_{p}^{i} \\ \hat{\mathbf{n}}_{p} \cdot \nabla \phi_{p}^{i} \end{pmatrix}$$
(2.23d)

$$\mathbf{x}^{\mathbf{A}-\phi\text{RDPIE }1} = \begin{pmatrix} \bar{\mathbf{a}} & \bar{\mathbf{b}} & \bar{\gamma} & \bar{\alpha} & \bar{\beta} \end{pmatrix}^{T}.$$
 (2.23e)

The second is create by eliminating  $\bar{\alpha}$ 

$$\mathcal{P}_{p}^{\mathbf{A}-\phi\text{RDPIE }2} = \operatorname{diag}\left(\frac{1}{\mu_{rp}}, -j\kappa_{0}\varepsilon_{p}, -j\kappa_{0}\varepsilon_{p}\epsilon_{rp}, \frac{1}{n_{p}^{2}}, \frac{\varepsilon_{p}\epsilon_{rp}}{c_{0}}\right)$$
(2.24a)

$$\underline{\mathcal{W}}_{p} = \operatorname{diag}\left(\mu_{rp}, \epsilon_{rp}, \frac{1}{\epsilon_{rp}}, \epsilon_{rp}, \frac{1}{\epsilon_{rp}}\right) \tag{2.24b}$$

$$\mathcal{Z}_{p}^{\mathbf{A}-\phi\text{RDPIE 2}} = \begin{pmatrix}
\mathcal{I} - \mathcal{K}_{p}^{\prime t} & -\kappa_{p}^{2} \mathcal{L}_{p}^{t} & 0 & \mathcal{Q}_{p}^{(1)} & 0 \\
\mathcal{J}_{p}^{(2)} & \mathcal{I} - \mathcal{K}_{p} & \mathcal{P}_{p}^{(2)} & \mathcal{Q}_{p}^{(2)} & 0 \\
\mathcal{J}_{p}^{(3)} & -\mathcal{M}_{p}^{(5)} & \mathcal{I} + \mathcal{D}_{p}^{\prime} & \mathcal{Q}_{p}^{(3)} & 0 \\
\mathcal{J}_{p}^{(4)} & 0 & -\kappa_{p}^{2} \mathcal{S}_{p} & \mathcal{I} - \mathcal{D}_{p} & 0 \\
0 & 0 & 0 & \frac{-j\omega}{\kappa_{p}^{2}} \mathcal{N}_{p} & \mathcal{I} + \mathcal{D}_{p}^{\prime}
\end{pmatrix} \tag{2.24c}$$

$$\mathbf{b}^{\mathbf{A}-\phi\text{RDPIE 2}} = \begin{pmatrix} \hat{\mathbf{n}}_p \times \hat{\mathbf{n}}_p \times \nabla \times \mathbf{A}_p^i \\ \hat{\mathbf{n}}_p \times \mathbf{A}_p^i \\ \hat{\mathbf{n}}_p \cdot \mathbf{A}_p^i \\ \nabla \cdot \mathbf{A}_p^i \\ \hat{\mathbf{n}}_p \cdot \nabla \phi_p^i \end{pmatrix}$$
(2.24d)

$$\mathbf{x}^{\mathbf{A}-\phi \text{RDPIE } 2} = \begin{pmatrix} \bar{\mathbf{a}} & \bar{\mathbf{b}} & \bar{\gamma} & \bar{\sigma} & \bar{\beta} \end{pmatrix}^{T}.$$
 (2.24e)

Additional  $\mathbf{A} - \phi$ -RDPIEs not shown here result from scaling and combining the fourth and fifth rows of the  $\mathbf{A} - \phi$ -DPIE after combining the fourth and fifth unknown functions.

# 2.5.4 F $-\psi$ -Decoupled Potential Integral Equation (F $-\psi$ -DPIE)

We can make use of the duality between the  $\mathbf{F} - \psi$ -DPIE and  $\mathbf{A} - \phi$ -DPIE formulations by replacing  $\mathbf{A}$  with  $\mathbf{F}$ ,  $\phi$  with  $\psi$ ,  $\mu$  with  $\epsilon$ , and  $\epsilon$  with  $\mu$  and arrive at the formulation.

Boundary conditions are expressed as

$$\underline{\mathcal{P}}_{1}^{\mathbf{F}-\psi \mathrm{DPIE}}\begin{pmatrix} \hat{\mathbf{n}}_{1} \times \hat{\mathbf{n}}_{1} \times \nabla \times \mathbf{F}_{1}^{t} \\ \hat{\mathbf{n}}_{1} \times \mathbf{F}_{1}^{t} \\ \hat{\mathbf{n}}_{1} \cdot \mathbf{F}_{1}^{t} \\ \nabla \cdot \mathbf{F}_{1}^{t} \\ \psi_{1} \\ \hat{\mathbf{n}}_{1} \cdot \nabla \psi_{1} \end{pmatrix} = \underline{\mathcal{P}}_{2}^{\mathbf{F}-\psi \mathrm{DPIE}}\begin{pmatrix} \hat{\mathbf{n}}_{2} \times \hat{\mathbf{n}}_{2} \times \nabla \times \mathbf{F}_{2}^{t} \\ \hat{\mathbf{n}}_{2} \times \mathbf{F}_{2}^{t} \\ \hat{\mathbf{n}}_{2} \cdot \mathbf{F}_{2}^{t} \\ \nabla \cdot \mathbf{F}_{2}^{t} \\ \psi_{2} \\ \hat{\mathbf{n}}_{2} \cdot \nabla \psi_{2} \end{pmatrix} = \begin{pmatrix} \bar{\mathbf{a}} \\ \bar{\mathbf{b}} \\ \bar{\mathbf{p}} \\ \bar{\sigma} \\ \bar{\sigma} \\ \bar{\beta} \end{pmatrix} (2.25a)$$

and the remaining matrices, operators, and vectors are

$$\underline{\mathcal{P}_{p}^{\mathbf{F}-\psi\text{DPIE}}} = \operatorname{diag}\left(\frac{1}{\epsilon_{rp}}, -j\kappa_{0}\varepsilon_{p}, -j\kappa_{0}\varepsilon_{p}\mu_{rp}, \frac{1}{n_{p}^{2}}, \frac{-j\kappa_{0}}{c_{0}}, \frac{\varepsilon_{p}\mu_{rp}}{c_{0}}\right)$$
(2.25b)

$$\underline{\mathcal{W}}_{p}^{\mathbf{F}-\psi \text{DPIE}} = \text{diag}\left(\epsilon_{rp}, \mu_{rp}, \frac{1}{\mu_{rp}}, \mu_{rp}, 1, \frac{1}{\mu_{rp}}\right)$$
(2.25c)

$$\mathcal{Z}_{p}^{\mathbf{F}-\psi\text{DPIE}} = \begin{pmatrix}
\mathcal{I} - \mathcal{K}_{p}^{\prime t} & -\kappa_{p}^{2} \mathcal{L}_{p}^{t} & 0 & \mathcal{Q}_{p}^{(1)} & 0 & 0 \\
\mathcal{J}_{p}^{(2)} & \mathcal{I} - \mathcal{K}_{p} & \mathcal{P}_{p}^{(2)} & \mathcal{Q}_{p}^{(2)} & 0 & 0 \\
\mathcal{J}_{p}^{(3)} & -\mathcal{M}_{p}^{(5)} & \mathcal{I} + \mathcal{D}_{p}^{\prime} & \mathcal{Q}_{p}^{(3)} & 0 & 0 \\
\mathcal{J}_{p}^{(4)} & 0 & -\kappa_{p}^{2} \mathcal{S}_{p} & \mathcal{I} - \mathcal{D}_{p} & 0 & 0 \\
0 & 0 & 0 & \mathcal{I} - \mathcal{D}_{p} & \mathcal{S}_{p} \\
0 & 0 & 0 & -\mathcal{N}_{p} & \mathcal{I} + \mathcal{D}_{p}^{\prime}
\end{pmatrix} \tag{2.25d}$$

$$\mathbf{b}_{p}^{\mathbf{F}-\psi \mathrm{DPIE}} = \begin{pmatrix} \hat{\mathbf{n}}_{p} \times \hat{\mathbf{n}}_{p} \times \nabla \times \mathbf{F}_{p}^{i} \\ \hat{\mathbf{n}}_{p} \times \mathbf{F}_{p}^{i} \\ \hat{\mathbf{n}}_{p} \cdot \mathbf{F}_{p}^{i} \\ \nabla \cdot \mathbf{F}_{p}^{i} \\ \psi_{p}^{i} \\ \hat{\mathbf{n}}_{p} \cdot \nabla \psi_{p}^{i} \end{pmatrix}$$

$$(2.25e)$$

$$\mathbf{x}^{\mathbf{F}-\psi \text{DPIE}} = \begin{pmatrix} \bar{\mathbf{a}} & \bar{\mathbf{b}} & \bar{\gamma} & \bar{\sigma} & \bar{\alpha} & \bar{\beta} \end{pmatrix}^{T}.$$
 (2.25f)

### 2.5.5 F $-\psi$ -Reduced Decoupled Potential Integral Equation (F $-\psi$ -RDPIE)

The same observation for the  $\mathbf{A} - \phi$ -RDPIE is applicable for the  $\mathbf{F} - \psi$ -RDPIE, and alternate formulations are possible due to the Lorenz gauge because  $\bar{\sigma} = \bar{\alpha}$ . The first of the two examples are created by eliminating  $\bar{\sigma}$ 

$$\underline{\mathcal{P}_{p}^{\mathbf{F}-\psi \text{RDPIE 1}}} = \operatorname{diag}\left(\frac{1}{\epsilon_{rp}}, -j\kappa_{0}\varepsilon_{p}, -j\kappa_{0}\varepsilon_{p}\mu_{rp}, \frac{-j\kappa_{0}}{c_{0}}, \frac{\varepsilon_{p}\mu_{rp}}{c_{0}}\right)$$
(2.26a)

$$\underline{\mathcal{W}}_{p}^{\mathbf{F}-\psi \text{RDPIE } 1} = \operatorname{diag}\left(\epsilon_{rp}, \mu_{rp}, \frac{1}{\mu_{rp}}, 1, \frac{1}{\mu_{rp}}\right)$$
(2.26b)

$$\mathcal{Z}_{p}^{\mathbf{F}-\psi \text{RDPIE 1}} = \begin{pmatrix}
\mathcal{I} - \mathcal{K}_{p}^{\prime t} & -\kappa_{p}^{2} \mathcal{L}_{p}^{t} & 0 & \frac{\kappa_{p}^{2}}{j\omega} \mathcal{Q}_{p}^{(1)} & 0 \\
\mathcal{J}_{p}^{(2)} & \mathcal{I} - \mathcal{K}_{p} & \mathcal{P}_{p}^{(2)} & \frac{\kappa_{p}^{2}}{j\omega} \mathcal{Q}_{p}^{(2)} & 0 \\
\mathcal{J}_{p}^{(3)} & -\mathcal{M}_{p}^{(5)} & \mathcal{I} + \mathcal{D}_{p}^{\prime} & \frac{\kappa_{p}^{2}}{j\omega} \mathcal{Q}_{p}^{(3)} & 0 \\
0 & 0 & \mathcal{I} - \mathcal{D}_{p} & \mathcal{S}_{p} \\
0 & 0 & 0 & -\mathcal{N}_{p} & \mathcal{I} + \mathcal{D}_{p}^{\prime}
\end{pmatrix} (2.26c)$$

$$\mathbf{b}_{p}^{\mathbf{F}-\psi \text{RDPIE 1}} = \begin{pmatrix} \hat{\mathbf{n}}_{p} \times \hat{\mathbf{n}}_{p} \times \nabla \times \mathbf{F}_{p}^{i} \\ \hat{\mathbf{n}}_{p} \times \mathbf{F}_{p}^{i} \\ \hat{\mathbf{n}}_{p} \cdot \mathbf{F}_{p}^{i} \\ \psi_{p}^{i} \\ \hat{\mathbf{n}}_{p} \cdot \nabla \psi_{p}^{i} \end{pmatrix}$$
(2.26d)

$$\mathbf{x}^{\mathbf{F}-\psi\text{RDPIE 1}} = \begin{pmatrix} \bar{\mathbf{a}} & \bar{\mathbf{b}} & \bar{\gamma} & \bar{\alpha} & \bar{\beta} \end{pmatrix}^{T}.$$
 (2.26e)

The second is create by eliminating  $\bar{\alpha}$ 

$$\underline{\mathcal{P}_{p}^{\mathbf{F}-\psi \text{RDPIE 2}}} = \operatorname{diag}\left(\frac{1}{\epsilon_{rp}}, -j\kappa_{0}\varepsilon_{p}, -j\kappa_{0}\varepsilon_{p}\mu_{rp}, \frac{1}{n_{p}^{2}}, \frac{\varepsilon_{p}\mu_{rp}}{c_{0}}\right)$$
(2.27a)

$$\underline{\mathcal{W}}_{p} = \operatorname{diag}\left(\epsilon_{rp}, \mu_{rp}, \frac{1}{\mu_{rp}}, \mu_{rp}, \frac{1}{\mu_{rp}}\right) \tag{2.27b}$$

$$\mathcal{Z}_{p}^{\mathbf{F}-\psi\text{RDPIE 2}} = \begin{pmatrix}
\mathcal{I} - \mathcal{K}_{p}^{\prime t} & -\kappa_{p}^{2} \mathcal{L}_{p}^{t} & 0 & \mathcal{Q}_{p}^{(1)} & 0 \\
\mathcal{J}_{p}^{(2)} & \mathcal{I} - \mathcal{K}_{p} & \mathcal{P}_{p}^{(2)} & \mathcal{Q}_{p}^{(2)} & 0 \\
\mathcal{J}_{p}^{(3)} & -\mathcal{M}_{p}^{(5)} & \mathcal{I} + \mathcal{D}_{p}^{\prime} & \mathcal{Q}_{p}^{(3)} & 0 \\
\mathcal{J}_{p}^{(4)} & 0 & -\kappa_{p}^{2} \mathcal{S}_{p} & \mathcal{I} - \mathcal{D}_{p} & 0 \\
0 & 0 & 0 & \frac{-j\omega}{\kappa_{p}^{2}} \mathcal{N}_{p} & \mathcal{I} + \mathcal{D}_{p}^{\prime}
\end{pmatrix} \tag{2.27c}$$

$$\mathbf{b}^{\mathbf{F}-\psi\text{RDPIE 2}} = \begin{pmatrix} \hat{\mathbf{n}}_{p} \times \hat{\mathbf{n}}_{p} \times \nabla \times \mathbf{F}_{p}^{i} \\ \hat{\mathbf{n}}_{p} \times \mathbf{F}_{p}^{i} \\ \hat{\mathbf{n}}_{p} \cdot \mathbf{F}_{p}^{i} \\ \nabla \cdot \mathbf{F}_{p}^{i} \\ \hat{\mathbf{n}}_{p} \cdot \nabla \psi_{p}^{i} \end{pmatrix}$$

$$(2.27d)$$

$$\mathbf{x}^{\mathbf{F}-\psi \text{RDPIE 2}} = \begin{pmatrix} \bar{\mathbf{a}} & \bar{\mathbf{b}} & \bar{\gamma} & \bar{\sigma} & \bar{\beta} \end{pmatrix}^{T}.$$
 (2.27e)

Again, combining the fourth and fifth rows of  $\mathbf{F} - \psi$ -DPIE, we can create further  $\mathbf{F} - \psi$ -RDPIEs formulations.

## 2.6 LC-CFIE

Thus far, the new formulations have been for dielectric objects. Indeed, my research goal was to advance dielectric formulations, and a subtle observation led to a new preconditioned formulation for PEC objects.

The system matrices that we have been working with are all Calderón type projectors. Specifically, we can view the system matrices  $\mathcal{Z}_p$  of some of the dielectric formulations (Müller (2.7c), DFIE (2.12c) (2.14d), DPIE (2.22c) (2.25d)) as projecting the traces of total fields or potentials on the surface to the incident traces on the surface. The complementary projector  $\mathcal{I} - \mathcal{Z}_p$  projects the traces of the total fields or potentials on the surface to the scattered

traces on the surface. From the perspective of projectors, it is obvious that the result of applying a projector and its complementary projector will be a block null operator matrix.

$$\mathcal{Z}_p \circ (\mathcal{I} - \mathcal{Z}_p) = 0. \tag{2.28}$$

Each entry in the operator matrix above will be the null operator, and Calderón type identities can be derived. One of these Calderón identities that results from using any of the new  $\mathcal{Z}_p^{\chi}$  in this chapter can be used to precondition the EFIE formulation

$$\mathcal{J}_p^{(2)} \circ \left(\kappa_p^2 \mathcal{L}_p\right) = \mathcal{K}_p \circ \left(\mathcal{I} - \mathcal{K}_p\right) - \mathcal{P}_p^{(2)} \circ \mathcal{M}_p^{(3)}. \tag{2.29}$$

With this identity, we can arrive at a Calderón preconditioned EFIE formulation

$$\mathcal{J}_1^{(2)} \circ \left( -j\kappa_1 \hat{\mathbf{n}}_1 \times \hat{\mathbf{n}}_1 \times \mathbf{E}_1^i \right) = \mathcal{J}_1^{(2)} \circ \left( \kappa_1^2 \eta_1 \mathcal{L}_1^t \circ \mathbf{J}_s \right). \tag{2.30}$$

This formulation can be combined with the MFIE to create a CFIE formulation.

$$\begin{pmatrix} \frac{\alpha}{\eta_0} & 1 \end{pmatrix} \begin{pmatrix} \mathcal{J}_1^{(2)} \circ \left( -j\kappa_1 \hat{\mathbf{n}}_1 \times \hat{\mathbf{n}}_1 \times \mathbf{E}_1^i \right) \\ \hat{\mathbf{n}}_1 \times \mathbf{H}_1^i \end{pmatrix} = \begin{pmatrix} \frac{\alpha}{\eta_0} & 1 \end{pmatrix} \begin{pmatrix} \mathcal{J}_1^{(2)} \circ \left(\kappa_1^2 \eta_1 \mathcal{L}_1^t\right) \\ \mathcal{I} - \mathcal{K}_1 \end{pmatrix} \circ \mathbf{J}_s. \tag{2.31}$$

This formulation has a null space because the MFIE and this Calderón EFIE share a null space. Fortunately, the stabilizing properties of  $\mathcal{J}_p^{(2)}$  are local, and we can use a lossy  $\tilde{\kappa}_1$  which not only shifts the null space but also improves high-frequency stability

$$\tilde{\mathcal{J}}_{p}^{(2)} \circ \mathbf{x} = \hat{\mathbf{n}}_{p} \times \tilde{\mathcal{S}}_{p} \circ (\hat{\mathbf{n}} \times \mathbf{x})$$
(2.32a)

$$\tilde{\mathcal{S}}_{p} \circ \mathbf{x} = \int \tilde{G}_{p}(\mathbf{r}, \mathbf{r}') \mathbf{x}(\mathbf{r}') dS'$$
 (2.32b)

$$\tilde{G}_p(\mathbf{r}, \mathbf{r}') = \frac{\exp(-j\tilde{\kappa}_p |\mathbf{r} - \mathbf{r}'|)}{4\pi |\mathbf{r} - \mathbf{r}'|}.$$
(2.32c)

arriving at

$$\begin{pmatrix} \frac{\alpha}{\eta_0} & 1 \end{pmatrix} \begin{pmatrix} \tilde{\mathcal{J}}_1^{(2)} \circ \left( -j\kappa_1 \hat{\mathbf{n}}_1 \times \hat{\mathbf{n}}_1 \times \mathbf{E}_1^i \right) \\ \hat{\mathbf{n}}_1 \times \mathbf{H}_1^i \end{pmatrix} = \begin{pmatrix} \frac{\alpha}{\eta_0} & 1 \end{pmatrix} \begin{pmatrix} \tilde{\mathcal{J}}_1^{(2)} \circ \left(\kappa_1^2 \eta_1 \mathcal{L}_1^t \right) \\ \mathcal{I} - \mathcal{K}_1 \end{pmatrix} \circ \mathbf{J}_s \qquad (2.32d)$$

which is unique and stable across a broad range of frequencies with the proper choice of  $\tilde{\kappa} = \kappa - j0.4H^{2/3}\kappa^{1/3}$  [Antoine et al., 2006] with H being the max mean curvature of the object.

Writing this in the common formulation framework results in

$$\underline{\mathcal{P}}_{1}^{\text{LC-CFIE}} = \begin{pmatrix} 1 & 1 \end{pmatrix} \tag{2.33a}$$

$$\underline{\mathcal{W}}_1 = \begin{pmatrix} \frac{\alpha}{\eta_0} & 1 \end{pmatrix} \tag{2.33b}$$

$$\mathcal{Z}_{1}^{\text{LC-CFIE}} = \operatorname{diag}\left(\tilde{\mathcal{J}}_{1}^{(2)} \circ \left(\kappa_{1}^{2} \eta_{1} \mathcal{L}_{1}^{t}\right), \mathcal{I} - \mathcal{K}_{1}\right)$$
(2.33c)

$$\mathbf{b}_{1}^{\text{LC-CFIE}} = \begin{pmatrix} \tilde{\mathcal{J}}_{1}^{(2)} \circ \left( -j\kappa_{1}\hat{\mathbf{n}}_{1} \times \hat{\mathbf{n}}_{1} \times \mathbf{E}_{1}^{i} \right) \\ \hat{\mathbf{n}}_{1} \times \mathbf{H}_{1}^{i} \end{pmatrix}$$
(2.33d)

$$\mathbf{x}^{\text{LC-CFIE}} = \mathbf{J}_s. \tag{2.33e}$$

# 2.7 Conclusion

The several formulations presented in this chapter cover most used in CEM. The direct method framework developed here is general and applicable to most formulations. The following chapter will build on this framework by discretizing these formulations.

#### CHAPTER 3

#### DISCRETIZATION

## 3.1 Introduction

The integral equations presented thus far are agnostic to the basis functions used to discretize these systems. For the formulations in Chapter 1, only vector unknowns need to be represented, but in formulations presented in Chapter 2, both vector and scalar unknowns are needed. We introduce some additional notation for ease of presentation (and implementation). Let the space of scalar basis functions be denoted using  $\underline{\mathcal{B}}_n^s$ , for  $n \in [1, N_s]$ . Likewise, the space of vector basis functions is denoted using  $\underline{\mathcal{B}}_n^s$ , for  $n \in [1, N_v]$ . In the above, we note that  $N_s$  and  $N_v$  are the number of scalar and vector basis functions. For the single, closed object scatterer, the number of degrees of freedom will be the  $N_b = n_s N_s + n_v N_v$  where  $n_s$  and  $n_v$  are the numbers of scalar and vector unknown source functions respectively. It follows that one can represent the collection of basis functions needed to represent all of the unknowns using  $\underline{\mathcal{F}}_{\chi} = \operatorname{diag}(\underline{\mathcal{B}}^s, \dots, \underline{\mathcal{B}}^v, \dots)$ , where "diag" here is used to mean a block-diagonal matrix and a  $\underline{\mathcal{B}}^s$  for each of the  $n_s$  scalar unknown functions and a  $\underline{\mathcal{B}}^v$  for each of the  $n_v$  vector unknown functions.

The discretized system for all formulations in this thesis is constructed through a Galerkin framework using inner products defined as

$$\langle g, f \rangle = \int g^*(\mathbf{r}) f(\mathbf{r}) dS$$
 (3.1a)

$$\langle \mathbf{g}, \mathbf{f} \rangle = \int \mathbf{g}^* (\mathbf{r}) \cdot \mathbf{f} (\mathbf{r}) dS$$
 (3.1b)

with \* indicating complex conjugate and g, f,  $\mathbf{g}$ , and  $\mathbf{f}$  denoting arbitrary scalar and vector functions of  $\mathbf{r}$ . For each region, we test (2.1b) over the limiting surface as  $\mathbf{r}$  approaches the interface from within  $\Omega_p$  and add the systems together, resulting in a single system, coupled through the boundary conditions, that can be written as

$$\mathbb{Z}^{\chi} y = b^{\chi} \tag{3.2a}$$

where the elements of this system are defined as

$$b_k^{\chi} = \left\langle \underline{\mathcal{F}}_k^{\chi}, \sum_{p=1}^{N_p} \underline{\mathcal{P}}_p^{\chi} \underline{\mathcal{W}}_p^{\chi} \mathbf{b}_p^{\chi} \right\rangle$$
 (3.2b)

$$\mathbb{Z}_{kn}^{\chi} = \left\langle \underline{\mathcal{F}}_{k}^{\chi}, \left( \sum_{p=1}^{N_{p}} \underline{\mathcal{P}}_{p}^{\chi} \underline{\mathcal{W}}_{p}^{\chi} \mathcal{Z}_{p}^{\chi} \left( \underline{\mathcal{P}}_{p}^{\chi} \right)^{-1} \right) \circ \underline{\mathcal{F}}_{n}^{\chi} \right\rangle. \tag{3.2c}$$

As the boundary conditions and scale factors manifest themselves as diagonal matrices, it is trivial to show that

$$b^{\chi} = \sum_{p=1}^{2} \underline{\bar{\mathcal{P}}}_{p}^{\chi} \underline{\bar{\mathcal{W}}}_{p}^{\chi} \left\langle \underline{\mathcal{F}}_{p}^{\chi}, \mathbf{b}_{p}^{\chi} \right\rangle \tag{3.3a}$$

$$\mathbb{Z}^{\chi} = \sum_{p=1}^{2} \underline{\bar{\mathcal{P}}}_{p}^{\chi} \underline{\bar{\mathcal{W}}}_{p}^{\chi} \left\langle \underline{\bar{\mathcal{F}}}_{p}^{\chi}, \mathcal{Z}_{p}^{\chi} \circ \underline{\bar{\mathcal{F}}}_{p}^{\chi} \right\rangle \left(\underline{\bar{\mathcal{P}}}_{p}^{\chi}\right)^{-1}$$
(3.3b)

where for the two region case  $\underline{\bar{\mathcal{W}}}_p^{\chi}$  and  $\underline{\bar{\mathcal{P}}}_p^{\chi}$  are built with either  $N_s$  or  $N_v$  repeated elements and  $\underline{\bar{\mathcal{F}}}_p^{\chi}$  is used to represent an individual region's unknown source and "source-like" functions. Effectively, with  $\underline{\bar{\mathcal{F}}}_p^{\chi}$  we test and measure each region individually and with  $\underline{\bar{\mathcal{W}}}_p^{\chi}$  and  $\underline{\bar{\mathcal{P}}}_p^{\chi}$  we scale and combine inner-products and enforce boundary conditions and scaling for the unknown source and "source-like" functions on their coefficients. As an aside for composite objects, there is an added step of selecting elements and functions only related to the particular region but conceptually the same.

All that is now required is to select the basis sets for  $\underline{\mathcal{B}}^s$  and  $\underline{\mathcal{B}}^v$ , which will be covered in the remainder of this chapter. For analytic analysis on a sphere, we will use spherical harmonics in Section 3.2. For numerical analysis on arbitrarily shaped tessellated objects, we will use piecewise RWG functions in Section 3.3.

## 3.2 Analytic Analysis

The functions used to extract characteristics for all formulations will be vector and scalar spherical harmonics basis and testing functions. These functions will represent the source and "source-like" unknowns and test the integral equations on the surface of a spherical scatterer with radius a. Because of the spherical harmonic expansion of Green's function and orthogonality properties of the spherical harmonics, we can compute all of the integrals

analytically. This is as in [Li et al., 2019, Yuan and Shanker, 2005, Hsiao and Kleinman, 1997].

We will use spherical harmonic indices l and m and understand that special care must be taken when l = 0 so that normalization terms do not introduce any division by 0. For simplicity of presentation, we will ignore this detail and set a = 1 m.

# 3.2.1 Scalar Spherical Harmonics for $\mathcal{B}^s$

To construct a basis for the space of scalar functions on the surface of a sphere, we utilize the orthonormalized spherical harmonics defined as

$$Y_l^m(\hat{\mathbf{r}}) = \sqrt{\frac{2l+1}{4\pi} \frac{(l-m)!}{(l+m)!}} P_l^m(\cos\theta) \exp(jm\phi)$$
(3.4a)

with  $P_l^m(\cos\theta)$  denoting associated Legendre polynomials,  $l \geq 0$ , and  $|m| \leq l$ .

With these basis functions, we can define  $\underline{\mathcal{B}}^s$  as

$$\underline{\mathcal{B}}^s = \left( Y_0^0 \dots Y_l^m \dots Y_{N_h}^{N_h} \right) \tag{3.4b}$$

with  $N_h$  being the highest order of harmonic examined and  $N_s = (N_h + 1)^2$ . For the remainder of this chapter,  $l = N_h = 2 \lceil \max_p \Re(\kappa_p a) \rceil + 2$  where  $\Re(\kappa_p a)$  takes the real component of  $\kappa_p a$  and  $\max_p$  takes the max over the single exterior region for the PEC case or the two regions for the dielectric case.

## 3.2.2 Vector Spherical Harmonics for $\mathcal{B}^v$

For the space of vector functions, we utilize orthonormalized vector spherical harmonics defined with respect to the scalar spherical harmonics

$$\mathbf{Y}_{l}^{m}\left(\hat{\mathbf{r}}\right) = \hat{\mathbf{r}} \mathbf{Y}_{l}^{m}\left(\theta,\phi\right) \tag{3.5a}$$

$$\mathbf{\Psi}_{l}^{m}\left(\hat{\mathbf{r}}\right) = -\hat{\mathbf{r}} \times \mathbf{\Phi}_{l}^{m}\left(\hat{\mathbf{r}}\right) = \frac{r\nabla Y_{l}^{m}\left(\hat{\mathbf{r}}\right)}{\sqrt{l\left(l+1\right)}}$$
(3.5b)

$$\mathbf{\Phi}_{l}^{m}(\hat{\mathbf{r}}) = \hat{\mathbf{r}} \times \mathbf{\Psi}_{l}^{m}(\hat{\mathbf{r}}) = \frac{\mathbf{r} \times \nabla Y_{l}^{m}(\hat{\mathbf{r}})}{\sqrt{l(l+1)}}$$
(3.5c)

The space of functions we want to represent is tangential to the surface. Because of this, we only require  $\Psi$  and  $\Phi$  type functions to represent them. With these basis functions, we can

define  $\underline{\mathcal{B}}^v$  as

$$\underline{\mathcal{B}}^{\Psi} = \begin{pmatrix} \Psi_0^0 & \dots & \Psi_l^m & \dots & \Psi_{N_h}^{N_h} \end{pmatrix}$$
 (3.6a)

$$\underline{\mathcal{B}}^{\Psi} = \begin{pmatrix} \mathbf{\Phi}_0^0 & \dots & \mathbf{\Phi}_l^m & \dots & \mathbf{\Phi}_{N_h}^{N_h} \end{pmatrix}$$
 (3.6b)

$$\underline{\mathcal{B}}^{v} = \left(\underline{\mathcal{B}}^{\Psi} \quad \underline{\mathcal{B}}^{\Phi}\right). \tag{3.6c}$$

with  $N_v = 2(N_h + 1)^2$ .

# 3.2.3 Zero-Mean Constraint

It is important to note that for some unknown functions, there are additional constraints. For example, when representing  $\gamma_p = \hat{\mathbf{n}}_p \cdot \mathbf{E}_p^t$  on the surface of a closed region p, it must satisfy a zero-mean constraint

$$\int \gamma_p(\mathbf{r}) \, dS = 0. \tag{3.7}$$

When using spherical harmonics to represent these unknowns, this can be performed by zeroing the coefficient associated with l=m=0.

# 3.2.4 Analytic Integration

Evaluation of all of the operators in the formulations in Chapter 2 can be performed exactly with the spherical harmonic basis sets by exploiting their orthogonality properties. Rather than stepping through each operator individually, the necessary tools will be given to perform all of the integrals, and only a single operator will be shown in complete detail. At the end of this section, all operators will be listed for completeness.

## 3.2.4.1 Additional Spherical Functions

Spherical Bessel functions are denoted using

$$\mathbf{b}_{l}^{(\alpha)}(z) = \begin{cases} \mathbf{j}_{l}(z) & \alpha = 1\\ \mathbf{y}_{l}(z) & \alpha = 2\\ \mathbf{h}_{l}^{(1)}(z) & \alpha = 3\\ \mathbf{h}_{l}^{(2)}(z) & \alpha = 4 \end{cases}$$

$$(3.8)$$

where the index  $\alpha$  is used to denote the kind of spherical Bessel function.

Using spherical Bessel and harmonic functions, the scalar and vector spherical wave functions that satisfy the wave equation are

$$\varphi_{lm}^{(\alpha)}(\kappa, \mathbf{r}) = \mathbf{b}_{l}^{(\alpha)}(\kappa r) \frac{\mathbf{Y}_{l}^{m}(\hat{\mathbf{r}})}{\sqrt{l(l+1)}}$$
(3.9a)

$$\mathbf{L}_{lm}^{(\alpha)}(\kappa, \mathbf{r}) = \nabla \varphi_{lm}^{(\alpha)}(\kappa, \mathbf{r}) \tag{3.9b}$$

$$\mathbf{M}_{lm}^{(\alpha)}(\kappa, \mathbf{r}) = \frac{1}{\kappa} \nabla \times \mathbf{N}_{lm}^{(\alpha)}(\kappa, \mathbf{r}) = -\mathbf{r} \times \nabla \varphi_{lm}^{(\alpha)}(\kappa, \mathbf{r})$$
(3.9c)

$$\mathbf{N}_{lm}^{(\alpha)}(\kappa, \mathbf{r}) = \frac{1}{\kappa} \nabla \times \mathbf{M}_{lm}^{(\alpha)}(\kappa, \mathbf{r})$$
(3.9d)

Note, in typical CEM spherical harmonic analysis, **E** and **H** are represented with  $\mathbf{M}_{lm}^{(\alpha)}$  and  $\mathbf{N}_{lm}^{(\alpha)}$  only and  $\mathbf{L}_{lm}^{(\alpha)}$  is not required because the fields do not radiate radially. However, that is not the case for representing the vector potentials **A** and **F** [Stratton, 2015].

# 3.2.4.2 Plane Wave Expansion

For completeness, we include plane wave expansion in terms of spherical wave functions. For  $\hat{\boldsymbol{\kappa}} = \hat{\mathbf{z}}$ ,  $\mathbf{E}_0 = \hat{\mathbf{x}}$  and  $\phi_0 = 1$ , we have  $\phi_1^i$ ,  $\mathbf{E}_1^i$ , and  $\mathbf{A}^i$ 

$$\phi_1^i(\mathbf{r}) = \exp\left(-j\kappa_1 \hat{\mathbf{z}} \cdot \mathbf{r}\right) = \sum_{l=0}^{\infty} \sum_{m=-l}^{l} a_{lm} \,\varphi_{lm}^{(1)}\left(\kappa_1, \mathbf{r}\right) \tag{3.10a}$$

$$\mathbf{E}_{1}^{i}\left(\mathbf{r}\right) = \hat{\mathbf{x}} \exp\left(-j\kappa_{1}\hat{\mathbf{z}} \cdot \mathbf{r}\right) = \sum_{l=0}^{\infty} \sum_{m=-l}^{l} b_{lm} \mathbf{M}_{lm}^{(1)}\left(\kappa_{1}, \mathbf{r}\right) + c_{lm} \mathbf{N}_{lm}^{(1)}\left(\kappa_{1}, \mathbf{r}\right)$$
(3.10b)

$$\mathbf{A}_{1}^{i}\left(\mathbf{r}\right) = \frac{-1}{i\omega} \left(\mathbf{E}_{1}^{i} + \nabla \phi_{1}^{i}\right) \tag{3.10c}$$

$$= \frac{-1}{j\omega} \sum_{l=0}^{\infty} \sum_{m=-l}^{l} a_{lm} \mathbf{L}_{lm}^{(1)}(\kappa_{1}, \mathbf{r}) + b_{lm} \mathbf{M}_{lm}^{(1)}(\kappa_{1}, \mathbf{r}) + c_{lm} \mathbf{N}_{lm}^{(1)}(\kappa_{1}, \mathbf{r}).$$
(3.10d)

For  $\hat{\mathbf{k}} = \hat{\mathbf{z}}$ ,  $\mathbf{H}_0 = \frac{1}{\eta_1} \hat{\mathbf{y}}$  and  $\psi_0 = \frac{j}{\eta_1}$ , we have  $\psi_1^i$ ,  $\mathbf{H}_1^i$ , and  $\mathbf{F}_1^i$ 

$$\psi_1^i(\mathbf{r}) = \frac{j}{\eta_1} \exp\left(-j\kappa_1 \hat{\mathbf{z}} \cdot \mathbf{r}\right) = \frac{j}{\eta_1} \sum_{l=0}^{\infty} \sum_{m=-l}^{l} a_{lm} \,\varphi_{lm}^{(1)}\left(\kappa_1, \mathbf{r}\right) \tag{3.10e}$$

$$\mathbf{H}_{1}^{i}(\mathbf{r}) = \frac{1}{\eta_{1}} \hat{\mathbf{y}} \exp\left(-j\kappa_{1}\hat{\mathbf{z}} \cdot \mathbf{r}\right)$$
(3.10f)

$$= \frac{j}{\eta_1} \sum_{l=0}^{\infty} \sum_{m=-l}^{l} c_{lm} \mathbf{M}_{lm}^{(1)}(\kappa_1, \mathbf{r}) + b_{lm} \mathbf{N}_{lm}^{(1)}(\kappa_1, \mathbf{r})$$
(3.10g)

$$\mathbf{F}_{1}^{i}\left(\mathbf{r}\right) = \frac{-1}{j\omega} \left(\mathbf{H}_{1}^{i} + \nabla \psi_{1}^{i}\right) \tag{3.10h}$$

$$= \frac{-1}{\omega \eta_1} \sum_{l=0}^{\infty} \sum_{m=-l}^{l} a_{lm} \mathbf{L}_{lm}^{(1)}(\kappa_1, \mathbf{r}) + c_{lm} \mathbf{M}_{lm}^{(1)}(\kappa_1, \mathbf{r}) + b_{lm} \mathbf{N}_{lm}^{(1)}(\kappa_1, \mathbf{r}).$$
(3.10i)

Defining in this way allows the coefficients  $a_{lm}$ ,  $b_{lm}$ , and  $c_{lm}$  to be shared

$$a_{lm} = \begin{cases} j^{-l} \sqrt{\frac{4\pi(2l+1)}{l(l+1)}} & m = 0\\ 0 & m \neq 0 \end{cases}$$
(3.11a)

$$b_{lm} = \begin{cases} j^{-l+|m|} \frac{\sqrt{\pi(2l+1)}}{l(l+1)} & |m| = 1\\ 0 & |m| \neq 1 \end{cases}$$
 (3.11b)

$$b_{lm} = \begin{cases} j^{-l+|m|} \frac{\sqrt{\pi(2l+1)}}{l(l+1)} & |m| = 1\\ 0 & |m| \neq 1 \end{cases}$$

$$c_{lm} = \begin{cases} j^{-(l+m)} \frac{\sqrt{\pi(2l+1)}}{l(l+1)} & |m| = 1\\ 0 & |m| \neq 1 \end{cases}$$

$$(3.11b)$$

$$c_{lm} = \begin{cases} j^{-(l+m)} \frac{\sqrt{\pi(2l+1)}}{l(l+1)} & |m| = 1\\ 0 & |m| \neq 1 \end{cases}$$

#### 3.2.4.3 Green's Function Expansion

The final ingredients necessary for the analytic evaluation of the integrals in all of the operators used in this thesis are the expansions of Green's functions. The scalar and dyadic Green's function expansions are

$$G_{p}(\mathbf{r}, \mathbf{r}') = -j\kappa_{p} \sum_{l=0}^{\infty} l(l+1) \sum_{m=-l}^{l} \varphi_{lm}^{(\alpha_{p})}(\kappa_{p}, \mathbf{r}) \varphi_{lm}^{(\beta_{p})*}(\kappa_{p}^{*}, \mathbf{r}')$$
(3.12a)

$$\underline{\underline{\underline{G}}}_{p}(\mathbf{r}, \mathbf{r}') = -j\kappa_{p} \sum_{l=0}^{\infty} \sum_{m=-l}^{l} \mathbf{M}_{lm}^{(\alpha_{p})}(\kappa_{p}, \mathbf{r}) \, \mathbf{M}_{lm}^{(\beta_{p})*}(\kappa_{p}^{*}, \mathbf{r}')$$

$$+ \mathbf{N}_{lm}^{(\alpha_{p})}(\kappa_{p}, \mathbf{r}) \, \mathbf{N}_{lm}^{(\beta_{p})*}(\kappa_{p}^{*}, \mathbf{r}')$$
(3.12b)

with

$$\alpha_p = \begin{cases} 4 & p = 1 \\ 1 & p = 2 \end{cases}$$
 (3.13a)

$$\beta_p = \begin{cases} 1 & p = 1 \\ 3 & p = 2 \end{cases}$$
 (3.13b)

These expressions and the spherical harmonic and wave functions constitute the underpinnings of our analytical analysis.

# 3.2.4.4 Candidate Inner Product Evaluation

As there are many different inner products to be evaluated, it is cumbersome to provide a detailed prescription for each. Indeed, there are 17 unique operators for all of the formulations presented in Chapters 1 and 2. As most of these follow the same template, we provide one illustrative example while leaving the reader with the necessary tools to follow the same steps for the others.

Our example is an operator that is less commonly encountered,  $\mathcal{P}_p^{(2)}$ . For illustration, we will focus on a single region and omit the scaling matrices, as these are diagonal and do not add to the integral. Specifically,

$$\mathbb{P}_{p}^{(2)}\big|_{kn} = \left\langle \underline{\mathcal{B}}_{k}^{v}, \mathcal{P}_{p}^{(2)} \circ \underline{\mathcal{B}}_{n}^{s} \right\rangle = \left\langle \underline{\mathcal{B}}_{k}^{v}, \hat{\mathbf{n}}_{p} \times \nabla \mathcal{S} \circ \underline{\mathcal{B}}_{n}^{s} \right\rangle \tag{3.14}$$

where  $k \in [1, N_v]$  and  $n \in [1, N_s]$  are the testing and basis indices for this matrix.

Substituting (3.12a) in leads to

$$\mathbb{P}_{p}^{(2)}\big|_{kn} = \int \underline{\mathcal{B}}_{k}^{v}(\mathbf{r}) \cdot \hat{\mathbf{n}}_{p} \times \nabla \int G(\mathbf{r}, \mathbf{r}') \underline{\mathcal{B}}_{n}^{s}(\mathbf{r}') dS' dS \qquad (3.15a)$$

$$= \int \underline{\mathcal{B}}_{k}^{v}(\mathbf{r}) \cdot \hat{\mathbf{n}}_{p} \times \nabla \int -j\kappa_{p} \sum_{l=0}^{\infty} l(l+1) \sum_{m=-l}^{l} \varphi_{lm}^{(\alpha_{p})}(\kappa_{p}, \mathbf{r}) \varphi_{lm}^{(\beta_{p})*}(\kappa_{p}^{*}, \mathbf{r}') \underline{\mathcal{B}}_{n}^{s}(\mathbf{r}') dS' dS \qquad (3.15b)$$

We use (3.4b) and (3.6c) for analytic analysis. If we "unroll" the testing index k into corresponding harmonic indices l and m for  $\Psi$  when  $k \leq (N_h + 1)^2$  and for  $\Phi$  when k > 1

 $(N_h + 1)^2$ , and "unroll" basis index n into corresponding to harmonic indices l' and m', it is easy to see that we can take advantage of the orthogonality of the spherical harmonics. When  $l \neq l'$  or  $m \neq m'$ , the system element is zero. This allows us to focus on a specific harmonic specified by l and m. We will use superscripts Y,  $\Psi$ , and  $\Phi$  to denote the basis and testing functions as in  $|_{lm}^{\Psi Y}$  to denote testing function  $\Psi_l^m$  and basis function  $Y_l^m$ . We analyze the two cases when k selects a testing function from  $\underline{\mathcal{B}}_{\Psi}$ 

$$\mathbb{P}_{p}^{(2)}\Big|_{lm}^{\mathbf{\Psi}\,\mathbf{Y}} = \left\langle \mathbf{\Psi}_{l}^{m}, \hat{\mathbf{n}}_{p} \times \nabla S \circ \mathbf{Y}_{l}^{m} \right\rangle 
= \int \mathbf{\Psi}_{l}^{m} \left( \hat{\mathbf{r}} \right) \cdot \hat{\mathbf{n}}_{p} \times \nabla \int -j\kappa_{p} l \left( l+1 \right) \varphi_{lm}^{(\alpha_{p})} \left( \kappa_{p}, \mathbf{r} \right) \varphi_{lm}^{(\beta_{p})*} \left( \kappa_{p}^{*}, \mathbf{r}' \right) \mathbf{Y}_{l}^{m} \left( \hat{\mathbf{r}}' \right) dS' dS$$
(3.16a)

(3.16b)

$$= -\varepsilon_{p} j \kappa_{p} l \left(l+1\right) \int \mathbf{\Psi}_{l}^{m} \left(\hat{\mathbf{r}}\right) \times \hat{\mathbf{r}} \cdot \mathbf{L}_{lm}^{(\alpha_{p})} \left(\kappa_{p}, \mathbf{r}\right) dS \left\langle \mathbf{Y}_{l}^{m}, \varphi_{lm}^{(\beta_{p})} \left(\kappa_{p}^{*}\right) \right\rangle^{*}$$
(3.16c)

$$=0 (3.16d)$$

and  $\underline{\mathcal{B}}_{\Phi}$  after skipping some shared steps

$$\mathbb{P}_{p}^{(2)}\Big|_{lm}^{\mathbf{\Phi} \, \mathbf{Y}} = \left\langle \mathbf{\Phi}_{l}^{m}, \hat{\mathbf{n}}_{p} \times \nabla \mathcal{S} \circ \mathbf{Y}_{l}^{m} \right\rangle \tag{3.16e}$$

$$= -\varepsilon_{p} j \kappa_{p} l \left(l+1\right) \int \mathbf{\Phi}_{l}^{m} \left(\hat{\mathbf{r}}\right) \times \hat{\mathbf{r}} \cdot \mathbf{L}_{lm}^{(\alpha_{p})} \left(\kappa_{p}, \mathbf{r}\right) dS \left\langle \mathbf{Y}_{l}^{m}, \varphi_{lm}^{(\beta_{p})} \left(\kappa_{p}^{*}\right) \right\rangle^{*}$$
(3.16f)

$$= -\varepsilon_{p} j \kappa_{p} l \left(l+1\right) \left\langle \mathbf{\Psi}_{l}^{m}, \mathbf{L}_{lm}^{(\alpha_{p})} \left(\kappa_{p}\right) \right\rangle \left\langle \mathbf{Y}_{l}^{m}, \varphi_{lm}^{(\beta_{p})} \left(\kappa_{p}^{*}\right) \right\rangle^{*}. \tag{3.16g}$$

## 3.2.4.5 All Operators

Below are all the operators used in Chapters 1 and 2 implemented with spherical harmonic basis functions. All pairs of test and basis functions not shown are analytically 0. The vector-vector operators are

$$\mathbb{K}_{p}^{\prime}\Big|_{lm}^{\Psi\Psi} = -\mathbb{K}_{p}^{\prime t}\Big|_{lm}^{\Psi\Psi} = \varepsilon_{p} j \kappa_{p}^{2} \left\langle \Psi_{l}^{m}, \mathbf{N}_{lm}^{(\alpha_{p})} \left(\kappa_{p}\right) \right\rangle \left\langle \Phi_{l}^{m}, \mathbf{M}_{lm}^{(\beta_{p})} \left(\kappa_{p}^{*}\right) \right\rangle^{*}$$
(3.17a)

$$\mathbb{K}_{p}^{\prime}\Big|_{lm}^{\mathbf{\Phi}\,\mathbf{\Phi}} = -\mathbb{K}_{p}^{\prime\prime}\Big|_{lm}^{\mathbf{\Phi}\,\mathbf{\Phi}} = -\varepsilon_{p}j\kappa_{p}^{2}\left\langle\mathbf{\Phi}_{l}^{m},\mathbf{M}_{lm}^{(\alpha_{p})}\left(\kappa_{p}\right)\right\rangle\left\langle\mathbf{\Psi}_{l}^{m},\mathbf{N}_{lm}^{(\beta_{p})}\left(\kappa_{p}^{*}\right)\right\rangle^{*}$$
(3.17b)

$$\mathbb{L}_{p}|_{lm}^{\mathbf{\Psi}\mathbf{\Psi}} = -\mathbb{L}_{p}|_{lm}^{\mathbf{\Psi}\mathbf{\Psi}} = -j\kappa_{p} \left\langle \mathbf{\Psi}_{l}^{m}, \mathbf{N}_{lm}^{(\alpha_{p})} \left(\kappa_{p}\right) \right\rangle \left\langle \mathbf{\Psi}_{l}^{m}, \mathbf{N}_{lm}^{(\beta_{p})} \left(\kappa_{p}^{*}\right) \right\rangle^{*}$$
(3.17c)

$$\mathbb{L}_{p}|_{lm}^{\mathbf{\Phi}\cdot\mathbf{\Phi}} = -\mathbb{L}_{p}^{t}|_{lm}^{\mathbf{\Phi}\cdot\mathbf{\Phi}} = -j\kappa_{p}\left\langle\mathbf{\Phi}_{l}^{m}, \mathbf{M}_{lm}^{(\alpha_{p})}\left(\kappa_{p}\right)\right\rangle\left\langle\mathbf{\Phi}_{l}^{m}, \mathbf{M}_{lm}^{(\beta_{p})}\left(\kappa_{p}^{*}\right)\right\rangle^{*}$$
(3.17d)

$$\mathbb{J}_{p}^{(2)}\Big|_{lm}^{\Psi\Psi} = j\kappa_{p} \left\langle \mathbf{\Phi}_{l}^{m}, \mathbf{M}_{lm}^{(\alpha_{p})} \left(\kappa_{p}\right) \right\rangle \left\langle \mathbf{\Phi}_{l}^{m}, \mathbf{M}_{lm}^{(\beta_{p})} \left(\kappa_{p}^{*}\right) \right\rangle^{*}$$

$$(3.17e)$$

$$\mathbb{J}_{p}^{(2)}\Big|_{lm}^{\boldsymbol{\Phi}\,\boldsymbol{\Phi}} = j\kappa_{p}\left(\left\langle\boldsymbol{\Psi}_{l}^{m}, \mathbf{N}_{lm}^{(\alpha_{p})}\left(\kappa_{p}\right)\right\rangle \left\langle\boldsymbol{\Psi}_{l}^{m}, \mathbf{N}_{lm}^{(\beta_{p})}\left(\kappa_{p}^{*}\right)\right\rangle^{*} \\
= \frac{l\left(l+1\right)}{\kappa_{p}^{2}}\left\langle\boldsymbol{\Psi}_{l}^{m}, \mathbf{L}_{lm}^{(\alpha_{p})}\left(\kappa_{p}\right)\right\rangle \left\langle\boldsymbol{\Psi}_{l}^{m}, \mathbf{L}_{lm}^{(\beta_{p})}\left(\kappa_{p}^{*}\right)\right\rangle^{*}\right) \tag{3.17f}$$

$$\mathbb{K}_{p}|_{lm}^{\mathbf{\Psi}\mathbf{\Psi}} = \varepsilon_{p} j \kappa_{p}^{2} \left\langle \mathbf{\Phi}_{l}^{m}, \mathbf{M}_{lm}^{(\alpha_{p})} \left( \kappa_{p} \right) \right\rangle \left\langle \mathbf{\Psi}_{l}^{m}, \mathbf{N}_{lm}^{(\beta_{p})} \left( \kappa_{p}^{*} \right) \right\rangle^{*}$$
(3.17g)

$$\mathbb{K}_{p}|_{lm}^{\mathbf{\Phi}\cdot\mathbf{\Phi}} = -\varepsilon_{p}j\kappa_{p}^{2} \left\langle \mathbf{\Psi}_{l}^{m}, \mathbf{N}_{lm}^{(\alpha_{p})} \left(\kappa_{p}\right) \right\rangle \left\langle \mathbf{\Phi}_{l}^{m}, \mathbf{M}_{lm}^{(\beta_{p})} \left(\kappa_{p}^{*}\right) \right\rangle^{*}.$$
(3.17h)

The vector-scalar operators are

$$\mathbb{Q}_{p}^{(1)}\Big|_{lm}^{\mathbf{\Phi}\,\mathbf{Y}} = \varepsilon_{p} j \kappa_{p}^{2} \left\langle \mathbf{\Phi}_{l}^{m}, \mathbf{M}_{lm}^{(\alpha_{p})} \left(\kappa_{p}\right) \right\rangle \left\langle \mathbf{Y}_{l}^{m}, \mathbf{N}_{lm}^{(\beta_{p})} \left(\kappa_{p}^{*}\right) \right\rangle^{*}$$

$$(3.17i)$$

$$\mathbb{P}_{p}^{(2)}\Big|_{lm}^{\mathbf{\Phi} \, \mathbf{Y}} = -\varepsilon_{p} j \kappa_{p} l \left(l+1\right) \left\langle \mathbf{\Psi}_{l}^{m}, \mathbf{L}_{lm}^{(\alpha_{p})} \left(\kappa_{p}\right) \right\rangle \left\langle \mathbf{Y}_{l}^{m}, \varphi_{lm}^{(\beta_{p})} \left(\kappa_{p}^{*}\right) \right\rangle^{*}$$
(3.17j)

$$\mathbb{Q}_{p}^{(2)}\Big|_{lm}^{\mathbf{\Phi} Y} = -j\kappa_{p}\left(\left\langle \mathbf{\Psi}_{l}^{m}, \mathbf{N}_{lm}^{(\alpha_{p})}\left(\kappa_{p}\right)\right\rangle \left\langle \mathbf{Y}_{l}^{m}, \mathbf{N}_{lm}^{(\beta_{p})}\left(\kappa_{p}^{*}\right)\right\rangle^{*} + \frac{l\left(l+1\right)}{\kappa_{p}^{2}}\left\langle \mathbf{Y}_{l}^{m}, \mathbf{L}_{lm}^{(\alpha_{p})}\left(\kappa_{p}\right)\right\rangle \left\langle \mathbf{\Psi}_{l}^{m}, \mathbf{L}_{lm}^{(\beta_{p})}\left(\kappa_{p}^{*}\right)\right\rangle^{*}\right).$$
(3.17k)

The scalar-vector operators are

$$\mathbb{J}_{p}^{(3)}\Big|_{lm}^{\mathbf{Y}\mathbf{\Phi}} = j\kappa_{p} \left( \left\langle \mathbf{Y}_{l}^{m}, \mathbf{N}_{lm}^{(\alpha_{p})} \left( \kappa_{p} \right) \right\rangle \left\langle \mathbf{\Psi}_{l}^{m}, \mathbf{N}_{lm}^{(\beta_{p})} \left( \kappa_{p}^{*} \right) \right\rangle^{*} + \frac{l(l+1)}{\kappa_{p}^{2}} \left\langle \mathbf{Y}_{l}^{m}, \mathbf{L}_{lm}^{(\alpha_{p})} \left( \kappa_{p} \right) \right\rangle \left\langle \mathbf{\Psi}_{l}^{m}, \mathbf{L}_{lm}^{(\beta_{p})} \left( \kappa_{p}^{*} \right) \right\rangle^{*} \right)$$
(3.17l)

$$\mathbb{M}_{p}^{(3)}\Big|_{lm}^{\mathbf{Y}\mathbf{\Phi}} = -\varepsilon_{p}j\kappa_{p}^{2}\left\langle\mathbf{Y}_{l}^{m},\mathbf{N}_{lm}^{(\alpha_{p})}\left(\kappa_{p}\right)\right\rangle\left\langle\mathbf{\Phi}_{l}^{m},\mathbf{M}_{lm}^{(\beta_{p})}\left(\kappa_{p}^{*}\right)\right\rangle^{*}$$
(3.17m)

$$\mathbb{J}_{p}^{(4)}\Big|_{lm}^{\mathbf{Y}\mathbf{\Phi}} = -\varepsilon_{p}j\kappa_{p}l\left(l+1\right)\left\langle\mathbf{Y}_{l}^{m},\varphi_{lm}^{(\alpha_{p})}\left(\kappa_{p}\right)\right\rangle\left\langle\mathbf{\Psi}_{l}^{m},\mathbf{L}_{lm}^{(\beta_{p})}\left(\kappa_{p}^{*}\right)\right\rangle^{*}.$$
(3.17n)

The scalar-scalar operators are

$$\mathbb{D}_{p}^{\prime}\Big|_{lm}^{\mathrm{YY}} = -\varepsilon_{p}j\kappa_{p}l\left(l+1\right)\left\langle\mathbf{Y}_{l}^{m},\mathbf{L}_{lm}^{(\alpha_{p})}\left(\kappa_{p}\right)\right\rangle\left\langle\mathbf{Y}_{l}^{m},\varphi_{lm}^{(\beta_{p})}\left(\kappa_{p}^{*}\right)\right\rangle^{*}$$
(3.170)

$$\mathbb{Q}_{p}^{(3)}\Big|_{lm}^{YY} = -j\kappa_{p}\left(\left\langle \mathbf{Y}_{l}^{m}, \mathbf{N}_{lm}^{(\alpha_{p})}\left(\kappa_{p}\right)\right\rangle \left\langle \mathbf{Y}_{l}^{m}, \mathbf{N}_{lm}^{(\beta_{p})}\left(\kappa_{p}^{*}\right)\right\rangle^{*} + \frac{l\left(l+1\right)}{\kappa_{p}^{2}}\left\langle \mathbf{Y}_{l}^{m}, \mathbf{L}_{lm}^{(\alpha_{p})}\left(\kappa_{p}\right)\right\rangle \left\langle \mathbf{Y}_{l}^{m}, \mathbf{L}_{lm}^{(\beta_{p})}\left(\kappa_{p}^{*}\right)\right\rangle^{*}\right)$$
(3.17p)

$$\mathbb{S}_{p}|_{lm}^{YY} = -j\kappa_{p}l\left(l+1\right)\left\langle \mathbf{Y}_{l}^{m}, \varphi_{lm}^{(\alpha_{p})}\left(\kappa_{p}\right)\right\rangle \left\langle \mathbf{Y}_{l}^{m}, \varphi_{lm}^{(\beta_{p})}\left(\kappa_{p}^{*}\right)\right\rangle^{*}$$
(3.17q)

$$\mathbb{D}_{p}|_{lm}^{\mathrm{YY}} = -\varepsilon_{p} j \kappa_{p} l \left(l+1\right) \left\langle \mathbf{Y}_{l}^{m}, \varphi_{lm}^{(\alpha_{p})}\left(\kappa_{p}\right) \right\rangle \left\langle \mathbf{Y}_{l}^{m}, \mathbf{L}_{lm}^{(\beta_{p})}\left(\kappa_{p}^{*}\right) \right\rangle^{*}$$
(3.17r)

$$\mathbb{N}_{p}|_{lm}^{\mathrm{YY}} = -j\kappa_{p}l\left(l+1\right)\left\langle \mathbf{Y}_{l}^{m}, \mathbf{L}_{lm}^{(\alpha_{p})}\left(\kappa_{p}\right)\right\rangle \left\langle \mathbf{Y}_{l}^{m}, \mathbf{L}_{lm}^{(\beta_{p})}\left(\kappa_{p}^{*}\right)\right\rangle^{*}.$$
(3.17s)

For completeness, additional vector-vector operators defined in Chapter 1 are provided here

$$\hat{\mathbf{n}}_{p} \times \mathbb{L}_{p} \Big|_{lm}^{\mathbf{\Psi} \mathbf{\Phi}} = \varepsilon_{p} j \kappa_{p} \left\langle \mathbf{\Phi}_{l}^{m}, \mathbf{M}_{lm}^{(\alpha_{p})} \left( \kappa_{p} \right) \right\rangle \left\langle \mathbf{\Phi}_{l}^{m}, \mathbf{M}_{lm}^{(\beta_{p})} \left( \kappa_{p}^{*} \right) \right\rangle^{*}$$
(3.17t)

$$\hat{\mathbf{n}}_{p} \times \mathbb{L}_{p} \Big|_{lm}^{\Phi \Psi} = -\varepsilon_{p} j \kappa_{p} \left\langle \mathbf{\Psi}_{l}^{m}, \mathbf{N}_{lm}^{(\alpha_{p})} \left( \kappa_{p} \right) \right\rangle \left\langle \mathbf{\Psi}_{l}^{m}, \mathbf{N}_{lm}^{(\beta_{p})} \left( \kappa_{p}^{*} \right) \right\rangle^{*}$$
(3.17u)

$$\hat{\mathbf{n}}_{p} \times \mathbb{K}_{p} \Big|_{lm}^{\mathbf{\Psi} \mathbf{\Phi}} = j \kappa_{p}^{2} \left\langle \mathbf{\Psi}_{l}^{m}, \mathbf{N}_{lm}^{(\alpha_{p})} \left( \kappa_{p} \right) \right\rangle \left\langle \mathbf{\Phi}_{l}^{m}, \mathbf{M}_{lm}^{(\beta_{p})} \left( \kappa_{p}^{*} \right) \right\rangle^{*}$$
(3.17v)

$$\hat{\mathbf{n}}_{p} \times \mathbb{K}_{p} \Big|_{lm}^{\Phi \Psi} = j \kappa_{p}^{2} \left\langle \Phi_{l}^{m}, \mathbf{M}_{lm}^{(\alpha_{p})} \left( \kappa_{p} \right) \right\rangle \left\langle \Psi_{l}^{m}, \mathbf{N}_{lm}^{(\beta_{p})} \left( \kappa_{p}^{*} \right) \right\rangle^{*}. \tag{3.17w}$$

## 3.2.5 Results

With these basis sets, we can analyze the eigenvalues and condition numbers of bandlimited versions of the operators, and compute Radar Cross Section (RCS) scattering from spheres. We do this by isolating the block of operators associated with a given harmonic specified by l and m. Because of the orthogonality of the basis functions, the system matrix becomes block diagonal with block size  $(2N_v + N_s) \times (2N_v + N_s)$ . The eigenvalues of the entire system comprise the  $2N_v + N_s$  eigenvalues of each block. Likewise, the singular values of the entire system comprise the  $2N_v + N_s$  singular values of each block. Computing each block's eigenvalues and singular values is significantly more efficient, and separating the eigenvalues by harmonic enables additional insight into the system's behavior. Also, the system is not dependent on harmonic index m. For this analysis, the first harmonic is excluded where l=m=0 and the highest harmonic is for  $l=N_h$ . The finite-dimensional expansion of the operator, in effect, creates a band-limited version. If the operator is compact, then this series converges, and the condition number represents the system for which  $N_h \to \infty$ . As is well known, the EFIE and PMCHWT integral equations have hyper-singular operators, so the operator's actual condition number is unbounded.

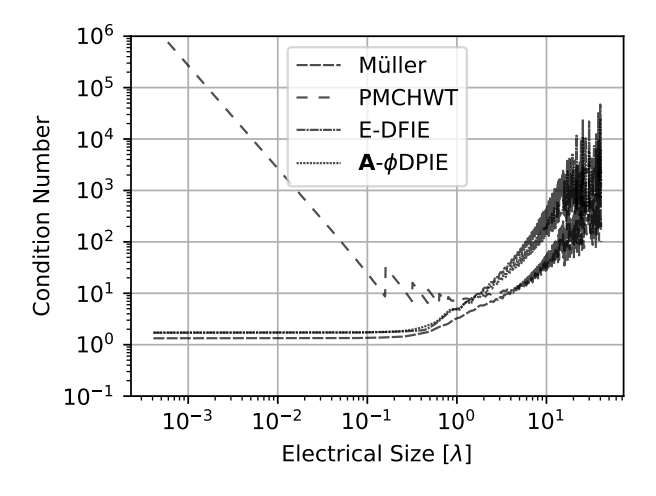
The eigenvalues are from the generalized eigenvalue problem,  $Av = \lambda Bv$  with  $A_{kn} = \mathbb{Z}_{kn}^{\chi}$  and  $B_{kn} = \langle \underline{\mathcal{F}}_{k}^{\chi}, \underline{\mathcal{F}}_{n}^{\chi} \rangle$  (or equivalently the regular eigenvalue problem  $B^{-1}Av = \lambda v$ ). Condition numbers are computed from the matrix  $B^{-1}A$ .

Rather than present results for each formulation, for dielectric formulations E-DFIE,  $\mathbf{A} - \phi$ -DPIE will be shown with PMCHWT and Müller as a reference, and for the PEC formulations LC-CFIE will be compared with EFIE and MFIE. For these comparisons, we will show the following:

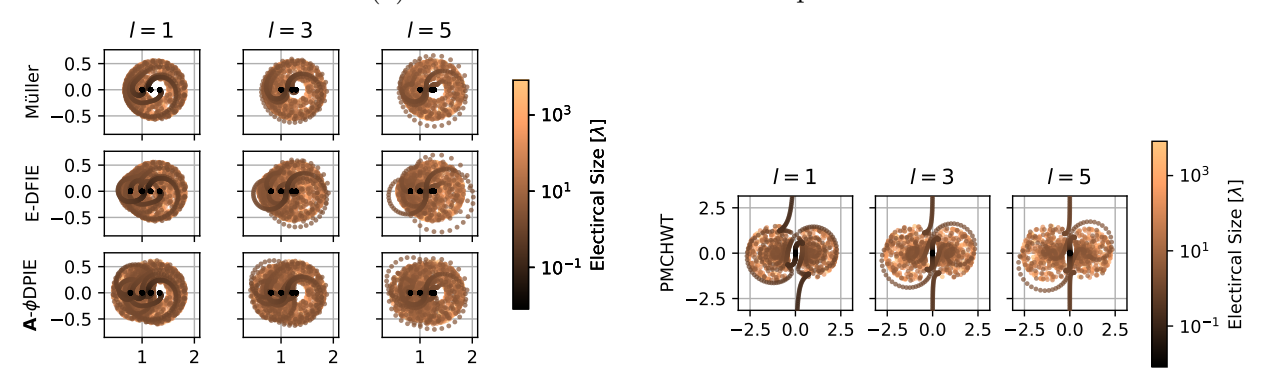
- 1. the condition number over frequency
- 2. the eigenvalue spectrum for several fixed orders l as frequency varies
- 3. the eigenvalue spectrum for all orders  $l < N_h$  for a specific frequency

## 3.2.5.1 Dielectric Formulations

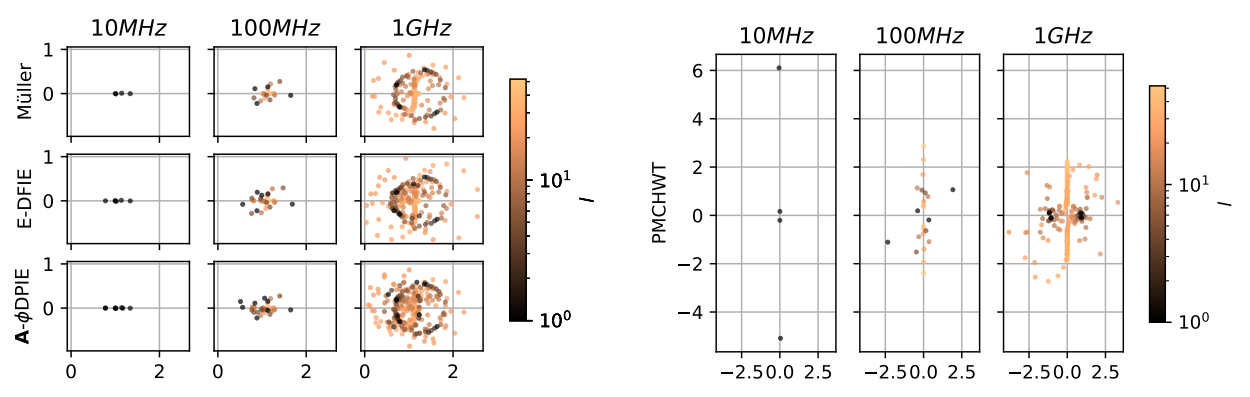
For the first case, we examine a low contrast scenario  $\mu_{r2} = 1$  and  $\epsilon_{r2} = 1.5$  in Figure 3.1. We see in Figure 3.1a that the condition number stays constant at low frequencies for Müller, DFIE, and DPIE but increases for PMCHWT. At high frequencies, all formulations grow at roughly the same rate. Next, we focus on the harmonics  $l \in [1,3,5]$  and m=0, as representatives of the whole system. We see in Figure 3.1b and 3.1c that at low frequency, the eigenvalues collect away from zero and are bounded at high frequency for Müller, DFIE, DPIE but collect at zero and infinity for PMCHWT. If the frequency is held constant at  $10 \, \text{MHz}$ ,  $100 \, \text{MHz}$ , and  $1 \, \text{GHz}$ , we notice that as frequency increases, we consider additional harmonics as designed. From Figures 3.1d and 3.1e, we can justify extrapolating the findings from examining l = 1, 3, 5 and see that the eigenvalues even for higher l are bounded and do



(a) Condition numbers across frequencies



- Müller, E-DFIE, and  $\mathbf{A} \phi$ -DPIE
- (b) Eigenvalues for fixed harmonic indices for (c) Eigenvalues for fixed harmonic indices for PMCHWT.



- E-DFIE, and  $\mathbf{A} \phi$ -DPIE
- (d) Eigenvalues for fixed frequencies for Müller, (e) Eigenvalues for fixed frequencies for PM-CHWT

Figure 3.1 Condition numbers and eigenvalues for different band-limited, dielectric integral equations using analytic basis sets for a dielectric sphere with  $\mu_{r2} = 1$  and  $\epsilon_{r2} = 1.5$ . Real and imaginary parts of eigenvalues on the x- and y-axes, respectively.

not collect at zero for Müller, DFIE, DPIE and collect closer and closer to zero and infinity as frequency goes down for PMCHWT.

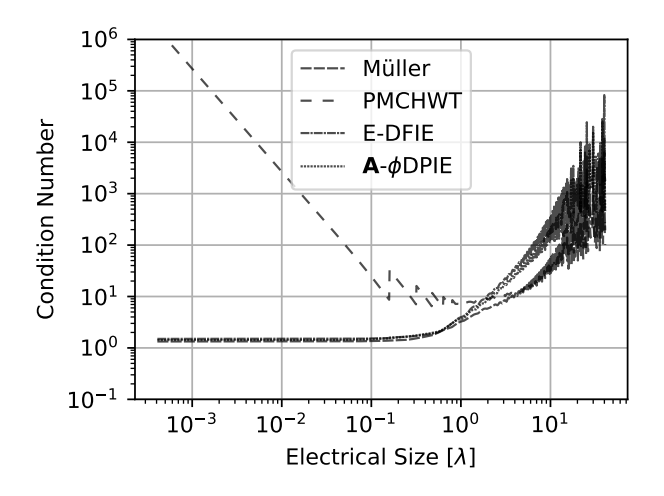
For the second case, we examine the dual scenario where  $\mu_{r2} = 1.5$  and  $\epsilon_{r2} = 1$  in Figure 3.2. This is equivalent to examining the first case with the dual formulations, H-DFIE and  $\mathbf{F} - \psi$ -DPIE. As evidenced by Figures 3.2, there is little noticeable difference between the first two scenarios.

For the third scenario, we consider a case where  $n_1^2 = n_2^2$  with  $\mu_{r2} = 1/1.5$  and  $\epsilon_{r2} = 1.5$  in Figure 3.3. This scenario is unique because the DPIE formulations are second-kind only under this condition. We see in Figure 3.3a that the condition number is much more flat for all formulations In Figure 3.3b and 3.3c, the eigenvalues seem to follow some additional structure but otherwise follow the same behavior as the first two cases. From Figures 3.3d and 3.3e, we again notice minimal distinction between the Müller, E-DFIE, and  $\mathbf{A} - \phi$ -DPIE formulations and similar takeaways for the PMCHWT formulation.

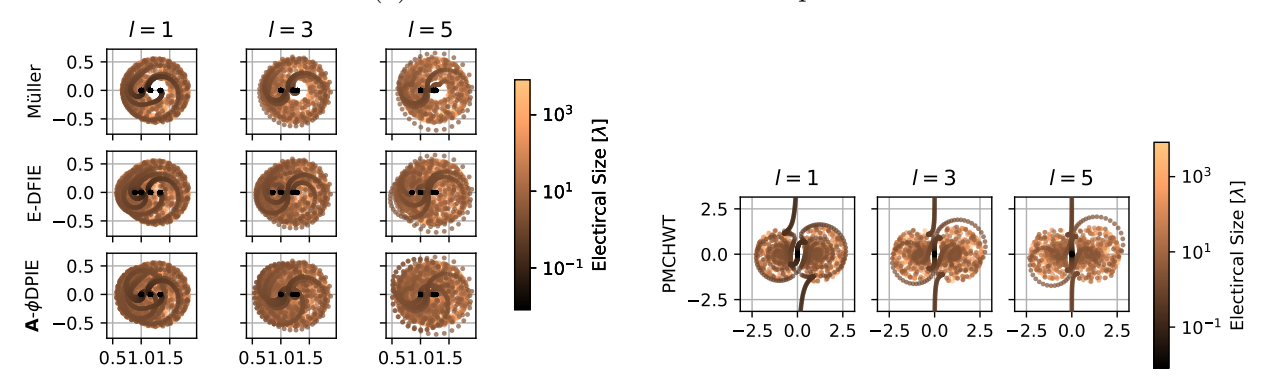
For the fourth and final case, we consider a high contrast scenario with  $\mu_{r2} = 1$  and  $\epsilon_{r2} = 20$  in Figure 3.4. We see in Figure 3.4a that the condition number is worse for all formulations. We also observe several "near-resonances" where the condition number spikes but not to infinity. Figure 3.4b and 3.4c show that the eigenvalues are still bounded but appear to be near and around zero. For certain frequencies, an eigenvalue will get relatively close to the origin, which will cause what we call a "near-resonance". From Figures 3.4d and 3.4e, we notice little significant difference between the three well-conditioned formulations and no new takeaways for the PMCHWT formulation.

# 3.2.5.2 PEC Formulations

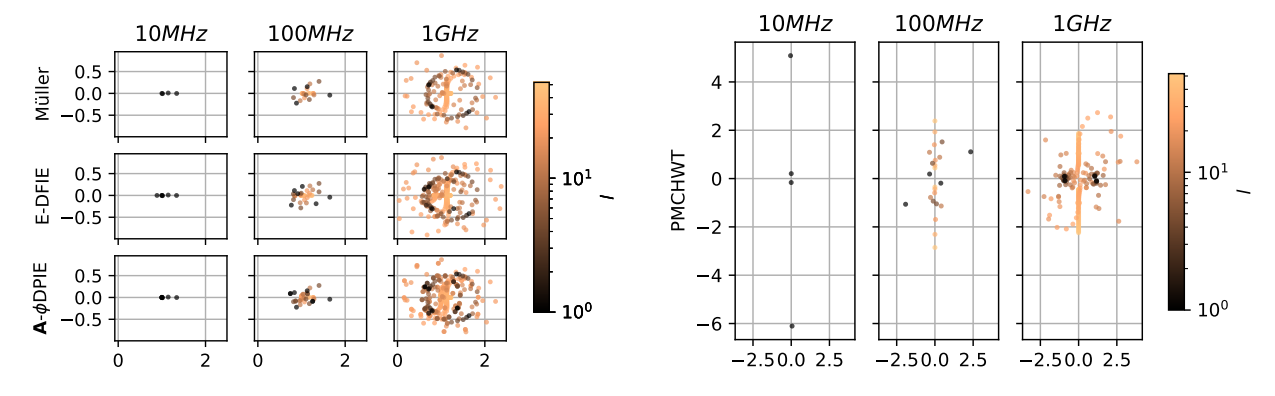
Before we examine the analytic results for the LC-CFIE formulation, we briefly describe the well-studied Calderón formulation [Andriulli et al., 2008] using the common framework. We will preface the existing Calderón formulation with  $\star$  to differentiate between the two



(a) Condition numbers across frequencies

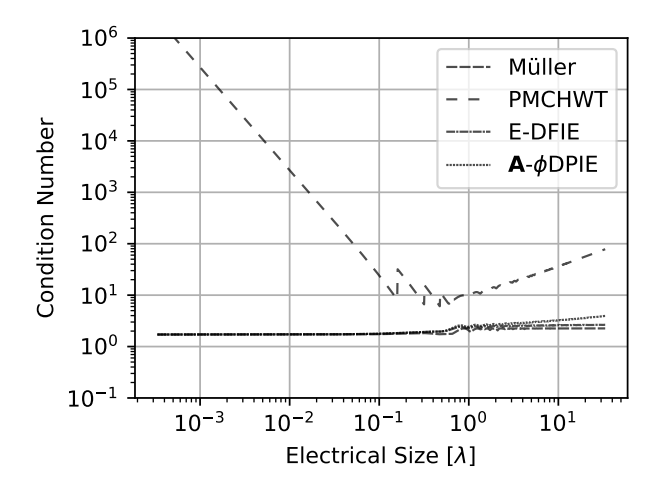


- (b) Eigenvalues for fixed harmonic indices for Müller, E-DFIE, and  ${\bf A}-\phi$ -DPIE
- (c) Eigenvalues for fixed harmonic indices for PMCHWT.

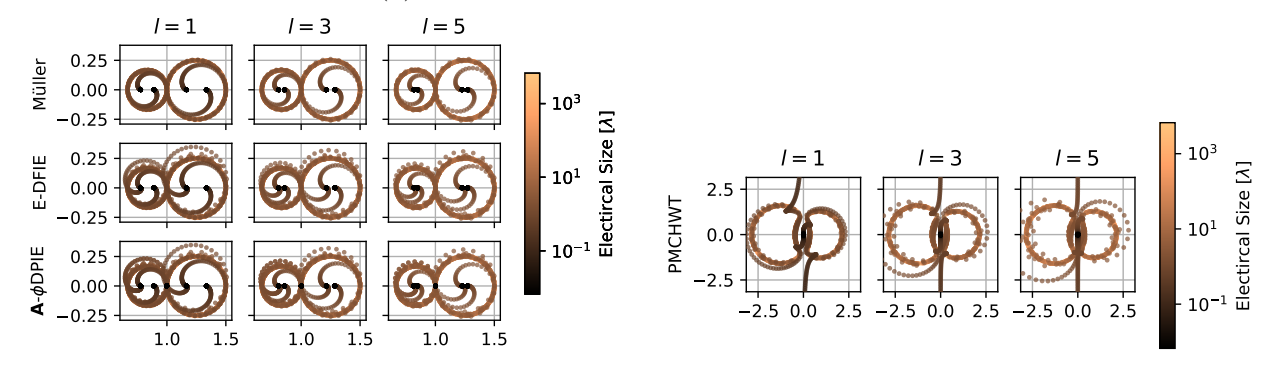


(d) Eigenvalues for fixed frequencies for Müller, (e) Eigenvalues for fixed frequencies for PM-E-DFIE, and  ${\bf A}-\phi$ -DPIE CHWT

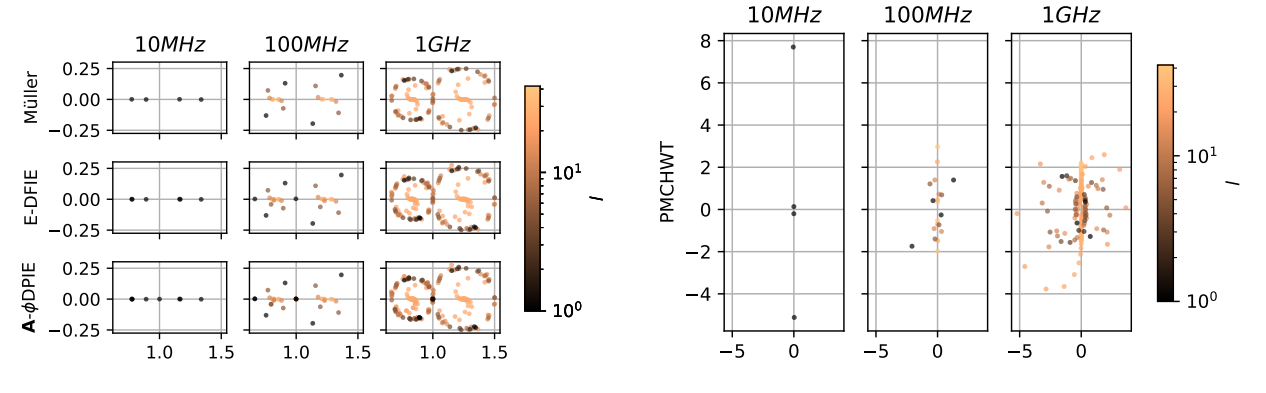
Figure 3.2 Condition numbers and eigenvalues for different band-limited, dielectric integral equations using analytic basis sets for a dielectric sphere with  $\mu_{r2} = 1.5$  and  $\epsilon_{r2} = 1$ . Real and imaginary parts of eigenvalues on the x- and y-axes, respectively.



(a) Condition numbers across frequencies

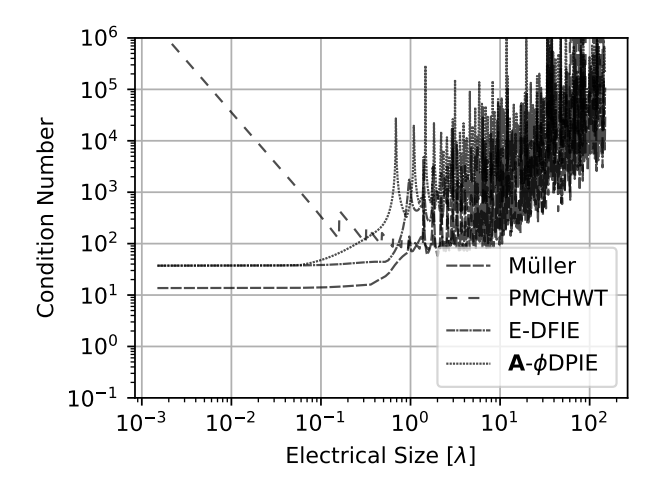


- (b) Eigenvalues for fixed harmonic indices for Müller, E-DFIE, and  ${\bf A}-\phi$ -DPIE
- (c) Eigenvalues for fixed harmonic indices for PMCHWT.

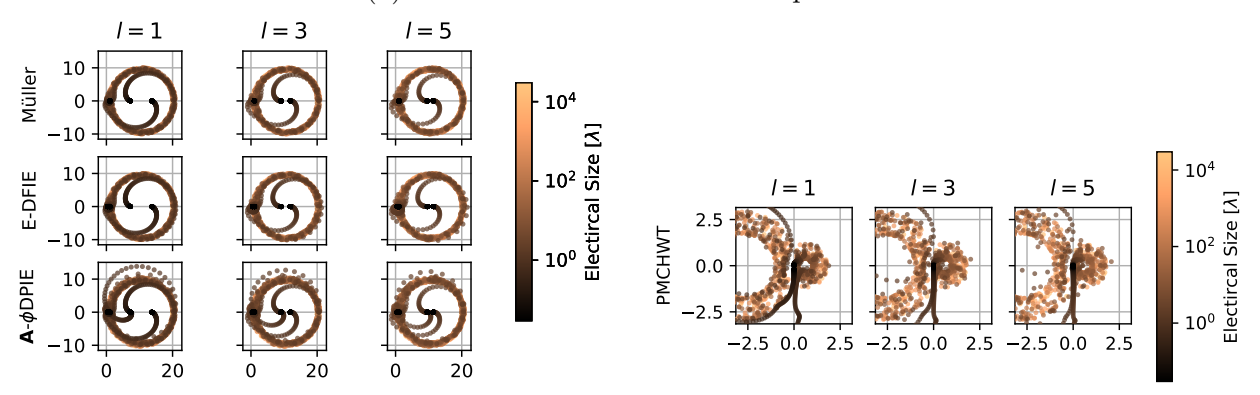


(d) Eigenvalues for fixed frequencies for Müller, (e) Eigenvalues for fixed frequencies for PM-E-DFIE, and  ${\bf A}-\phi$ -DPIE CHWT

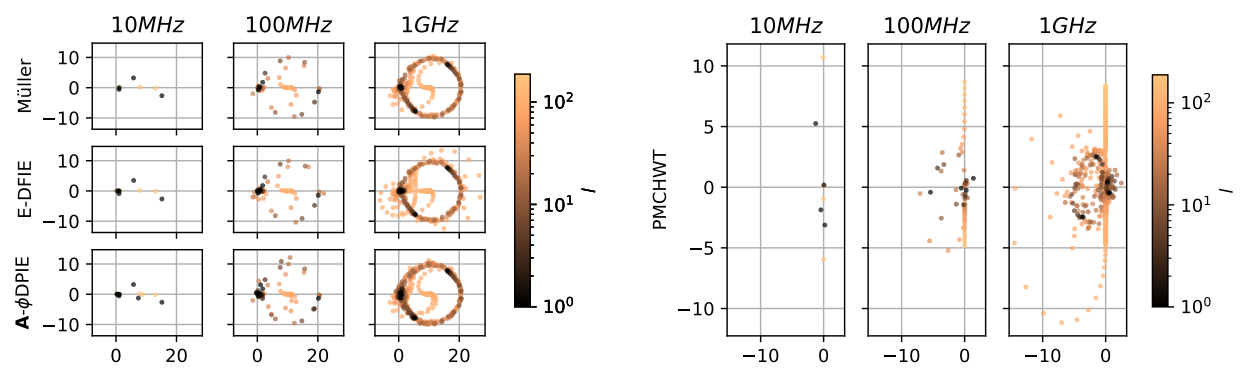
Figure 3.3 Condition numbers and eigenvalues for different band-limited, dielectric integral equations using analytic basis sets for a dielectric sphere with  $\mu_{r2} = 1/1.5$  and  $\epsilon_{r2} = 1.5$ . Real and imaginary parts of eigenvalues on the x- and y-axes, respectively.



(a) Condition numbers across frequencies



- (b) Eigenvalues for fixed harmonic indices for Müller, E-DFIE, and  $\mathbf{A} - \phi$ -DPIE
- (c) Eigenvalues for fixed harmonic indices for PMCHWT.



- E-DFIE, and  $\mathbf{A} \phi$ -DPIE
- (d) Eigenvalues for fixed frequencies for Müller, (e) Eigenvalues for fixed frequencies for PM-CHWT

Figure 3.4 Condition numbers and eigenvalues for different band-limited, dielectric integral equations using analytic basis sets for a dielectric sphere with  $\mu_{r2}=1$  and  $\epsilon_{r2}=20$ . Real and imaginary parts of eigenvalues on the x- and y-axes, respectively.

formulations.

$$\underline{\mathcal{P}}_{1}^{\star \text{LC-CFIE}} = \begin{pmatrix} 1 & 1 \end{pmatrix} \tag{3.18a}$$

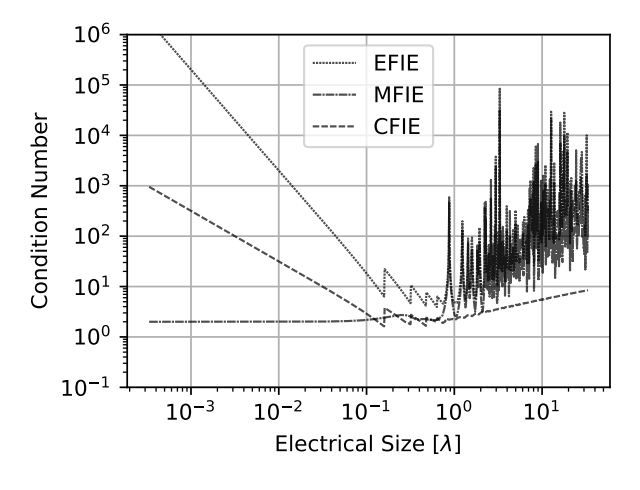
$$\underline{\mathcal{W}}_1 = \begin{pmatrix} \underline{\alpha} & 1 \end{pmatrix} \tag{3.18b}$$

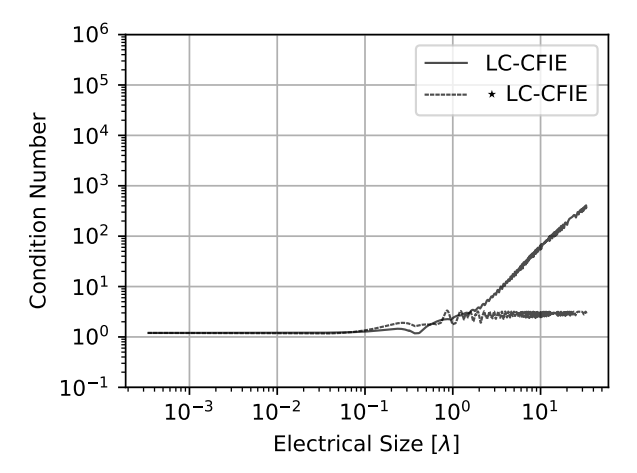
$$\mathcal{Z}_{1}^{\star LC\text{-CFIE}} = \operatorname{diag}\left(\hat{\mathbf{n}}_{1} \times \tilde{\mathcal{L}}_{1} \circ \left(\kappa_{1}^{2} \eta_{1} \hat{\mathbf{n}}_{1} \times \mathcal{L}_{1}\right), \mathcal{I} - \mathcal{K}_{1}\right)$$
(3.18c)

$$\mathbf{b}_{1}^{\star \text{LC-CFIE}} = \begin{pmatrix} \hat{\mathbf{n}}_{1} \times \tilde{\mathcal{L}}_{1} \circ \left( j \kappa_{1} \mathbf{E}_{1}^{i} \times \hat{\mathbf{n}}_{1} \right) \\ \hat{\mathbf{n}}_{1} \times \mathbf{H}_{1}^{i} \end{pmatrix}$$
(3.18d)

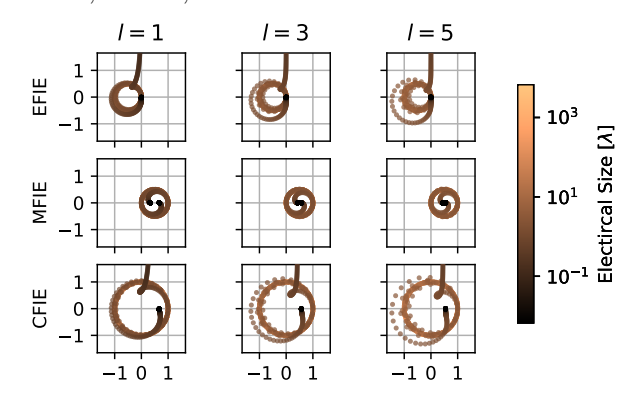
$$\mathbf{x}^{\star \text{LC-CFIE}} = \mathbf{J}_s. \tag{3.18e}$$

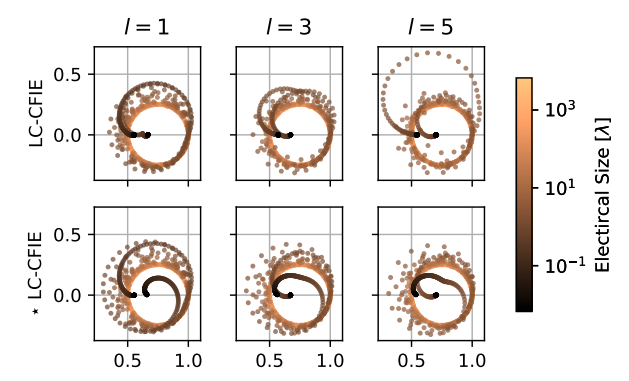
We examine the results in Figure 3.5 where we show the standard EFIE, MFIE, and CFIE behavior for reference and the related LC-CFIE and  $\star$  LC-CFIE formulations. What is immediately noticeable from Figure 3.5a is that neither the EFIE, MFIE, nor CFIE formulation are well-conditioned at either low or high frequencies. In contrast, in Figure 3.5b, we see excellent conditioning for  $\star$  LC-CFIE and excellent low-frequency and comparable high-frequency conditioning from the LC-CFIE. From Figure 3.5c, we observe that the EFIE and CFIE are unbounded and how the MFIE and CFIE do not collect at the origin at low frequencies. That is not to say that the MFIE does not have resonances. The CFIE has no resonances as all the eigenvalues are away from the origin. In contrast, both the LC-CFIE and \* LC-CFIE are bounded, do not collect at the origin, and are far from the origin. The main difference between the two Calderón formulations is that the new LC-CFIE formulation has a "bubble" that grows with harmonic index l. This is directly responsible for the difference in high-frequency behavior from the starred counterpart. Finally, in Figures 3.5e and 3.5f, we see eigenvalues always clustering away from zero for the LC-CFIE and  $\star$  LC-CFIE formulations but not so with the EFIE, MFIE, or CFIE formulation, and for the LC-CFIE formulation, the "bubble" manifests itself at higher frequencies and is the cause of the increased conditioning compared to  $\star$  LC-CFIE.



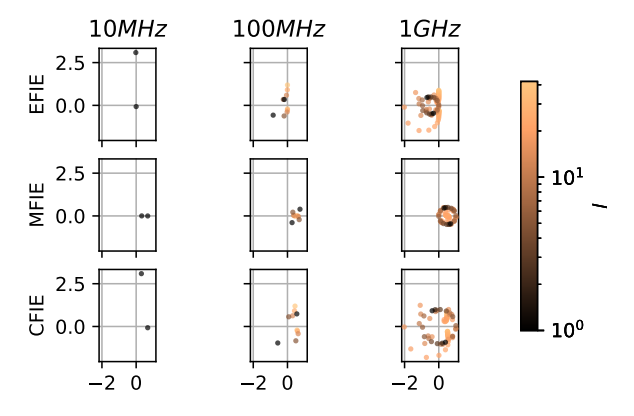


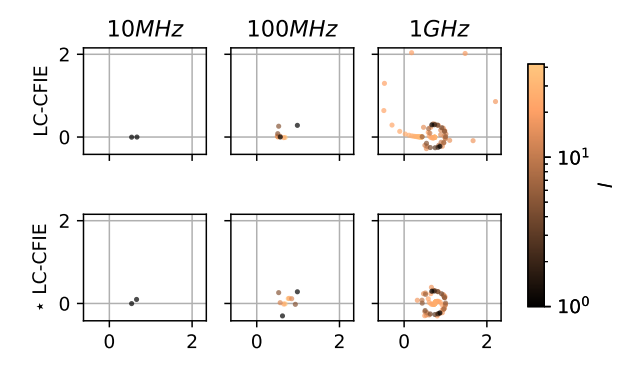
- (a) Condition numbers across frequencies for EFIE, MFIE, and CFIE
- (b) Condition numbers across frequencies for LC-CFIE and  $\star$  LC-CFIE





- (c) Eigenvalues for fixed harmonic indices for EFIE, MFIE, and CFIE
- (d) Eigenvalues for fixed harmonic indices for LC-CFIE and  $\star$  LC-CFIE.





- MFIE, and CFIE
- (e) Eigenvalues for fixed frequencies for EFIE, (f) Eigenvalues for fixed frequencies for LC-CFIE and  $\star$  LC-CFIE.

Figure 3.5 Condition numbers and eigenvalues for different band-limited, integral equations using analytic basis sets for a PEC sphere. Real and imaginary parts of eigenvalues on the xand y-axes, respectively.

# 3.3 Piecewise Analysis

For analysis on non-spherical objects, we can utilize a triangular mesh with  $N_f$  flattriangles,  $N_e$  edges, and  $N_n$  nodes to approximate the true surface as is typically done. Piecewise basis and testing functions will not have the helpful analytic integration properties of the spherical harmonics. However, they will enable the analysis of arbitrarily shaped objects, which is necessary for practical utility.

# 3.3.1 RWG functions for $\underline{\mathcal{B}}^v$

RWG functions are a heavily utilized set of basis functions for representing vector functions in CEM. They are excellent for demonstrating how to implement the formulations presented in Chapter 1 and 2. These functions are defined for each edge with a domain of the two connected triangles as

$$\mathbf{f}_{n_e}(\mathbf{r}) = \begin{cases} \frac{l_{n_e}}{2A_{n_e}^{\pm}} \boldsymbol{\varrho}_{n_e}^{\pm}(\mathbf{r}) & \mathbf{r} \in T_{n_e}^{\pm} \\ \mathbf{0} & \text{otherwise} \end{cases}$$
(3.19a)

where

$$\varrho_{n_e}^{\pm}(\mathbf{r}) = \begin{cases}
\pm \left(\mathbf{r} - \mathbf{p}_{n_e}^{\pm}\right) & \mathbf{r} \in T_{n_e}^{\pm} \\
\mathbf{0} & \text{otherwise}
\end{cases}$$
(3.19b)

In the above equations,  $l_{n_e}$  is the length of edge  $n_e$ ,  $A_{n_e}^{\pm}$  is the area associated with triangle  $T_{n_e}^{\pm}$ , and  $\mathbf{p}_{n_e}^{\pm}$  is the node of the triangle  $T_{n_e}^{\pm}$  opposite the edge  $n_e$  [Rao et al., 1982]. With these basis functions, we can define  $\underline{\mathcal{B}}^v$  as

$$\underline{\mathcal{B}}^{v} = \begin{pmatrix} \mathbf{f}_{1} & \dots & \mathbf{f}_{n_{e}} & \dots & \mathbf{f}_{N_{e}} \end{pmatrix}$$
 (3.20)

with  $N_v = N_e$ .

## 3.3.2 Pulse functions for $\mathcal{B}^s$

Pulse functions are the simplest basis functions to represent scalar functions over a triangular mesh. These functions are constant over each face of the mesh

$$p_{n_f}(\mathbf{r}) = \begin{cases} 1 & \mathbf{r} \in T_{n_f} \\ 0 & \text{otherwise} \end{cases}$$
 (3.21)

where  $T_{n_f}$  is the  $n_f$  triangle.

With these basis functions, we can define  $\underline{\mathcal{B}}^s$  as

$$\underline{\mathcal{B}}^s = \begin{pmatrix} p_1 & \dots & p_{n_f} & \dots & p_{N_f} \end{pmatrix} \tag{3.22}$$

with  $N_s = N_f$ .

# 3.3.3 Hat functions for $\underline{\mathcal{B}}^s$

While hat functions have been implemented for these new formulations, they are unnecessary for the primary purpose of this chapter. Rather than showing two sets of results, one with pulse functions and one with hat functions, pulse functions are used for the remainder of this thesis. This section serves as a reminder of how additional basis sets can be used to construct  $\underline{\mathcal{B}}^v$  and  $\underline{\mathcal{B}}^s$  without any change to the underlying formulation.

The second most straightforward scalar functions on a triangular mesh are hat functions (pyramidal functions). These functions are associated with each node and linearly decrease from 1 at the node to 0 at the edges, forming a ring around the node. We can define these functions fairly simply by reusing RWG functions

$$h_{n_n} = \begin{cases} 1 - \hat{\mathbf{u}}_{n_n}^i \cdot \mathbf{f}_{n_n}^i & \mathbf{r} \in T_{n_n}^i \\ 0 & \text{otherwise} \end{cases}$$
(3.23)

where each node has  $N_{n_n}$  triangles connected to it with index  $i \in [1, N_{n_n}]$ . Each triangle  $T_{n_n}^i$  has an edge that does not include node  $n_n$ . Those edges have unit normal vectors  $\hat{\mathbf{u}}_{n_n}^i$  perpendicular to them pointing out of the triangle and an RWG function  $\mathbf{f}_{n_n}^i$  oriented such that  $T_{n_n}^i$  is its positive triangle.

With these basis functions, we can define  $\underline{\mathcal{B}}^s$  as

$$\underline{\mathcal{B}}^s = \begin{pmatrix} h_1 & \dots & h_{n_n} & \dots & h_{N_n} \end{pmatrix} \tag{3.24}$$

with  $N_s = N_n$ .

These functions typically result in fewer unknowns for  $\underline{\mathcal{B}}^s$  than the pulse functions because  $N_n \leq N_f$  for closed objects. However, more quadrature points will be needed for each integral

because the domain of support covers more than one triangle. If we count the number of integrals, each triangle is integrated over once for pulse functions but three times for hat functions.

# 3.3.4 Zero-Mean Constraint

In order to effect the zero-mean constraint for a closed tessellated object through the basis function coefficients, we use a Lagrange multiplier as in [Dault and Shanker, 2015]. This adds a row and column to the matrix for each Lagrange multiplier while not significantly modifying the convergence properties of the formulation as confirmed experimentally.

As an alternative, a rank-1 update will avoid the matrix with the added cost of an additional matrix solution as done in [Hawkins et al., 2022].

# 3.3.5 Numeric Integration

The key challenge of working with piecewise tessellations is evaluating these operators when the k testing domain is close to or shared with the n basis domain. While several operators are familiar, some are not. We have taken a straightforward approach to evaluating these integrals—singularity subtraction. There are other methods of evaluating these integrals [Tihon and Craeye, 2018]. However, they are not necessary to demonstrate the crux of this chapter—the demonstration of how to implement the new formulations for discrete piecewise tessellations and their properties. To that end, we note that even though there are several unfamiliar operators, the singular integrals necessary are the same as those encountered in the EFIE and MFIE; all other singular integrals can be evaluated via a combination of four base singular integrals. These singular integrals, along with an example of the complete treatment of one of the operators, are presented in the next section. Standard quadrature techniques are applicable for numeric integration when the basis and testing domains are sufficiently separated and not discussed here.

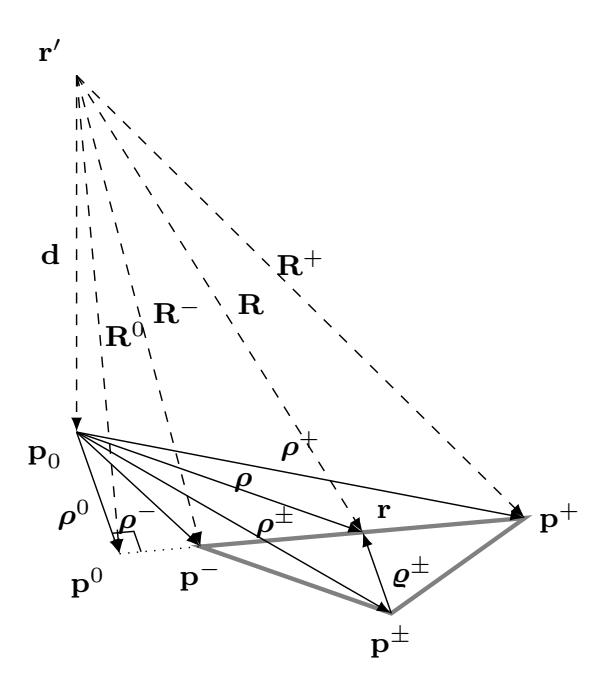


Figure 3.6 Vector and point definitions for singular integration over a testing triangle.

# 3.3.5.1 Singular Integrals

We subtract the first two terms from the Taylor series expansion of the exponential function. As will be evident, the singular integrals needed are identical to the ones needed for the EFIE and MFIE and can be found in [Wilton et al., 1984, Hodges and Rahmat-Samii, 1997]. It follows that, if necessary, one can use better rules [Fink et al., 2008, Botha, 2013, Tihon and Craeye, 2018] if so desired. We use Figure 3.6 to set the stage for definitions, and it is here purely for completeness. The definitions here follow those in [Wilton et al., 1984].

It is well known that the following integrals can be evaluated analytically as  $\mathbf{r}'$  approaches a testing triangle.

$$\mathcal{I}_{1/R} = \int \frac{1}{R} dS \tag{3.25a}$$

$$\mathcal{I}_{\rho/R} = \int \frac{\boldsymbol{\rho}}{R} dS \tag{3.25b}$$

$$\mathcal{I}_{1/R^3} = \int \frac{1}{R^3} dS$$
 (3.25c)

$$\mathcal{I}_{\rho/R^3} = \int \frac{\rho}{R^3} dS \tag{3.25d}$$

where the integrals are defined according to Figure 3.6. Similar integrals can be defined and evaluated as  $\mathbf{r}$  approaches a source triangle with the only difference being that  $\mathbf{R}$  points away from the triangle, so the integrals involving  $\mathbf{R}$  have an extra factor of -1. Singular integrals over the source domain will be denoted with a prime.

We used a seven-point Gauss-Legendre rule for the integrals over a triangle to effect the integration. For the hypersingular integral  $\mathbb{N}_p$ , we treat it as in [Terai, 1980] and use a fourteen-point Gauss-Legendre rule for the line integral.

As an aside, two issues naturally crop up when surfaces are modeled using higher-order geometric representations: (a) evaluation of singular integrals and (b) cost of a higher-order quadrature rule. The integrals in (3.25) have been dealt with in the community using either a mapping of the contour to a flat patch, which allows the use of singularity subtraction or singularity cancellation techniques. Amelioration of the costs associated with the evaluation of these integrals for higher order geometries has been dealt with in [Alsnayyan et al., 2020, Dault and Shanker, 2015] by integrating with a wideband Fast Multipole Method (FMM), which uses a combination of an adaptive quadrature rule and singularity cancellation around a small neighborhood of the singularity.

The techniques used below rely on the fact that we use a flat tessellation and are specialized in using RWG and pulse functions for basis and testing functions.

# 3.3.5.2 Candidate Inner Product Evaluation

To illustrate a general approach, consider the evaluation of  $\mathbb{P}_p^{(2)}\Big|_{kn}$  as defined in (3.14). The integration is over the testing domain  $T_k^{\pm}$  and the basis domain  $T_n$ . To simplify the presentation, only consider  $T_k^+$  (the other follows trivially). Given that  $\hat{\mathbf{n}}_p$  is constant over  $T_k^+$ , manipulation of the integral results in

$$\mathbb{P}_{p}^{(2)}\big|_{kn} = \int_{T_{k}^{+}} \mathbf{f}_{k}(\mathbf{r}) \cdot \hat{\mathbf{n}}_{p} \times \nabla \int_{T_{n}} G_{p}(\mathbf{r}, \mathbf{r}') p_{n}(\mathbf{r}') dS' dS$$
(3.26a)

$$= \int_{T_n} p_n(\mathbf{r}') \,\hat{\mathbf{n}}_p \cdot \int_{T_k^+} \nabla G_p(\mathbf{r}, \mathbf{r}') \times \mathbf{f}_k(\mathbf{r}) \, dS dS'. \tag{3.26b}$$

As is usually done for singularity subtraction, we use a Taylor series expansion for  $G_p$  or  $\nabla G_p$  depending on the integral. We then decompose the integral into two parts: one with a removable singularity and another non-singular integral that can be evaluated numerically. As mentioned earlier, we subtract the first two terms of the expansions to construct the singular part (although the second terms are not singular), and the rest of the series is captured in the non-singular part

$$G_{p}(\mathbf{r}, \mathbf{r}') = \frac{1}{4\pi} \left( \frac{1}{R} - j\kappa_{p} \right) + \mathcal{O}(R)$$
(3.27a)

$$\underbrace{\frac{1}{4\pi} \left( \frac{1}{R} - j\kappa_p \right)}_{\text{Singular}} + \underbrace{\left( G - \frac{1}{4\pi} \left( \frac{1}{R} - j\kappa_p \right) \right)}_{\text{Non-singular}}$$
(3.27b)

$$\nabla G_p(\mathbf{r}, \mathbf{r}') = \frac{1}{4\pi} \left( -\frac{\mathbf{R}}{R^3} - \frac{\kappa_p^2 \mathbf{R}}{2R} \right) + \mathbf{R} \mathcal{O}(1)$$
(3.27c)

$$= \underbrace{\frac{1}{4\pi} \left( -\frac{\mathbf{R}}{R^3} - \frac{\kappa_p^2 \mathbf{R}}{2R} \right)}_{\text{Singular}} + \underbrace{\left( \nabla \mathbf{G} - \frac{1}{4\pi} \left( -\frac{\mathbf{R}}{R^3} - \frac{\kappa_p^2 \mathbf{R}}{2R} \right) \right)}_{\text{Non-singular}}$$
(3.27d)

We only discuss the singular portion of the integral denoted below using superscript S as in S. For (3.26), this can be written as

$$\left. \mathbb{P}_{p}^{(2)} \right|_{kn}^{S} = \frac{-1}{4\pi} \int_{T_{n}} \hat{\mathbf{n}}_{p} \cdot \left( \int_{T_{k}^{+}} \frac{\mathbf{R}}{R^{3}} \times \mathbf{f}_{k} \left( \mathbf{r} \right) dS + \frac{\kappa_{p}^{2}}{2} \int_{T_{k}^{+}} \frac{\mathbf{R}}{R} \times \mathbf{f}_{k} \left( \mathbf{r} \right) dS \right) dS'. \tag{3.28}$$

It follows that to evaluate this integral we need to evaluate  $\int \frac{\mathbf{R}}{R^3} \times \mathbf{f}_k(\mathbf{r}) dS$  and  $\int \frac{\mathbf{R}}{R} \times \mathbf{f}_k(\mathbf{r}) dS$ . In this example, the integral over the source domain can be evaluated numerically.

From (3.25), one can derive the following analytic integrals:

$$\mathcal{I}_{\mathbf{R}/R} = \int \frac{\mathbf{R}}{R} dS = \mathcal{I}_{\rho/R} + \mathbf{d}\mathcal{I}_{1/R}$$
 (3.29a)

$$\mathcal{I}_{\mathbf{R}/R\times\mathbf{f}} = \int_{T_k^{\pm}} \frac{\mathbf{R}}{R} \times \mathbf{f}_k(\mathbf{r}) dS = \pm \frac{l_k}{2A_k^{\pm}} \left( \mathbf{d} + \boldsymbol{\rho}^{\pm} \right) \times \mathcal{I}_{\mathbf{R}/R}$$
(3.29b)

$$\mathcal{I}_{f/R} = \int_{T_k^{\pm}} \frac{\mathbf{f}_k(\mathbf{r})}{R} dS = \pm \frac{l_k}{2A_k^{\pm}} \left( \mathcal{I}_{\rho/R} - \boldsymbol{\rho}^{\pm} \mathcal{I}_{1/R} \right)$$
(3.29c)

$$\mathcal{I}_{\mathbf{R}/R^3} = \int \frac{\mathbf{R}}{R^3} dS = \mathcal{I}_{\rho/R^3} + \mathbf{d}\mathcal{I}_{1/R^3}$$
(3.29d)

$$\mathcal{I}_{\mathbf{R}/R^{3}\times\mathbf{f}} = \int_{T_{k}^{\pm}} \frac{\mathbf{R}}{R^{3}} \times \mathbf{f}_{k}(\mathbf{r}) dS = \pm \frac{l_{k}}{2A_{k}^{\pm}} \left(\mathbf{d} + \boldsymbol{\rho}^{\pm}\right) \times \mathcal{I}_{\mathbf{R}/R^{3}}.$$
 (3.29e)

The integral  $\mathcal{I}_{\mathbf{f}_{k}/R}$  is not necessary for this example but is for the other operators in the following section.

We finally arrive at

$$\left. \mathbb{P}_p^{(2)} \right|_{kn}^S = \frac{-1}{4\pi} \int_{T_n} \hat{\mathbf{n}}_p \cdot \left( \mathcal{I}_{\mathbf{R}/R^3 \times \mathbf{f}} + \frac{\kappa_p^2}{2} \mathcal{I}_{\mathbf{R}/R \times \mathbf{f}} \right) dS'. \tag{3.30}$$

# 3.3.5.3 All Operators

The process for addressing the rest of the singular integrals is similar. Again, the integrals are defined according to Figure 3.6 where the integration is over a testing triangle, and it is important to remember if integrating over the source domain to add an extra factor of -1 for singular integrals involving  $\mathbf{R}$ . Singular integrals over the source domain will be denoted with a prime.

Note, the singular integrals are either due to  $G_p$  or  $\nabla G_p$ , are over either testing or source domains, and can all be formed as combinations of (3.25). Just as the normal over each triangle is constant due to the flat-tessellation,  $\hat{\mathbf{n}} \cdot \mathbf{R}$  and  $\hat{\mathbf{n}}' \cdot \mathbf{R}$  are also constant over the testing and source domains respectively. In addition,  $\nabla_s \cdot \mathbf{f}$  and  $\nabla_s' \cdot \mathbf{f}'$  are constant.

Below, the expressions we use to treat the singular integrals are cataloged. This catalog is one of several equivalent sets of expressions that can be used for singularity subtraction. The singular integrals for the vector-vector operators are

$$\mathbb{K}_p' \Big|_{kn}^S = - \mathbb{K}_p'^t \Big|_{kn}^S = \frac{-1}{4\pi} \int_{T_n^+} \left( \hat{\mathbf{n}}_p' \times \mathbf{f}_n' \right) \cdot \left( \mathcal{I}_{\mathbf{R}/R^3 \times \mathbf{f}} + \frac{\kappa_p^2}{2} \mathcal{I}_{\mathbf{R}/R \times \mathbf{f}} \right) dS'$$
 (3.31a)

$$\mathbb{L}_{p}|_{kn}^{S} = -\mathbb{L}_{p}^{t}|_{kn}^{S} = \frac{1}{4\pi} \int_{T_{k}^{+}} \mathbf{f}_{k} \cdot \left( \mathcal{I}_{\mathbf{f}/R}' - j\kappa_{p} \int_{T_{n}^{+}} \mathbf{f}_{n}' dS' \right) \\
- \frac{1}{\kappa_{p}^{2}} \nabla_{s} \cdot \mathbf{f}_{k} \nabla_{s}' \cdot \mathbf{f}_{n}' \left( \mathcal{I}_{1/R}' - j\kappa_{p} A_{n}^{+} \right) dS \tag{3.31b}$$

$$\mathbb{J}_{p}^{(2)}\big|_{kn}^{S} = \frac{1}{4\pi} \int_{T_{r}^{+}} \left( \hat{\mathbf{n}}_{p} \times \mathbf{f}_{k} \right) \cdot \left( \hat{\mathbf{n}}_{p}^{\prime} \times \left( \mathcal{I}_{\mathbf{f}/R}^{\prime} - j\kappa_{p} \int_{T_{p}^{+}} \mathbf{f}_{n}^{\prime} dS^{\prime} \right) \right) dS \tag{3.31c}$$

$$\mathbb{K}_p|_{kn}^S = \frac{1}{4\pi} \int_{T_k^+} \left( \hat{\mathbf{n}}_p \times \mathbf{f}_k \right) \cdot \left( \mathcal{I}'_{\mathbf{R}/R^3 \times \mathbf{f}} + \frac{\kappa_p^2}{2} \mathcal{I}'_{\mathbf{R}/R \times \mathbf{f}} \right) dS.$$
 (3.31d)

The singular integrals for the vector-scalar operators are

$$\mathbb{Q}_p^{(1)}\big|_{kn}^S = \frac{-1}{4\pi} \int_{T_n} \hat{\mathbf{n}}_p' \cdot \left( \mathcal{I}_{\mathbf{R}/R^3 \times \mathbf{f}} + \frac{\kappa_p^2}{2} \mathcal{I}_{\mathbf{R}/R \times \mathbf{f}} \right) dS'$$
 (3.31e)

$$\left. \mathbb{P}_p^{(2)} \right|_{kn}^S = \frac{-1}{4\pi} \int_{T_n} \hat{\mathbf{n}}_p \cdot \left( \mathcal{I}_{\mathbf{R}/R^3 \times \mathbf{f}} + \frac{\kappa_p^2}{2} \mathcal{I}_{\mathbf{R}/R \times \mathbf{f}} \right) dS'$$
 (3.31f)

$$\mathbb{Q}_p^{(2)}\big|_{kn}^S = \frac{-1}{4\pi} \int_{T_n} \hat{\mathbf{n}}_p' \cdot \hat{\mathbf{n}}_p \times \left( \mathcal{I}_{f/R} - j\kappa_p \int_{T_k^+} \mathbf{f}_k dS \right) dS'. \tag{3.31g}$$

The singular integrals for the scalar-vector operators are

$$\mathbb{J}_p^{(3)}\Big|_{kn}^S = \frac{1}{4\pi} \int_{T_k} \hat{\mathbf{n}}_p \cdot \hat{\mathbf{n}}_p' \times \left( \mathcal{I}_{f/R}' - j\kappa_p \int_{T_n^+} \mathbf{f}_n' dS' \right) dS$$
 (3.31h)

$$\mathbb{M}_{p}^{(3)}\big|_{kn}^{S} = \frac{-1}{4\pi} \int_{T_{k}} \hat{\mathbf{n}}_{p} \cdot \left( \mathcal{I}_{\mathbf{R}/R^{3} \times \mathbf{f}}' + \frac{\kappa_{p}^{2}}{2} \mathcal{I}_{\mathbf{R}/R \times \mathbf{f}}' \right) dS \tag{3.31i}$$

$$\mathbb{J}_{p}^{(4)}\Big|_{kn}^{S} = \frac{1}{4\pi} \int_{T_{k}} \hat{\mathbf{n}}_{p}' \cdot \left( \mathcal{I}_{\mathbf{R}/R^{3} \times \mathbf{f}}' + \frac{\kappa_{p}^{2}}{2} \mathcal{I}_{\mathbf{R}/R \times \mathbf{f}}' \right) dS. \tag{3.31j}$$

The singular integrals for the scalar-scalar operators are

$$\mathbb{D}_p' \Big|_{kn}^S = \frac{-1}{4\pi} \int_{T_n} \left( \hat{\mathbf{n}}_p \cdot \mathbf{R} \right) \left( \mathcal{I}_{1/R^3} + \frac{\kappa_p^2}{2} \mathcal{I}_{1/R} \right) dS'$$
 (3.31k)

$$\mathbb{Q}_p^{(3)}\big|_{kn}^S = \frac{1}{4\pi} \int_{T_k} \hat{\mathbf{n}}_p \cdot \hat{\mathbf{n}}' \left( \mathcal{I}_{1/R} - j\kappa_p A_n^+ \right) dS \tag{3.311}$$

$$\mathbb{S}_p|_{kn}^S = \frac{1}{4\pi} \int_{T_k} \mathcal{I}_{1/R} - j\kappa_p A_n^+ dS \tag{3.31m}$$

$$\mathbb{D}_p|_{kn}^S = \frac{1}{4\pi} \int_{T_k} \left( \hat{\mathbf{n}}_p' \cdot \mathbf{R} \right) \left( \mathcal{I}_{1/R^3} + \frac{\kappa_p^2}{2} \mathcal{I}_{1/R} \right) dS.$$
 (3.31n)

As stated earlier in this chapter, the  $\mathbb{N}_p$  operator is hyper-singular and is dealt with as in [Terai, 1980] rather than with singularity subtraction.

For completeness, additional vector-vector operators defined in Chapter 1 are provided here

$$\hat{\mathbf{n}}_p \times \mathbb{L}_p \Big|_{kn}^S = \frac{1}{4\pi} \int_{T_k^+} \left( \mathbf{f}_k \times \hat{\mathbf{n}}_p \right) \cdot \left( \left( \mathcal{I}'_{\mathbf{f}/R} - j\kappa_p \int_{T_n^+} \mathbf{f}'_n dS' \right) \right)$$
(3.310)

$$-\frac{1}{\kappa_p^2} \nabla_s' \cdot \mathbf{f}_n' \left( \mathcal{I}_{\mathbf{R}/R^3}' + \frac{\kappa_p^2}{2} \mathcal{I}_{\mathbf{R}/R}' \right) \right) dS$$

$$\hat{\mathbf{n}}_{p} \times \mathbb{K}_{p} \Big|_{kn}^{S} = \frac{1}{4\pi} \int_{T_{k}^{+}} \mathbf{f}_{k} \cdot \left( \mathcal{I}'_{\mathbf{R}/R^{3} \times \mathbf{f}} + \frac{\kappa_{p}^{2}}{2} \mathcal{I}'_{\mathbf{R}/R \times \mathbf{f}} \right) dS.$$
 (3.31p)

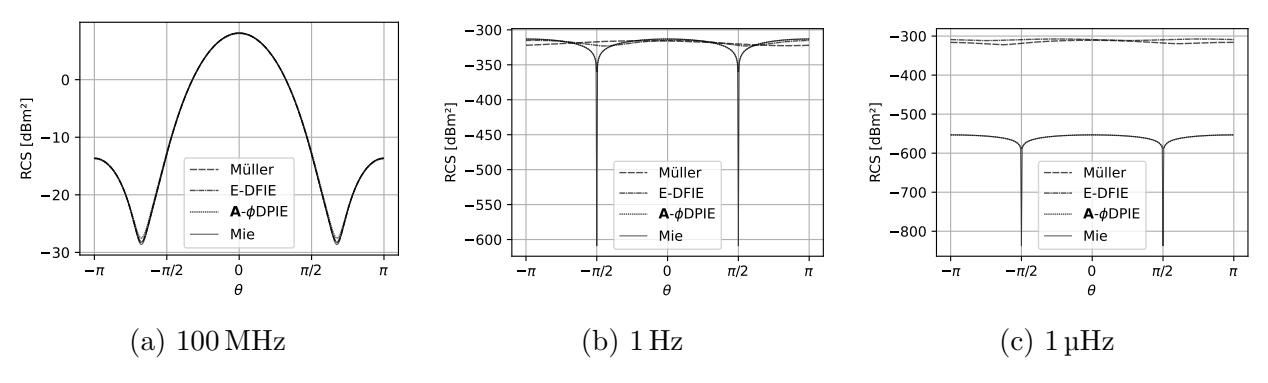


Figure 3.7 RCS of the dielectric sphere with  $\mu_{r2} = 1$  and  $\epsilon_{r2} = 1.5$ .

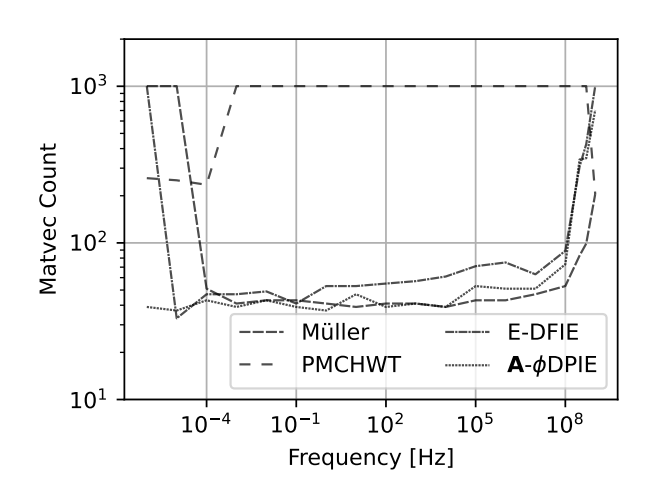
The integrals  $\int_{T_k^+} \mathbf{f}_k dS$  and  $\int_{T_n^+} \mathbf{f}'_n dS'$  are not singular and can be evaluated analytically or numerically.

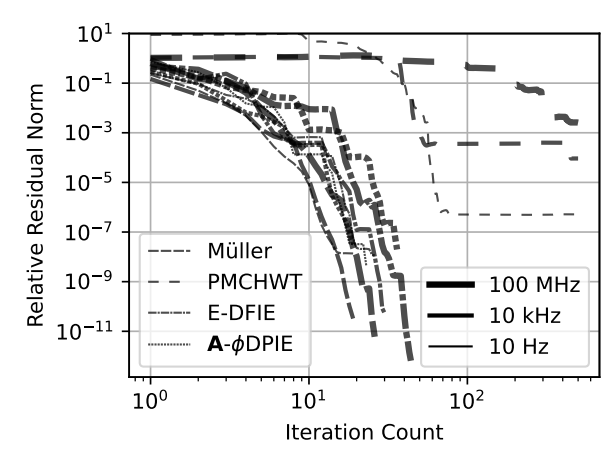
Piecewise geometric descriptions come with the challenge of accurately describing the scattering physics from objects with singular features, e.g., cones, tips, edges, These are well-known challenges (and the formulations from Chapter 2 are not immune to these as they arise from the geometry as opposed to the formulation), and one could use singular basis functions [Graglia et al., 2013] or adaptive basis functions [Nair and Shanker, 2011, Dault and Shanker, 2015] to overcome some of the bottlenecks partially.

Utilizing hat instead of pulse functions changes the expressions above but not in a way that requires additional singular integrals and is relatively straightforward due to how hat functions defined in (3.23) are related to RWG functions.

# 3.3.6 Results

We begin the piecewise analysis by considering the scattering from the dielectric sphere with radius 1 m. The sphere is meshed into 1280 patches and 1920 edges with an average edge length at 100 MHz of about  $^{\lambda_1}/_{19.9}$  with  $\lambda_1$  being the wavelength in the exterior region. In Figures 3.7, we examine RCS data at three different frequencies, specifically at 100 MHz, 1 Hz, and 1  $\mu$ Hz due to an incident wave with an arrival vector of  $\hat{\mathbf{k}} = \hat{\mathbf{z}}$ , polarized along  $\mathbf{E}_0 = \hat{\mathbf{x}}$ , and measured at points along  $\theta \in [-\pi, \pi]$  and  $\phi = 0$ . In Figure 3.7a, we see that there is good agreement among all formulations, including the analytic formulation at 100 MHz. In Figure 3.7b, we see that the E-DFIE, Müller, and PMCHWT formulations have already





(a) Matvec count using TFQMR method for different integral equations across frequencies.

(b) Convergence plot of the relative residual ||residual|| / ||RHS|| using the TFQMR method for different integral equations. The thickness of the line indicates the frequency, while the style (dotted, dashed, solid) indicates the formulation.

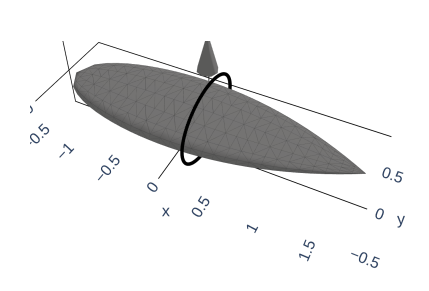
Figure 3.8 Results from the dielectric sphere discretized with RWG and pulse basis sets with  $\mu_{r2} = 1$  and  $\epsilon_{r2} = 1.5$ .

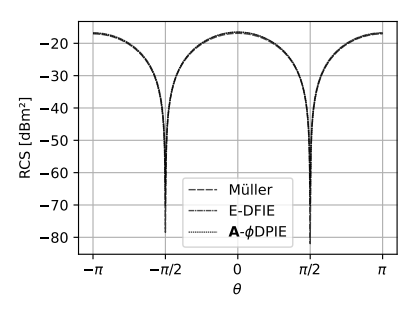
diverged from the analytic solution at 1 Hz whereas the  $\mathbf{A} - \phi$ -DPIE and Mie agree very well with each other. Finally, in Figure 3.7c, we see that the DPIE still matches the analytic solution while the E-DFIE and Müller solutions are off the chart at 1  $\mu$ Hz.

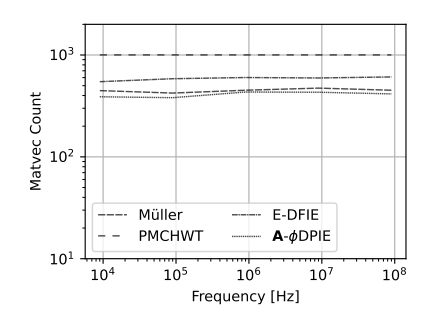
For this next experiment, we used the same piecewise discretized sphere and collected data from  $1\,\mu\text{Hz}$  to  $100\,\text{MHz}$ . For this demonstration, we use the Transpose-Free Quasi-Minimal Residual (TFQMR), but we have verified that other iterative solvers show similar behavior. A relative tolerance of  $10^{-12}$  is used for two reasons. First, low-frequency convergence, especially to  $-500\,\text{dB}\,\text{m}^2$ , necessitated the need for a smaller than typical tolerance and a relative as opposed to absolute tolerance

$$||residual|| \le tol \times ||RHS||$$
. (3.32)

Second, as we examine convergence across frequencies, we wanted to keep the relative tolerance constant so that the iteration count comparison would be fair. The TFQMR solver is stopped after 500 iterations unless it stops due to a TFQMR related breakdown or the tolerance has been met. For TFQMR, there are two matrix-vector multiplications (matvecs) per iteration.







(a) Tessellated geometry with incident and observation angles.

(b) RCS at 90 MHz.

(c) Matvec count using TFQMR method for different integral equations across frequencies

Figure 3.9 The dielectric National Aeronautics and Space Administration (NASA) Almond using piecewise basis sets with  $\mu_{r2} = 1$  and  $\epsilon_{r2} = 1.5$ .

From Figure 3.8a, it is apparent that the matvec and iteration count remains low as the frequency goes toward 0 Hz. It is also evident that PMCHWT requires significantly more iterations than the threshold except at 1  $\mu$ Hz, where the iterative solver does converge within the tolerance but not to the correct solution. There is a moderate increase for the E-DFIE and  $\mathbf{A} - \phi$ -DPIE as one tends to higher frequencies. This trend mirrors that seen in the Müller system [Li et al., 2019]. We note that methods to mollify the behavior of Müller systems have been addressed by using intermediate Buffa-Christianssen basis sets [Yan et al., 2010], but investigating these phenomena lies outside the main goals of this thesis and can be investigated in the future.

We turn our attention to the convergence of the iterative solver. In Figure 3.8b, we see that the E-DFIE,  $\mathbf{A} - \phi$ -DPIE, and Müller formulations converge very quickly in a few iterations to a solution within the relative tolerance specified. The E-DFIE and Müller formulation are well-conditioned but do not recover the RCS at a low enough frequency. In other words, even though the solver finds a solution within a few iterations, it is not helpful in the low-frequency regime.

The results of Figure 3.8 demonstrate fast convergence for the E-DFIE and  $\mathbf{A} - \phi$ -DPIE

# 3.3.6.1 Dielectric Almond

Next, we analyze scattering from a dielectric NASA almond, as seen in Figure 3.9a. The NASA almond meshes into 896 patches and 1344 edges. The average edge length at 90 MHz is about  $\lambda_1/28.5$ .

In Figure 3.9b, the RCS is shown at 90 MHz with an incident wave arriving from  $\hat{\boldsymbol{\kappa}} = \hat{\mathbf{z}}$ , polarization  $\mathbf{E}_0 = \hat{\mathbf{y}}$ , and measured at points along  $\theta \in [-\pi, \pi]$  and  $\phi = \frac{\pi}{2}$ . We see that there is excellent agreement among the E-DFIE,  $\mathbf{A} - \phi$ -DPIE, and Müller formulations at 90 MHz.

Next, the number of TFQMR iterations needed to converge to an error of  $10^{-12}$  is shown in Figure 3.9c. The data shown in this figure is for a range of frequencies from 9 kHz to 90 MHz. Again, at the lower frequencies, only  $\mathbf{A} - \phi$ -DPIE is the only formulation that is accurate. The number of iterations is relatively constant for the E-DFIE,  $\mathbf{A} - \phi$ -DPIE, and Müller.

Overall, as is evident from Figure 3.9, the favorable properties of the E-DFIE and  $\mathbf{A} - \phi$ -DPIE hold for non-canonical geometries.

# 3.4 Conclusion

Discretization with spherical harmonics enables analysis that provides insight into the formulations, even more than what is presented here. With piecewise basis functions, we can use these formulations to analyze arbitrary shapes and model actual use cases.

Implementing both discretizations provides a very practical advantage because they can be used to cross-validate each other. A simple change of basis from piecewise functions to spherical harmonics of a particular order can help identify implementation issues and give valuable insight into discretization limitations.

At this point in the thesis, a framework for formulations was presented in Chapter 2, and all of the formulations are implementable using the framework and integrals provided in this chapter. In addition, indirect formulations and formulations that are developed under different frameworks but involve the same operators are implementable with what is covered above.

## CHAPTER 4

## ACCELERATION

#### 4.1 Introduction

As noted earlier, the formulations introduced in Chapter 2 involve more operators than encountered in the classical formulations and result in large systems. As shown in Chapter 3, it is possible to implement these formulations using piecewise basis sets and construct a dense system of equations to solve for the unknown coefficients of (3.3b). However, an increased system size typically translates to a significant increase in solve time even if the system is well-conditioned due to the necessity of evaluating each entry in the system. Fortunately, this burden can be alleviated by using the MLFMA for computing far interactions, which constitute most of the system. The advantages are realized by reconstructing the potential or fields before they (or their derivatives or traces) are measured. While it is well understood, we briefly overview the MLFMA to introduce the vocabulary necessary to discuss modifications to evaluate the new operators.

#### 4.2 MLFMA Background

The derivation of FMM and its multilevel variant MLFMA are well known [Coifman et al., 1993, Song and Chew, 1995, Song et al., 1997, Sarvas, 2003, Vikram et al., 2009, Hughey et al., 2018]. Without any loss of generality, we will present the MLFMA through the 2-level description and drop the region index p from the notation. FMM starts with the integral representation of the Green's function

$$G(\mathbf{X} + \mathbf{d}) \approx -\frac{j\kappa}{(4\pi)^2} \int_{S^2} \exp(-j\kappa \cdot \mathbf{d}) T(\kappa, \mathbf{X}) d^2 \hat{\kappa},$$
 (4.1)

where the translation operator T is given by

$$T(\boldsymbol{\kappa}, \mathbf{X}) = \sum_{n=0}^{\infty} (-j)^n (2n+1) h_n^{(2)}(\kappa X) P_n(\hat{\boldsymbol{\kappa}} \cdot \hat{\mathbf{X}}), \qquad (4.2)$$

with  $\kappa = \kappa \hat{\kappa}$ . Here,  $S^2$  denotes the unit  $\hat{\kappa}$ -sphere, parameterized by  $(\theta, \phi) \in [0, \pi] \times [0, 2\pi]$ . We note that  $\hat{\kappa} = \hat{\kappa}(\theta, \phi)$ , and use these notations interchangeably. As in any MLFMA scheme, the computational domain is embedded into a bounding box that is used to construct a uniform oct-tree, the smallest of whose boxes we refer to as leaf boxes. As usual, one designs operators to map from sources in the leaf boxes to observers in other leaf boxes, provided the boxes satisfy an interaction criterion.

# 4.3 Implementation Details

As is evident from how all of the formulations in this thesis are constructed, the representation equations relate the scattered potential or field to traces and traces of derivatives acting on the total potential or field collectively referred to as  $\mathbf{x}$  in (2.1b). Likewise, one measures traces or traces of derivatives acting on the scattered potential or field. Within an MLFMA scheme, all these operators can be evaluated spectrally before and after translation. This implies that one can send scattered potentials or fields up and down the tree and then evaluate the necessary derivatives (and their traces) just before testing.

Consider a source box s whose domain is denoted by  $\Omega_s$  and centroid by  $\mathbf{r}_s^c$ . The potential or field radiated by these sources is observed in an observation box with domain  $\Omega_o$  and centroid  $\mathbf{r}_o^c$ . Assume that in the source box, there exist  $N_f^s$  functions and  $N_e^s$  RWG basis functions. Each representation integral is evaluated using a quadrature rule. Each pulse basis function is evaluated at  $N_q^f$  quadrature points located at  $\mathbf{r}'_{n_f i}$  with quadrature weights  $w_{n_f i}$ . Each RWG basis function is evaluated at  $N_q^e$  quadrature points located at  $\mathbf{r}'_{n_e i}$  with quadrature weights  $w_{n_e i}$  and unit normal  $\hat{\mathbf{n}}'_{n_e i}$  (which changes based on which triangle  $T_{n_e}^{\pm}$  of the RWG function the quadrature point resides on).

Several formulations are presented in this thesis, each with slightly different representation integrals. The following presents the most general representation integrals (1.20) and (2.17). We will utilize placeholders  $\mathbf{x}$  and x to denote any vector and scalar that satisfies the vector and scalar Helmholtz equation, respectively. In that way, the following prescription will cover all of the DFIE and DPIE formulations. For clarity, the coefficients in y will be split into coefficients  $\alpha_{n_f}$ ,  $\beta_{n_f}$ ,  $a_{n_e}$ ,  $b_{n_e}$ ,  $\gamma_{n_f}$ , and  $\sigma_{n_f}$  as needed for the formulations and for simplicity  $\underline{\mathcal{P}}$  and  $\underline{\mathcal{W}}$  will be omitted without any loss in generality. Then Charge-to-Multipole (C2M)

expansions are as follows

$$f_s(\mathbf{r}, \boldsymbol{\kappa}) = \exp\left(-j\boldsymbol{\kappa} \cdot (\mathbf{r}_s^c - \mathbf{r})\right) \tag{4.3a}$$

$$V_s^x(\boldsymbol{\kappa}) = \sum_{n_f=1}^{N_f^s} \sum_{i=1}^{N_q^f} w_{n_f i} f_s\left(\mathbf{r}'_{n_f i}, \boldsymbol{\kappa}\right)$$
(4.3b)

$$\left(j\boldsymbol{\kappa}\cdot\hat{\mathbf{n}}_{n_f}'\alpha_{n_f}-\beta_{n_f}\right)p_{n_f}\left(\mathbf{r}_{n_fi}'\right)$$

$$\mathbf{V}_{s}^{\mathbf{x}}(\boldsymbol{\kappa}) = \sum_{n_{f}=1}^{N_{f}^{s}} \sum_{i=1}^{N_{q}^{f}} w_{n_{f}i} f_{ns} \left( \mathbf{r}_{n_{f}i}', \boldsymbol{\kappa} \right)$$

$$\left( j\boldsymbol{\kappa} \gamma_{n_{f}} - \hat{\mathbf{n}}_{n_{f}} \sigma_{n_{f}} \right) p_{n_{f}} \left( \mathbf{r}_{n_{f}i}' \right)$$

$$+ \sum_{n_{e}=1}^{N_{e}^{s}} \sum_{i=1}^{N_{q}^{e}} w_{n_{e}i} f_{s} \left( \mathbf{r}_{n_{e}i}', \boldsymbol{\kappa} \right)$$

$$\left( -\hat{\mathbf{n}}_{n_{e}i} a_{n_{e}} - j\boldsymbol{\kappa} b_{n_{e}} \right) \times \mathbf{f}_{n_{e}i} \left( \mathbf{r}_{n_{e}i}' \right).$$

$$(4.3c)$$

Multipole-to-Local (M2L) transformations from  $\Omega_s$  multipoles to local expansion  $\Omega_o$  are unchanged

$$U_o^x(\kappa) = \sum_s T(\kappa, \mathbf{r}_o^c - \mathbf{r}_s^c) V_s^x(\kappa)$$
(4.4a)

$$\mathbf{U}_{o}^{\mathbf{x}}\left(\boldsymbol{\kappa}\right) = \sum_{s} \mathbf{T}\left(\boldsymbol{\kappa}, \mathbf{r}_{o}^{c} - \mathbf{r}_{s}^{c}\right) \mathbf{V}_{s}^{\mathbf{x}}\left(\boldsymbol{\kappa}\right). \tag{4.4b}$$

As an aside for the multilevel case, Multipole-to-Multipole (M2M) and Local-to-Local (L2L) expansions and M2L translations on all levels are unchanged.

For Local-to-Observer (L2O) measurements, dipole and monopole observations are located

at  $\mathbf{r} \in \text{box } \Omega_o$  can be evaluated using requisite inner products with

$$g_o(\mathbf{r}, \boldsymbol{\kappa}) = \frac{-j\kappa}{(4\pi)^2} \exp\left(-j\boldsymbol{\kappa} \cdot (\mathbf{r} - \mathbf{r}_o^c)\right)$$
(4.5a)

$$x^{FF}(\mathbf{r}) = \int_{S^2} g_o(\mathbf{r}, \boldsymbol{\kappa}) U_o^x(\boldsymbol{\kappa}) d^2 \hat{\boldsymbol{\kappa}}$$
(4.5b)

$$\nabla x^{FF}(\mathbf{r}) = \int_{S^2} -j\kappa g_o(\mathbf{r}, \kappa) U_o^x(\kappa) d^2 \hat{\kappa}$$
 (4.5c)

$$\mathbf{x}^{FF}(\mathbf{r}) = \int_{S^2} g_o(\mathbf{r}, \boldsymbol{\kappa}) \, \mathbf{U}_o^{\mathbf{x}}(\boldsymbol{\kappa}) \, d^2 \hat{\boldsymbol{\kappa}}$$
(4.5d)

$$\nabla \times \mathbf{x}^{FF}(\mathbf{r}) = \int_{S^2} -j\boldsymbol{\kappa} \times g_o(\mathbf{r}, \boldsymbol{\kappa}) \, \mathbf{U}_o^{\mathbf{x}}(\boldsymbol{\kappa}) \, d^2 \hat{\boldsymbol{\kappa}}$$
(4.5e)

$$\nabla \cdot \mathbf{x}^{FF}(\mathbf{r}) = \int_{S^2} -j\boldsymbol{\kappa} \cdot g_o(\mathbf{r}, \boldsymbol{\kappa}) \,\mathbf{U}_o^{\mathbf{x}}(\boldsymbol{\kappa}) \,d^2\boldsymbol{\hat{\kappa}}. \tag{4.5f}$$

Here, superscript FF denotes the far-field scattered quantity. Minor modifications are necessary to use this for the reduced formulations, for example, setting  $\sigma = 0$  for the Reduced-Decoupled Field Integral Equation (R-DFIE) and utilizing  $\sigma = \frac{\kappa^2}{j\omega}\alpha$  for R-DPIE. For the classical formulations, utilize their respective representation integrals to develop the proper C2M operator.

We note the following: (a) only changes to an existing MLFMA implementation to accommodate the new formulations are at the leaf levels in the C2M and L2O operators. (b) For the DPIE, we chose to have a four-tree configuration to represent the three Cartesian components of  $\mathbf{A}^s$  and  $\phi^s$  or  $\mathbf{F}^s$  and  $\psi^s$  and a three-tree configuration for the DFIE to represent the Cartesian components of  $\mathbf{E}^s$  or  $\mathbf{H}^s$ . We chose to send the Cartesian (rather than  $\theta - \phi$ ) components primarily to enable simpler future integration with wideband MLFMA [Vikram et al., 2009]. Furthermore, (c) because we take all derivatives spectrally, we must carefully account for the overall spectral content to design integration rules.

## 4.4 Results

The main results of this chapter are twofold: the efficacy of DFIE and DPIE for analysis of electrically large objects and the effectiveness of the MLFMA. To that end, we will show several RCS plots for a variety of objects and timings of the MLFMA accelerated (i.e. far-field) portion of the matrix-vector multiplications.

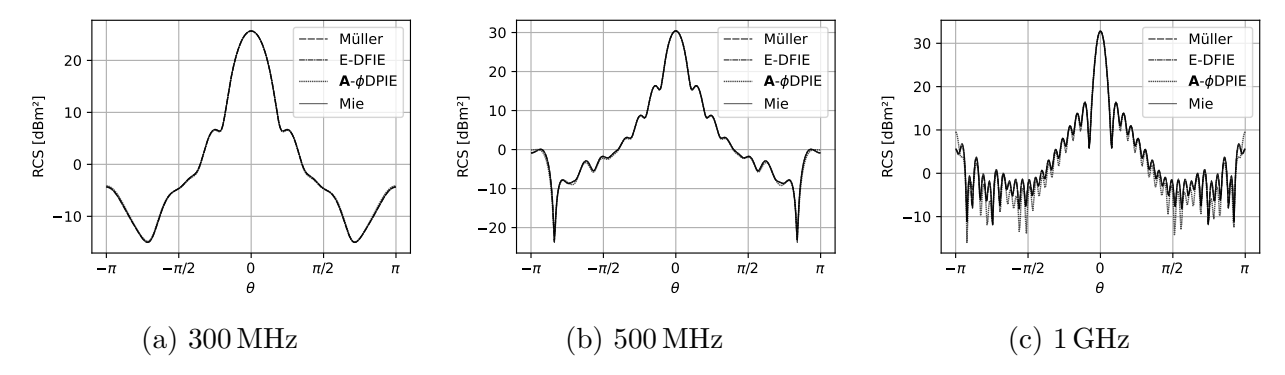


Figure 4.1 RCS plots from MLFMA accelerated solutions for a 1 m radius, dielectric sphere with  $\mu_{r2} = 1$  and  $\epsilon_{r2} = 1.5$ .

Like before, rather than showing results for each form of the DFIE and DPIE, we choose to focus on the E-DFIE and  $\mathbf{A} - \phi$ -DPIE as representatives. The main reference point will be the three-tree MLFMA accelerated Müller formulation.

# 4.4.1 Accuracy

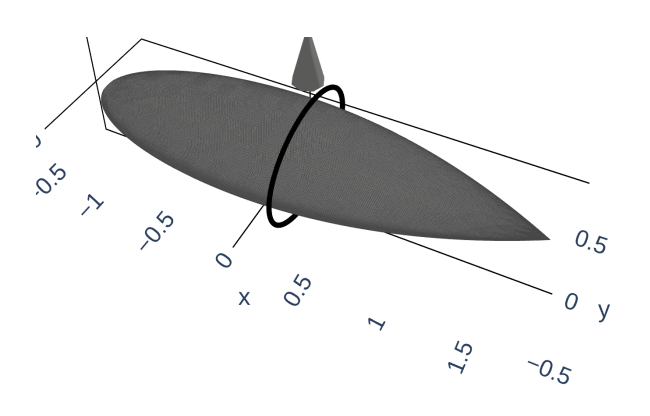
We first examine the accuracy of the MLFMA by comparing the RCS to the Mie series RCS. After that, we show agreement between the different formulations of arbitrarily shaped objects.

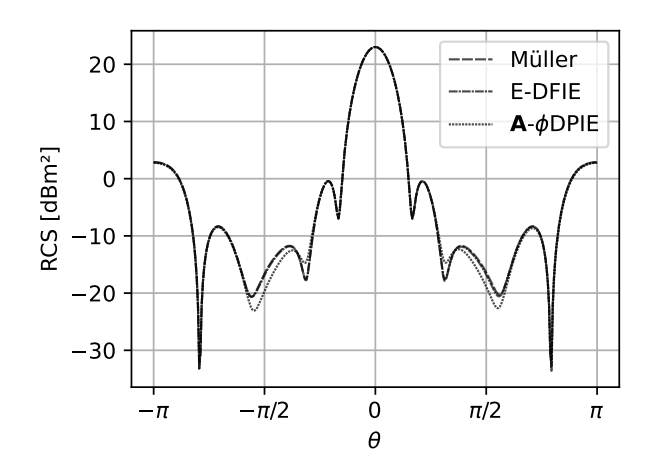
#### 4.4.1.1 Spheres

We begin by considering the scattering from different refinements of a dielectric sphere with a radius of 1 m. We present three RCS measurements due to an incident plane wave arriving from  $\hat{\mathbf{\kappa}} = \hat{\mathbf{z}}$ , polarized along  $\mathbf{E}_0 = \hat{\mathbf{x}}$ , and measured at points along  $\theta \in [-\pi, \pi]$  and  $\phi = 0$ . These are compared against the Mie series solution.

The first result is the RCS of a sphere meshed into 20,480 patches and 30,720 edges with an average edge length of about  $\lambda_1/26.6$  with an incident plane wave at 300 MHz. A three-level MLFMA tree is used for this result. Figure 4.1a shows excellent agreement between the formulations with almost no noticeable disagreement at any  $\theta$ .

The second result is the RCS of a sphere meshed into 103,680 patches and 155,520 edges with an average edge length of about  $\lambda_1/35.7$  with an incident wave at 500 MHz. A four-level MLFMA tree is used for this result. We see in Figure 4.1b excellent agreement between all of





- (a) The NASA almond geometry with incident and observation angles.
- (b) The RCS at 900 MHz.

Figure 4.2 The dielectric NASA almond with  $\mu_{r2} = 1$  and  $\epsilon_{r2} = 1.5$ .

the formulations with only slight disagreement with the DPIE formulation for certain RCS valleys.

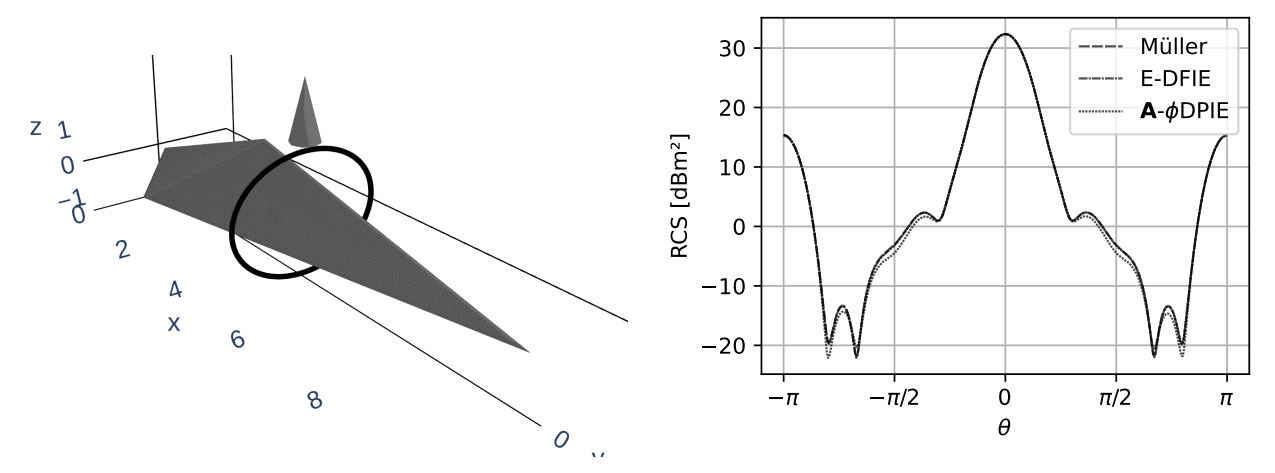
The third result is the RCS of a sphere meshed into 184,320 patches and 276,480 edges with an average edge length of about  $^{\lambda_1/23.8}$  with an incident wave at 1 GHz. A five-level MLFMA tree is used for this result. We see in Figure 4.1c excellent agreement between all of the formulations except the DPIE formulation, which still captures the general shape but misses the peaks of some side lobes by up to 5 dB m<sup>2</sup> for  $|\theta| > \pi/8$ .

In Figure 4.1, we have shown that the accuracy is not impacted by the MLFMA acceleration and have identified that the RCS from the  $\mathbf{A} - \phi$ -DPIE starts to deviate at higher frequencies.

## 4.4.1.2 Arbitrary Objects

Next, we analyze scattering from a dielectric NASA almond, as seen in Figure 4.2a. The NASA almond is meshed into 72,576 patches and 108,864 edges with an average edge length of about  $^{\lambda_1}/_{25.6}$  with an incident 900 MHz plane wave with  $\hat{\boldsymbol{\kappa}} = \hat{\mathbf{z}}$ , polarization  $\mathbf{E}_0 = \hat{\mathbf{y}}$ , and measured at points along  $\theta \in [-\pi, \pi]$  and  $\phi = \frac{\pi}{2}$ . A five-level MLFMA tree is used for this result. Figure 4.2b shows excellent agreement between the formulations with slight disagreement with the DPIE formulation for certain RCS valleys.

Finally, we analyze scattering from a dielectric arrowhead, as seen in Figure 4.3a. This is a challenging geometry in that it has sharp tips and edges. The arrowhead is meshed into



(a) The arrowhead geometry with incident and (b) The RCS of the dielectric arrowhead at observation angles.

300 MHz.

Figure 4.3 The dielectric arrowhead with  $\mu_{r2} = 1$  and  $\epsilon_{r2} = 1.5$ .

23,024 patches and 34,536 edges with an average edge length of about  $\lambda_1/15.6$  with an incident 300 MHz plane wave directed along  $\hat{\boldsymbol{\kappa}} = \hat{\mathbf{z}}$ , polarization  $\mathbf{E}_0 = \hat{\mathbf{y}}$ , and measured at points along  $\theta \in [-\pi, \pi]$  and  $\phi = \frac{\pi}{2}$ . A five-level MLFMA tree is used for this result.

We see in Figure 4.3b excellent agreement between all of the formulations with almost no noticeable disagreement at any  $\theta$ .

The results from the analysis of the sphere in Figure 4.1, almond in Figure 4.2, and arrow in Figure 4.3 are for geometries that result in systems that are much larger than those from Chapter 3. The results presented in this chapter would be too large to fit in memory on the machines we were utilizing if solved without MLFMA acceleration. In addition, they were solved significantly faster than some of the smaller problems from Chapter 3. The following section will explore a timing study for our implementation.

## 4.4.2 **Timing**

For the timing study, we use a  $1 \text{ m} \times 1 \text{ m} \times 1 \text{ m}$  cube with a variety of meshes discretized with different edge lengths. The frequency is chosen for each mesh so that the edge lengths are approximately  $\lambda_1/15$ . Only the outer region's discretized system  $\langle \mathcal{F}, \mathcal{Z}_1 \circ \mathcal{F} \rangle y$  is timed for the various formulations because all other matrices involved are sparse. The number of unknowns N for a given mesh depends on the formulation:  $2N_v$ ,  $2N_s + 2N_s$ , and  $2N_v + 4N_s$ 

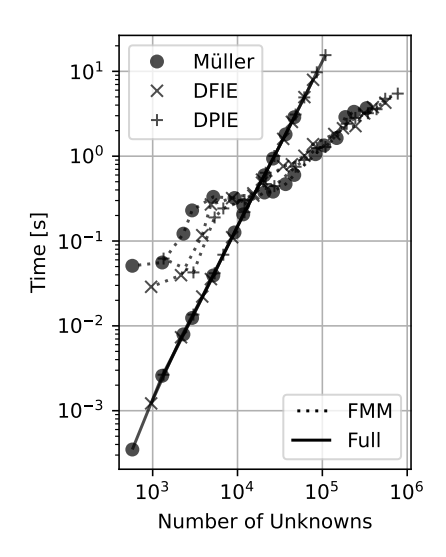


Figure 4.4 Timings for direct and MLFMA accelerated matvecs.

for the Müller, DFIE, and DPIE formulations respectively. As is seen in Figure 4.4, the direct matrix vector computation scales with  $\mathcal{O}(N^2)$  and we confirm that the MLFMA accelerated computation scales with  $\mathcal{O}(N \log N)$ . The cost of MLFMA can start paying dividends for relatively small meshes because the cross-over point occurs on the order of thousands of unknowns. However, the exact cross-over point of around  $3 \times 10^4$  unknowns is not meaningful. It is somewhat of an upper bound because many standard MLFMA optimizations have been omitted in our implementation. The grand takeaway is that the additional operators and basis function types of the DFIE and DPIE formulations do not change the scaling properties nor significantly increase the matvec computation time compared to standard MLFMA accelerated formulations.

# 4.5 Conclusion

This chapter presents how to accelerate both the DFIE and DPIE with MLFMA. As is observed in canonical and non-canonical geometries, the discrete piecewise systems are accurate, and MLFMA successfully accelerates the formulations with only minor modifications to existing implementations.

### CHAPTER 5

### CONCLUSION

To briefly summarize, in this thesis, a generalized formulation process for the direct method is developed and applied to both classic and several new formulations in Chapter 2, details required for discretizing the operators involved in all formulations with spherical harmonics and piecewise basis functions with results detailing the characteristics of each formulation were provided in Chapter 3. The necessary modifications needed to implement all of the formulations with MLFMA with RCS and timing results are given in Chapter 4.

This thesis pushes the state-of-the-art forward by (1) generalizing the direct method formulation process and utilizing it to present old and new formulations, (2) explicitly describing how to implement all of the formulations with analytic basis sets, enabling eigenvalue and condition number analysis in a unified manner, (3) developing the required integrals for implementing all operators used in many formulations on piecewise basis and testing functions, and (4) demonstrating how to accelerate these formulations using a common MLFMA framework.

#### 5.1 Future Work

Some areas of further development include but are not limited to

- additional excitations such as point sources
- impedance boundary conditions
- extending the framework to support multiply connected and open geometries
- more advanced singularity treatment for the piecewise basis sets
- alternate basis functions and non-Galerkin testing such that the testing functions lie in the dual space of the range of each operator
- higher order piecewise basis functions
- hybrid Multilevel Accelerated Cartesian Expansion (MLACE)-MLFMA acceleration for wide-band performance
- FEBI with DFIE and DPIE formulations

Much of this work can be accomplished abstractly, as was done in this thesis, such that comparisons to existing formulations and methods are always apples-to-apples and share as much logic and implementation as possible. Future novel formulations will also benefit from this and can be more quickly matured with less effort.

## **BIBLIOGRAPHY**

- [Adrian et al., 2019] Adrian, S. B., Andriulli, F. P., and Eibert, T. F. (2019). On a refinement-free calderón multiplicative preconditioner for the electric field integral equation. *Journal of Computational Physics*, 376:1232–1252.
- [Alsnayyan et al., 2020] Alsnayyan, A., Li, J., Hughey, S., Diaz, A., and Shanker, B. (2020). Efficient isogeometric boundary element method for analysis of acoustic scattering from rigid bodies. *The Journal of the Acoustical Society of America*, 147(5):3275–3284.
- [Andriulli et al., 2008] Andriulli, F. P., Cools, K., Bagci, H., Olyslager, F., Buffa, A., Christiansen, S., and Michielssen, E. (2008). A multiplicative calderon preconditioner for the electric field integral equation. *IEEE Transactions on Antennas and Propagation*, 56(8):2398–2412.
- [Antoine et al., 2006] Antoine, X., Darbas, M., and Lu, Y. Y. (2006). Computer methods in applied mechanics and engineering. Arch. Elektr. Ubertrag, 195(33-36):4060–4074.
- [Balanis, 2012] Balanis, C. A. (2012). Advanced engineering electromagnetics. John Wiley & Sons.
- [Botha, 2013] Botha, M. M. (2013). A family of augmented duffy transformations for near-singularity cancellation quadrature. *IEEE Transactions on Antennas and Propagation*, 61(6):3123–3134.
- [Burton and Kashyap, 1995] Burton, M. and Kashyap, S. (1995). A study of a recent moment method algorithm that is accurate to very low frequencies. *Applied Computational Electromagnetics Society Journal*, 10(3):58–68.
- [Chew, 2014] Chew, W. C. (2014). Vector potential electromagnetics with generalized gauge for inhomogeneous media: Formulation. *Progress In Electromagnetics Research*, 149:69–84.
- [Coifman et al., 1993] Coifman, R., Rokhlin, V., and Wandzura, S. (1993). The fast multipole method for the wave equation: A pedestrian prescription. *IEEE Antennas and Propagation magazine*, 35(3):7–12.
- [Cools et al., 2009a] Cools, K., Andriulli, F. P., Olyslager, F., and Michielssen, E. (2009a). Nullspaces of mfie and calderÓn preconditioned effe operators applied to toroidal surfaces. *IEEE Transactions on Antennas and Propagation*, 57(10):3205–3215.
- [Cools et al., 2009b] Cools, K., Andriulli, F. P., Olyslager, F., and Michielssen, E. (2009b). Time domain calderÓn identities and their application to the integral equation analysis of scattering by pec objects part i: Preconditioning. *IEEE Transactions on Antennas and Propagation*, 57(8):2352–2364.

- [Costabel, 1991] Costabel, M. (1991). A coercive bilinear form for maxwell's equations. Journal of Mathematical Analysis and Applications, 157(2):527–541.
- [Costabel and Stephan, 1988] Costabel, M. and Stephan, E. P. (1988). Strongly elliptic boundary integral equations for electromagnetic transmission problems. *Proceedings of the Royal Society of Edinburgh: Section A Mathematics*, 109(3-4):271–296.
- [Dault and Shanker, 2015] Dault, D. and Shanker, B. (2015). An interior penalty method for the generalized method of moments. *IEEE Transactions on Antennas and Propagation*, 63(8):3561–3568.
- [Dault and Shanker, 2015] Dault, D. and Shanker, B. (2015). A mixed potential mlfma for higher order moment methods with application to the generalized method of moments. *IEEE Transactions on Antennas and Propagation*, 64(2):650–662.
- [Dely, 2020] Dely, A. (2020). Computational strategies for impedance boundary condition integral equations in frequency and time domains. PhD thesis, Ecole nationale supérieure Mines-Télécom Atlantique.
- [Epstein and Greengard, 2010] Epstein, C. L. and Greengard, L. (2010). Debye sources and the numerical solution of the time harmonic maxwell equations. *Communications on Pure and Applied Mathematics*, 63(4):413–463.
- [Fink et al., 2008] Fink, P. W., Wilton, D. R., and Khayat, M. A. (2008). Simple and efficient numerical evaluation of near-hypersingular integrals. *IEEE Antennas and Wireless Propagation Letters*, 7:469–472.
- [Fu et al., 2017] Fu, X., Li, J., Jiang, L. J., and Shanker, B. (2017). Generalized debye sources-based efie solver on subdivision surfaces. *IEEE Transactions on Antennas and Propagation*, 65(10):5376–5386.
- [Glisson, 1984] Glisson, A. (1984). An integral equation for electromagnetic scattering from homogeneous dielectric bodies. *IEEE Transactions on Antennas and Propagation*, 32(2):173–175.
- [Graglia et al., 2013] Graglia, R. D., Peterson, A. F., and Matekovits, L. (2013). Singular, hierarchical scalar basis functions for triangular cells. *IEEE Transactions on Antennas and Propagation*, 61(7):3674–3692.
- [Hawkins et al., 2022] Hawkins, J., Baumann, L., Aktulga, H., Dault, D., and Shanker, B. (2022). Analytic preconditioners for decoupled potential integral equations for wideband analysis of scattering from pec objects. arXiv preprint arXiv:2211.10560.
- [Helsing et al., 2020] Helsing, J., Karlsson, A., and Rosén, A. (2020). Comparison of integral equations for the maxwell transmission problem with general permittivities.

- [Hodges and Rahmat-Samii, 1997] Hodges, R. E. and Rahmat-Samii, Y. (1997). The evaluation of mfie integrals with the use of vector triangle basis functions. *Microwave and Optical Technology Letters*, 14(1):9–14.
- [Hsiao and Kleinman, 1997] Hsiao, G. C. and Kleinman, R. E. (1997). Mathematical foundations for error estimation in numerical solutions of integral equations in electromagnetics. *IEEE Transactions on Antennas and Propagation*, 45(3):316–328.
- [Hughey et al., 2018] Hughey, S., Aktulga, H., Vikram, M., Lu, M., Shanker, B., and Michielssen, E. (2018). Parallel wideband mlfma for analysis of electrically large, nonuniform, multiscale structures. *IEEE Transactions on Antennas and Propagation*, 67(2):1094–1107.
- [Kress and Roach, 1978] Kress, R. and Roach, G. F. (1978). Transmission problems for the helmholtz equation. *Journal of Mathematical Physics*, 19(6):1433–1437.
- [Li et al., 2014] Li, J., Dault, D., Nair, N., and Shanker, B. (2014). Analysis of scattering from complex dielectric objects using the generalized method of moments. *JOSA A*, 31(11):2346–2355.
- [Li et al., 2017] Li, J., Fu, X., and Shanker, B. (2017). Potential integral equations in electromagnetics. In 2017 IEEE International Symposium on Antennas and Propagation USNC/URSI National Radio Science Meeting.
- [Li et al., 2019] Li, J., Fu, X., and Shanker, B. (2019). Decoupled potential integral equations for electromagnetic scattering from dielectric objects. *IEEE Transactions on Antennas and Propagation*, 67(3):1729–1739.
- [Liu et al., 2015] Liu, Q. S., Sun, S., and Chew, W. C. (2015). An integral equation method based on vector and scalar potential formulations. In 2015 IEEE International Symposium on Antennas and Propagation USNC/URSI National Radio Science Meeting, pages 744–745.
- [Marx, 1984] Marx, E. (1984). Integral equation for scattering by a dielectric. *IEEE Transactions on Antennas and Propagation*, 32(2):166–172.
- [Müller, 1969] Müller, C. (1969). Electromagnetic Waves in a Homogeneous Medium. Springer Berlin Heidelberg, Berlin, Heidelberg.
- [Nair and Shanker, 2011] Nair, N. V. and Shanker, B. (2011). Generalized method of moments: A novel discretization technique for integral equations. *IEEE transactions on antennas and propagation*, 59(6):2280–2293.
- [Poggio and Miller, 1973] Poggio, A. and Miller, E. (1973). Chapter 4 integral equation solutions of three-dimensional scattering problems. In Mittra, R., editor, *Computer Techniques for Electromagnetics*, International Series of Monographs in Electrical Engineering, pages 159 264. Pergamon.

- [Qian and Chew, 2009] Qian, Z. and Chew, W. C. (2009). Fast full-wave surface integral equation solver for multiscale structure modeling. *IEEE Transactions on Antennas and Propagation*, 57(11):3594–3601.
- [Qian and Chew, 2008] Qian, Z. G. and Chew, W. C. (2008). A quantitative study on the low frequency breakdown of efie. *Microwave and Optical Technology Letters*, 50(5):1159–1162.
- [Rao et al., 1982] Rao, S., Wilton, D., and Glisson, A. (1982). Electromagnetic scattering by surfaces of arbitrary shape. *IEEE Transactions on Antennas and Propagation*, 30(3):409–418.
- [Roth and Chew, 2018] Roth, T. E. and Chew, W. C. (2018). Development of stable A- $\phi$  time-domain integral equations for multiscale electromagnetics. *IEEE Journal on Multiscale and Multiphysics Computational Techniques*, 3:255–265.
- [Roth and Chew, 2020] Roth, T. E. and Chew, W. C. (2020). Radiation gauge potential-based time domain integral equations for penetrable regions. *Progress In Electromagnetics Research*, 168:73–86.
- [Sarvas, 2003] Sarvas, J. (2003). Performing interpolation and anterpolation entirely by fast fourier transform in the 3-d multilevel fast multipole algorithm. SIAM Journal on Numerical Analysis, 41(6):2180–2196.
- [Song et al., 1997] Song, J., Lu, C.-C., and Chew, W. C. (1997). Multilevel fast multipole algorithm for electromagnetic scattering by large complex objects. *IEEE transactions on antennas and propagation*, 45(10):1488–1493.
- [Song and Chew, 1995] Song, J. M. and Chew, W. C. (1995). Multilevel fast-multipole algorithm for solving combined field integral equations of electromagnetic scattering. *Microwave and optical technology letters*, 10(1):14–19.
- [Stratton, 2015] Stratton, J. A. (2015). Spherical Waves, chapter VII, pages 392–423. John Wiley & Sons, Ltd.
- [Terai, 1980] Terai, T. (1980). On calculation of sound fields around three dimensional objects by integral equation methods. *Journal of Sound and Vibration*, 69(1):71 100.
- [Tihon and Craeye, 2018] Tihon, D. and Craeye, C. (2018). All-analytical evaluation of the singular integrals involved in the method of moments. *IEEE Transactions on Antennas and Propagation*, 66(4):1925–1936.
- [Vecchi, 1999] Vecchi, G. (1999). Loop-star decomposition of basis functions in the discretization of the efie. *IEEE Transactions on Antennas and Propagation*, 47(2):339–346.

- [Vico et al., 2016] Vico, F., Ferrando, M., Greengard, L., and Gimbutas, Z. (2016). The decoupled potential integral equation for time-harmonic electromagnetic scattering. *Communications on Pure and Applied Mathematics*, 69(4):771–812.
- [Vico et al., 2015] Vico, F., Ferrando-Bataller, M., Jiménez, T. B., and Berenguer, A. (2015). A high order locally corrected nyström implementation of the decoupled potential integral equation. In 2015 9th European Conference on Antennas and Propagation (EuCAP), pages 1–4.
- [Vico et al., 2018] Vico, F., Greengard, L., and Ferrando, M. (2018). Decoupled field integral equations for electromagnetic scattering from homogeneous penetrable obstacles. Communications in Partial Differential Equations, 43(2):159–184.
- [Vikram et al., 2009] Vikram, M., Huang, H., Shanker, B., and Van, T. (2009). A novel wideband fmm for fast integral equation solution of multiscale problems in electromagnetics. *IEEE Transactions on Antennas and Propagation*, 57(7):2094–2104.
- [Wilcox, 1956] Wilcox, C. H. (1956). An expansion theorem for electromagnetic fields. Communications on Pure and Applied Mathematics, 9(2):115–134.
- [Wilde, 1987] Wilde, P. (1987). Transmission problems for the vector helmholtz equation. *Proceedings of the Royal Society of Edinburgh: Section A Mathematics*, 105(1):61–76.
- [Wilton et al., 1984] Wilton, D., Rao, S., Glisson, A., Schaubert, D., Al-Bundak, O., and Butler, C. (1984). Potential integrals for uniform and linear source distributions on polygonal and polyhedral domains. *IEEE Transactions on Antennas and Propagation*, 32(3):276–281.
- [Wilton and Glisson, 1981] Wilton, D. R. and Glisson, A. W. (1981). On improving the electric field integral equation at low frequencies. In *URSI National Radio Science Meeting Digest*, page 24.
- [Wu et al., 1995] Wu, W., Glisson, A. W., and Kajfez, D. (1995). A study of two numerial solution procedures for the electric field integral equation at low frequency. *Applied Computational Electromagnetics Society Journal*, 10(3):69–80.
- [Yan et al., 2010] Yan, S., Jin, J., and Nie, Z. (2010). Calderón preconditioner: From efie and mfie to n-müller equations. *IEEE Transactions on Antennas and Propagation*, 58(12):4105–4110.
- [Yla-Oijala and Taskinen, 2005] Yla-Oijala, P. and Taskinen, M. (2005). Well-conditioned muller formulation for electromagnetic scattering by dielectric objects. *IEEE Transactions on Antennas and Propagation*, 53(10):3316–3323.

[Ylä-Oijala et al., 2005] Ylä-Oijala, P., Taskinen, M., and Sarvas, J. (2005). Surface integral equation method for general composite metallic and dielectric structures with junctions. *Progress In Electromagnetics Research*, 52:81–108.

[Yuan and Shanker, 2005] Yuan, J. and Shanker, B. (2005). Analysis of the spectrum of the single integral equation for scattering from dielectric objects. In 2005 IEEE Antennas and Propagation Society International Symposium, volume 2B, pages 93–96 vol. 2B.